Light matter interactions: quantum memories and atom-photon gates

G. P. Teja

A thesis submitted for the partial fulfilment of

the degree of Doctor of philosophy

Department of Physical sciences

Indian Institute of Science Education and Research Mohali

Knowlege city, sector 81, SAS Nagar, Manauli PO, Mohali 140306, Punjab, India

Declaration

The work presented in this thesis has been carried out by me under the guidance of Dr. Sandeep K. Goyal at the Indian Institute of Science Education and Research Mohali. This work has not been submitted in part or in full for a degree, a diploma, or a fellowship to any other university or institute. Whenever contributions of others are involved, every effort is made to indicate this clearly, with due acknowledgement of collaborative research and discussions. This thesis is a bona fide record of original work done by me and all sources listed within have been detailed in the bibliography.

G. P. Teja

In my capacity as the supervisor of the candidate's thesis work, I certify that the above statements by the candidate are true to the best of my knowledge.

Supervisor:

Dr. Sandeep K. Goyal

Acknowledgements

I would like to thank my supervisor for his persistent encouragement and motivation to pursue interesting problems. I'm grateful for time he catered for discussions and for persuading me to become an independent researcher.

I would like to thank my collaborators Christoph Simon, Thomas Konrad, Manabendra Nath Bera, Chanchal and Rajeev Gangwar. Working with them broadened my perspective and helped me in exploring new topics with ease.

I also like to thank my group members for their academic and non-academic assistance. I thank my friends and family for their support.

Publications

- ✓[1] G. P. Teja, C. Simon, and S. K. Goyal, "Photonic quantum memory using an intra-atomic frequency comb," *Physical Review A*, vol. 99, May 2019.
- ✓ G. Teja and S. K. Goyal, "Studying the effect of fluctuating environment on intra-atomic frequency comb based quantum memory," *Scientific Reports*, vol. 11, no. 1, pp. 1–9, 2021.
- ✗[2] Chanchal, G. P. Teja, C. Simon, and S. K. Goyal, "Storing vector-vortex states of light in an intra-atomic frequency-comb quantum memory," *Phys. Rev. A*, vol. 104, p. 043713, Oct 2021.
- ☆[3] R. Gangwar, M. L. Bera, G. P. Teja, S. K. Goyal, and M. N. Bera, "Making noisy quantum channels transparent," *arXiv* .2106.04425, 2021.
- ✗ Chanchal, G. P. Teja and S. K. Goyal, "Single atom quantum memory using intra-atomic frequency-comb ," *Manuscript under preparation.*
- ✓ G. P. Teja, T. Konrad and S. K. Goyal "Atomic state preparation with off resonant pulses," *Manuscript under preparation.*

[1] ✓ represents articles completely included in the thesis.
[2] ✗ represents articles not included in the thesis.
[3] ☆ represents articles partly included in the thesis.

Abstract

Light-matter interactions play a central role in realizing practical quantum computers and long distance quantum communication. Some of the essential tools in realizing quantum communication are quantum memory (QM) and quantum gates. Photonic quantum memory is a device capable of storing and retrieving the quantum states of photons on demand. They are typically realized in atoms or artificial-atoms such as quantum dots. Most of the present day QM's are proposed using light-matter interactions and have been demonstrated on various platforms such as solid-state systems, atom traps and vapour cells. Quantum gates are the operations performed on quantum systems in order to implement quantum algorithms.

In the first part of the thesis, we have devised a novel photonic quantum memory using an intra-atomic frequency comb (I-AFC). The frequency comb is constructed between two degenerate energy levels of an atom. Since the frequency comb is constructed from individual atoms, these atoms can be used individually or in ensembles to realize the quantum memory. The I-AFC based quantum memory is efficient and robust against environmental fluctuations. Also it provides the possibility for realizing on-chip quantum memory for photons.

Second part of the thesis deals with atom-photon quantum gates. In this part we study light-matter interactions in atom-cavity setups to realize certain operations on atom-photon combined systems. Using these gates, we demonstrate an efficient scheme to prepare arbitrary atomic states using a chain of single photons interacting sequentially with the atom. We also use the atom-photon gates to implement the quantum channel transparency protocol on an atomic system.

Contents

Chapter 1

Introduction

The idea of a classical computer is well known to us. A computer in its rudimentary form is a device that takes information in terms of classical bits, performs logic gates on the bits and yields output-bits. Whereas a quantum computer (QC) uses two-level quantum systems (qubits) for computation. In QC's the qubits are typically initialized in a desired state or a superposition state. Then unitary rotations (gate-operations) are applied and finally the output states are measured. A variety of systems are being explored to realize a practical quantum computer e.g. superconducting qubits (SQ) [1, 2], trapped ions [3], Rydberg atoms [4], quantum dots [5, 6] and photonic systems [7, 8].

The physical systems that act as qubits are realized using the various degrees of freedom of the system, e.g. energy levels of atoms and ions, charge states in quantum dots and the charge and flux states of SQ. The initialization, gate operations and readout of the qubits are performed using light-matter interactions. For photonic qubits polarization can be used for encoding a qubit. Such encoding is ideal for communication, as the polarization qubits doesn't have a bath. But the two-qubit gate operations are difficult with polarization qubits, as photons do not interact easily. For quantum computation with photons, the qubits are encoded in an infinite-dimensional harmonic oscillator [9], and the gate operations are performed using beams splitters, phase shifters, homodyne detectors and number resolving detectors.

A feature essential to QC is the superposition states of a qubit. To have longer computation times it is crucial to preserve the coherence of the superposition states. Nevertheless a realistic qubit is under constant interaction with the environment resulting in the decoherence of the qubit. The decoherence will eventually make the qubit ineffective

and all computations on the qubit should be completed within the coherence time. Coherence times depend on type of system and the noise. Till the present day the best coherence times for trapped ions is ~ 50 s [3], for for SQ is ~ 1 ms [1], Rydberg atoms is ~ 10 μs [4] and for semi-conductor qubits the coherence times range from few nano-seconds to few hours [6].

Another important metric for a practical QC is the gate-error. Single qubit gates are typically achieved with very high fidelities and the two-qubit operations have gate fidelities $\gtrsim 99\%$. The present day errors for two-qubit gates are at $\sim 0.3\%$ in SQ [1], $\sim 0.1\%$ in trapped-ions [3], $> 1\%$ in Rydberg atoms [4] and $\sim 0.8\%$ in semi-conductor qubits [10]. Although the error for two qubit gate operation is less, it can get accumulated while performing large number of operations. However, similar to a classical computer these faulty gates can be used to perform precise operations by using fault-tolerant techniques The gate-errors are corrected by encoding a single logical qubit into multiple qubits, thus higher gate errors require more qubits for the encoding of a single logical qubit and the exact number of qubits depends on the form of the noise. Nevertheless it's clear that, to perform useful and reliable computation we require large number of qubits. Rough estimates show that to built a fault-tolerant quantum computer with 100 qubits requires a million qubits [11].

Scientists and industries are in constant pursuit to control more qubits. And in the matter qubits (atoms, trapped ions, quantum dots and SQ), it will be a challenging task to scale-up the system to a million qubits. In photonic quantum computers, bosonic modes of photons are used as qubits and can be produced in large numbers. The drawback of using bosonic modes is that the gate operations are not feasible for practical computations. Instead, a computation scheme known as measurement based quantum computation (MBQC) will be suitable to build a QC using photons [12, 13, 14].

So far we have discussed only the computation with qubits. Another equally important aspect is quantum communication i.e. distribution of quantum states over long distances. To transmit the quantum states we can map the qubits into a photon and transmit the photons using optical fibers. To avoid the losses of optical fibers, amplifiers are required at regular intervals but the no-cloning theorem forbids a quantum amplifier [15]. To overcome this, entanglement between distant nodes can be used for long distance communication. A photonic channel can be used to share entanglement between distant nodes but the

degree of entanglement drops exponentially with the length of the channel and to avoid noise, exponentially large number of partially entangled states are required to create one highly entangled state [16]. Due to the exponential scaling, photonic channels are not viable for entanglement sharing over long distances. An alternative approach to sharing entanglement is the quantum repeater [15]. In quantum repeaters the distance is split into shorter links. Each link contains two Quantum Memories (QM), which convert photons into atomic excitations, and vice versa. The entanglement process starts by absorbing a photon and creating an atomic excitation at both QM's. Then the excitations are converted into photons using light pulses. Finally the photons from the QM's are mixed at a beam splitter and the detection of a single photon will herald the entanglement of two QM's [15]. Once an entanglement is generated between two links of QM's it can be swapped to give an entanglement over a long distance [15]. For example, two pairs of QM's (A, B) and (C, D) are spatially separated and entanglement is generated between $A \leftrightsquigarrow B$ and $C \leftrightsquigarrow D$ [17]. Then to swap the entanglement i.e. to entangle $A \leftrightsquigarrow D$, atomic excitations form the QM B and C are converted into photons and mixed at a beam splitter, then the detection of a single photon will herald the entanglement of $A \leftrightsquigarrow D$ [17].

From the above discussion it is obvious that quantum memory and the quantum gates are essential for photonic quantum computation and long distance quantum communication. In this thesis we study the light-matter interaction to construct efficient and robust photonic quantum memories and efficient photon-photon and atom-photon gates.

Photonic quantum memory is a device capable of storing and re-emitting the photons on demand. Atoms or artificial-atoms have been the typical platforms for photonic quantum memories. All of the present-day QM are proposed using light-mater interactions and have been demonstrated in solid-sate systems, atom traps and vapour cells [18, 19]. Some of the popular QM's in atomic ensembles are based on Electromagnetically Induced Transparency (EIT), Controlled Reversible Inhomogeneous Broadening (CRIB), Gradient Echo Mechanism (GEM) and the Atomic Frequency Comb (AFC). Till the present day the highest efficiencies for EIT is 85% [20], for CRIB is 15% [21], for GEM is 85% [22] and for AFC is 10% [23]. In all of these protocols the longest memory times are $\sim \mu$s.

Atom-photon gates are crucial for computation in cavity-QED setups. The atom-photon gates are realized by reflecting photons of a strongly coupled atom-cavity setup.

Further applying the atom-photon gates on two photons, a photon-photon quantum gate can be implemented. Apart from the gates for computation, studying light-matter interactions of atom-cavity systems [24, 25] have been instrumental in realizing a wide range of application ranging from single photon generation, atom-photon gates, generating entanglement between two nodes, quantum transducers, generating cat-states [26] and atomic clocks [27].

In this thesis we propose a photonic quantum memory called the Intra-AFC, this memory scheme is similar to the AFC. AFC typically consists of rare-earth ions doped in crystals that have optical transition between the ground state $|g\rangle$ and the excited state $|e\rangle$. This transition has a narrow homogeneous bandwidth γ and a large inhomogeneous bandwidth Γ_{in} ($\Gamma_{\text{in}} \gg \gamma$). The absorption profile of $|e\rangle$-$|g\rangle$ transitions is shaped into series of peaks, with spacing Δ using the technique of spectral hole-burning [28]. In spectral hole burning a narrow transmission window is created in a large inhomogeneous profile, by coherently transferring the atoms into a long-lived auxiliary state. Repeating this protocol at different frequencies results in an atomic density function with series of equispaced narrow peaks (teeth), resulting in a comb like structure in frequency modes. A single photon absorbed in the AFC system is re-emitted after a delay time of $2\pi/\Delta$. To store the excitation for a long time the excitation is transferred to a long-lived spin state by applying a control pulse. This excitation can be retrieved at a later time by applying another control pulse which transfers the excitation from the spin state to the excited state from where we can observe a photon echo at time $2\pi/\Delta$.

To overcome the difficulty of preparation of frequency combs through hole-burning, we propose an intra-atomic frequency comb (I-AFC) with hyper-fine levels of a single atom. The I-AFC is realized by splitting the hyper-fine levels with an external magnetic filed. We constructed an I-AFC in Cs and Rb atoms and showed that it results in an efficient quantum memory.

One of the limitation of the I-AFC is that the frequency combs obtained in natural atomic systems are not always uniform. The non-uniformity can be due to unequal absorption or due to unequal spacing between different hyperfine states. This may severely affect the storage quality, forcing us to choose the atomic systems which have almost uniform frequency combs. To study the effects of various environmental factors on intra-atomic frequency comb (I-AFC) based quantum memory. We introduced random

fluctuations and non-uniformity in the parameters such as comb spacing and the optical depth, of the frequency comb.

We found that the fluctuations in different parameters in the I-AFC affect the quality of the photon storage differently. The non-uniformity in the height of the teeth has negligible effect on the efficiency. Whereas the fluctuations in the comb spacing has significant effect. Fortunately, this adverse effect can be mitigated by increasing the finesse of the frequency comb, which can be done by increasing the external magnetic field. Similarly, the fidelity between the input and the output states is robust against the fluctuation in the absorption and the comb spacing. Furthermore, we found that the non-uniform frequency combs without any fluctuations in the comb parameters can also yield efficient quantum memory. Since the intra-atomic frequency combs found in natural atomic systems are often non-uniform, our results suggest that a large class of these systems can be used for I-AFC based efficient quantum memory.

By realizing frequency combs for right and left circular polarizations , I-AFC can be used as a quantum memory for the polarization qubit [29]. Since the I-AFC is present in a single atom it can be used to realize on-chip single photon sources and a single atom quantum memory with long storage times.

In the second part of the thesis we use atom-cavity setups to realize two-qubit atom-photon gates and swap operation. The atom cavity setup consists of a Λ-type atom with $|0\rangle$ as the excited states and $|\pm 1\rangle$ as the degenerate ground states.

The atom-cavity system is typically driven in two important regimes. The bad cavity regime ($\kappa \gg g^2/\kappa \gg \gamma$) where the decay of the cavity mode (κ) dominates over atom-cavity coupling (g) and the atom decay rate (γ). Since cavity decay is much larger than coherence, photon in this regime quickly leaks out of the cavity. Contrary to bad cavity regime is the strong coupling regime ($g \gg \kappa, \gamma$) where the coherent emission and absorption of photon is dominant over decay. Driving the atom-cavity in strong coupling regime results in a conditional phase shift. This conditional phase along with a Λ-type atom results in atom-photon gates, $C_{j=x,y,z} = |0\rangle\langle 0| \otimes \mathbb{1} + |1\rangle\langle 1| \otimes \sigma_j$.

We use these atom-photon gates to propose an implementation scheme for Quantum channel transparency (QCT). QCT is a protocol where the action of bath on a system (S) is suppressed by interacting the system with two ancillary systems (A and B). In

QCT the environment effects are formulated in the form of Linblad operators without assuming a specific noise model, hence it works for any general environment. QCT relies on performing unitary operations of the form [30]

$$\begin{aligned} U_{ABS} =& \ |00\rangle\langle 00|^{AB} \otimes \mathbb{1}^S + |01\rangle\langle 01|^{AB} \otimes \sigma_z^S + |10\rangle\langle 10|^{AB} \otimes \sigma_x^S - i\,|11\rangle\langle 11|^{AB} \otimes \sigma_y^S. \\ V_{ABS} =& (H \otimes H \otimes \mathbb{1})\ U_{ABS}\ (H \otimes H \otimes \mathbb{1}) \qquad \text{with} \quad H = \begin{pmatrix} 1 & 1 \\ 1 & -1 \end{pmatrix} \end{aligned} \tag{1.1}$$

where A, B represent the ancilla's and S the system. H is Hadamard operation on the ancilla's A and B

We implement the U_{ABS} operation using atom-photon gates, with atom and photons as the system and the ancilla's. We first decompose U_{ABS} as a product of two controlled operators

$$U_{ABS} = \left(\mathbb{1}_B \otimes C_x^{AS}\right)\left(\mathbb{1}_A \otimes C_z^{BS}\right), \tag{1.2}$$

where $C_x^{AS} = |0\rangle\langle 0|^A \otimes \mathbb{1}^S + |1\rangle\langle 1|^A \otimes \sigma_x^S$ and $C_z^{BS} = |0\rangle\langle 0|^B \otimes \mathbb{1}^S + |1\rangle\langle 1|^B \otimes \sigma_z^S$ are respectively the control-NOT and control-Phase gates acting on one photon and the atom. Therefore, the unitary U_{ABS} can be implemented by sequentially interacting the two photons with the atom-cavity system similarly the unitary V_{ABS} by performing a Hadamard operation on the ancillas.

We also use the atom-cavity setup to implement an atomic state preparation protocol using the technique of coherent feedback control and weak swap gate. Swap operation can be a useful tool in mapping the state of system A to system B. This can be convenient when the state preparation is easier for one of the system e.g. it's easier to prepare the polarization states of a photon than to prepare superposition of atomic states. Hence with an efficient swap operation one can map the polarization to the atomic superposition.

In a coherent feedback control formalism, the state of a system is asymptotically pushed towards a target state $|T\rangle$ by sequentially applying weak measurements on the system [31]. Consider a trace-preserving quantum channel \$ described by an n-element set of Kraus operators K_i. If the Kraus operators satisfy the fix-point condition and complete span

condition, i.e,

$$K_i |T\rangle = z_i |T\rangle , \tag{1.3}$$

$$\text{span}\{K_i^\dagger |T\rangle\}_{i=0,\ldots,n-1} = \mathcal{H}_s, \tag{1.4}$$

where $\mathcal{H}_s$ is Hilbert space of the system. Upon satisfying Eq. (1.3) and Eq. (1.4) for all $i = 0, \ldots, n-1$ with $z_i \in \mathbb{C}$, an arbitrary initial state ρ of the system converges to target state $|T\rangle$ under repeated application of the channel \$, i.e., $\$^n(\rho) \to |T\rangle \langle T|$ as $n \to \infty$.

An atom-cavity setup driven in the bad cavity regime was used to realize a weak swap operation between atom and photon [32]. And the ideal swap operation was possible only at atom-photon resonance. We showed that the weak swap operation with off-resonant pulses satisfies the required conditions for the coherent control. Hence sequentially reflecting photons off the atom-cavity setup converges the weak swap to an ideal swap operation. Thus mapping the photonic polarization state to atomic state. The precision of the fidelity can be improved by increasing the number of photons . This protocol can be demonstrated with existing technologies and can be an efficient and fast technique for state preparation e.g. reflecting ~ 10 photons gives fidelities > 99.99 and a single-photon source producing 10^9 photons/sec [33], gives protocol times around ~ 10ns.

The thesis is organised as follows:

Part-I

- **Chapter 2: Light-matter interactions**

  This chapter introduces the basics of light-matter interactions. We derive the optical Bloch equations of two-level systems and the multi-level systems are shown as genralizaiton of two-level systems. We also study phenomenons such as electromagnetically induced transparency (EIT), Autler-Townes effect and stimulated Raman adiabatic passage (STIRAP).

- **Chapter 3: Quantum memories**

  The optical Bloch equations are used to study the existing quantum memory protocols e.g. EIT based memories, controlled reversible inhomogeneous broadening (CRIB) and the atomic frequency comb (AFC).

- **Chapter 4: Intra atomic frequency comb (I-AFC)**

  We propose a frequency comb using the hyper-fine levels of a single atom. We then

show that this I-AFC works similar to a AFC type quantum memory.

- **Chapter 5: Randomness in I-AFC**

  The role of non-uniformities on I-AFC based memory is studied in the chapter. The non-uniformities are introduced in absorption and the comb spacing and we show that even an imperfect I-AFC results in an efficient quantum memory. As examples, we numerically show the frequency comb in the Cesium (Cs) and Rubidium (Rb) atoms.

Part-II

- **Chapter 6: Atom-cavity interactions**

  The basics of atom-cavity interactions are introduced in the chapter. We also study phenomenons such as photon blockade and cavity-STIRAP.

- **Chapter 7: Atom-photon gates**

  The gate operations between atoms and photons are studied. We then use these atom-photon gates to generate Cat-states, swap operation between atom and a photon and non-destructive GHZ state analyser.

- **Chapter 8: Applications of atom-photon gates**

  Atom-photon gates are used to propose an implementation scheme for the quantum channel transparency (QCT). We also propose a state preparation scheme using swap operation and coherent feedback control.

- **Chapter 9: Conclusion**

  In this chapter we summarize the results of the thesis.

Chapter 2

Light-matter interactions

Quantum optics in its broad sense is the study of light-matter interactions. The matter can be any quantum mechanical system with discrete energy levels e.g. atoms, quantum dots and superconducting qubits.

A general light-matter interaction can be visualized as follows: when light interacts with atoms it causes transitions which in turn results in an atomic dipole moment (i.e. atomic polarization). This change in dipole moment gives raise to source terms in maxwell equations and thus can affect the propagation of light in the medium. Quantum memories and slow light are few examples where propagation and atomic polarization are mutually affected.

The complete dynamics of atom-light interactions are given by the atomic polarization and light propagation. The dynamics of light propagation can be ignored when we are interested only in absorption or transmission spectrum of the atom, typical examples are STIRAP (stimulated Raman adiabatic passage), EIT (electromagnetically induced transparency), CPT (coherent population trapping), optical Free Induction Decay (FID) [34] and superradiance [35].

To understand the physics of atom-light interactions. We start with a simple and basic interaction in quantum optics, a two-level system interacting with the electric field. Then the three and multi-level systems interacting with light can be seen as extension of these techniques.

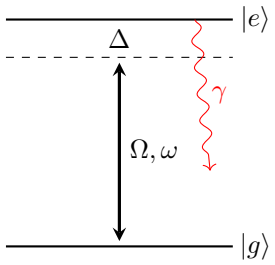

FIGURE 2.1: Two-level atom with transition frequency ω_{eg}, interacting with a light of frequency ω and detuning Δ from the atomic transition. γ is the spontaneous decay rate from $|e\rangle$ to $|g\rangle$

2.1 Two-level atom interacting with light

The Hamiltonian for a two-level atom with excited ($|e\rangle$) and ground ($|g\rangle$) states separated by frequency of ($\omega_{eg} = \omega_e - \omega_g$) can be written as $H_0 = \hbar\omega_{eg} |e\rangle\langle e|$. The interaction of a dipole with the electric field is given as $H_{\text{int}} = -\mathbf{d} \cdot \mathbf{E}$, where $\mathbf{d} = e\mathbf{r}$ is the dipole moment operator of the atom and $\mathbf{E}$ is the classical electric field. For simplicity we consider an electric pulse with narrow spectral width propagating in z direction and polarized along $\hat{x}$

$$\mathbf{E}(t) = \mathcal{E}(t)\cos(kz - \omega t + \phi)\hat{x} \rightleftharpoons \frac{1}{2}\Big(\mathcal{E}(t)e^{-i(kz-\omega_0 t)}e^{-i\phi} + c.c\Big)\hat{x}, \tag{2.1}$$

where $k = 2\pi/\lambda$ and ω_0 is the mean frequency of the light. The ϕ is phase at $t = z = 0$. The amplitude $\mathcal{E}(t)$ gives the shape of the pulse in time and for a typical quasi monochromatic pulse this is centred around ω_0 with a narrow spread. The Hamiltonian in the basis $\{|e\rangle, |g\rangle\}$ is given as [36]

$$H = \hbar\omega_{eg} |e\rangle\langle e| - \mathcal{E}(t)[d_{eg}e^{-i\omega_0 t}e^{i\phi} |e\rangle\langle g| + d_{ge}e^{i\omega_0 t}e^{-i\phi} |g\rangle\langle e| + h.c]. \tag{2.2}$$

where $d_{eg} = \langle e|\hat{x}|g\rangle$ is the dipole matrix element. The terms e^{ikz} are dropped under the called dipole approximation. In a typical system dipole approximation ($kz \equiv 2\pi z/\lambda \ll 1$) is well justified, as the interacting fields are in the visible region ($\lambda = 10^{-7}$m) and $z \sim 10^{-10}$m is the typical size of an atom.

The Hamiltonian Eq. (2.2) in the interaction picture is given as

$$H_I \equiv e^{\frac{iH_0 t}{\hbar}} H e^{-\frac{iH_0 t}{\hbar}} \equiv -\Big[\Omega e^{it\Delta} |e\rangle\langle g| e^{i\phi} + \Omega e^{i(\omega_{eg}+\omega_0)t} |e\rangle\langle g| e^{-i\phi} + h.c.\Big], \tag{2.3}$$

where $\Delta = \omega_{eg} - \omega_0$ is the detuning and $\Omega = \frac{d_{eg} \cdot \mathcal{E}}{\hbar}$ is the Rabi frequency. Typically we work with optical transitions and $\Delta \ll \omega_{eg}, \omega_0$. The dynamics of the system evolve with a time scale of Ω^{-1}. Since $\omega_0 + \omega_{eg} \gg \Omega$ the fast rotating terms $\exp[\pm i(\omega_0 + \omega_{eg})t]$ in the Eq. (2.3) will be averaged out and are dropped under the rotating wave approximation (RWA). Then the Hamiltonian reads

$$H_I = -\Big[\Omega e^{i\Delta t} e^{i\phi} \left|e\right\rangle\!\left\langle g\right| + h.c.\Big], \tag{2.4}$$

and with another transformation of the form $e^{-i\Delta t|e\rangle\langle e|}(\hbar\Delta \left|e\right\rangle\!\left\langle e\right| + H_I)e^{i\Delta t|e\rangle\langle e|}$ gives

$$H = \hbar\Delta \left|e\right\rangle\!\left\langle e\right| - \frac{\hbar}{2}\Omega(\left|e\right\rangle\!\left\langle g\right| e^{i\phi} + \left|g\right\rangle\!\left\langle e\right| e^{-i\phi}), \tag{2.5}$$

where we assume the Rabi frequency (Ω) to be real. The two-level Hamiltonian with $\phi = 0$ can be written as

$$H = \begin{pmatrix} \Delta & -\Omega/2 \\ -\Omega/2 & 0 \end{pmatrix}. \tag{2.6}$$

The eigenvalues and vectors are obtained to be

$$E_\pm = \frac{\Delta}{2} \pm \frac{\Omega}{2}\sqrt{\left(\frac{\Delta}{\Omega}\right)^2 + 1}, \qquad \left|\pm\right\rangle = \frac{1}{\sqrt{\left|2E_\pm\right|^2 + \left|\Omega\right|^2}}(2E_\pm \left|e\right\rangle + \Omega \left|g\right\rangle). \tag{2.7}$$

Thus when the interaction strength is very high $\Omega \gg \Delta$ we get $E_\pm = \pm\frac{\Omega}{2}$ with $\left|\pm\right\rangle = \left|e\right\rangle \pm \left|g\right\rangle$ as the corresponding eigenvectors. This shifting of two-level system under strong field interaction is called Autler-Townes effect. This effect can be observed by probing the system with another weak light. Also the eigenstates $\left|\pm\right\rangle$ are called dressed states and the states $\left|e\right\rangle$ and $\left|g\right\rangle$ are called bare states.

To obtain the evolution of the two-level system, we start with $\left|\psi\right\rangle$ of the form $\left|\psi(t)\right\rangle = c_g(t)\left|g\right\rangle + c_e(t)\left|e\right\rangle$. The Schrödinger equation $i\hbar\frac{\partial\left|\psi\right\rangle}{\partial t} = H\left|\psi\right\rangle$ with Eq. (2.5) gives

$$\begin{aligned} \dot{c}_g &= \frac{i}{2}\Omega(t)e^{-i\phi}c_e, \\ \dot{c}_e &= -i\Delta c_e + \frac{i}{2}\Omega(t)e^{i\phi}c_g, \end{aligned} \tag{2.8}$$

The general solution of Eq. (2.8) is not possible but when $\Omega(t)$ is time independent the solution for Eq. (2.8) reads

$$\begin{aligned} c_g(t) &= \frac{1}{2\Omega'}\, e^{-\frac{1}{2}i(\Delta+\Omega')t} e^{-i\phi} \left[\beta\Omega(e^{i\Omega' t}-1) + \alpha e^{i\phi}\Big\{(\Omega'-\Delta) + e^{i\Omega' t}(\Omega'+\Delta)\Big\}\right], \\ c_e(t) &= \frac{1}{2\Omega'}\, e^{-\frac{1}{2}i(\Delta+\Omega')t} \left[\alpha\Omega e^{i\phi}(e^{i\Omega' t}-1) + \beta\Big\{(\Omega'+\Delta) + e^{i\Omega' t}(\Omega'-\Delta)\Big\}\right], \end{aligned} \tag{2.9}$$

with $\Omega' = \sqrt{\Omega^2+\Delta^2}$.

Also with the resonance condition, i.e $\Delta = 0$ the Eq. (2.8) can be analytically solved. Making the transformation $\partial\tau = \Omega(t)\partial t \rightarrow \tau = \int_0^t \Omega(t')\partial t'$ gives

$$\frac{\partial^2}{\partial\tau^2} c_g + (1/4) c_g = 0 \tag{2.10}$$

where τ is called the area of the pulse. Also note that this simplification is not possible with off-resonance or decay terms. The Eq. (2.10) with in the initial condition $|\psi(0)\rangle = \alpha\,|g\rangle + \beta\,|e\rangle$ gives

$$\begin{aligned} c_g(\tau) &= \alpha\cos\left(\frac{\tau}{2}\right) + ie^{-i\phi}\beta\sin\left(\frac{\tau}{2}\right), \\ c_e(\tau) &= ie^{i\phi}\alpha\sin\left(\frac{\tau}{2}\right) + \beta\cos\left(\frac{\tau}{2}\right), \end{aligned} \tag{2.11}$$

2.1.1 π-pulses and superposition states

In light-matter interactions e.g. in quantum memory protocols, an excitation has to be transferred to a stable state with long lifetimes. This transfer is typically achieved using a π-pulse. Also while performing quantum computation it is important to prepare superposition state of the atom and perform a general unitary rotations on the atom both these operations can be performed by varying the area of the pulse.

Starting the atom in the ground state ($\beta = 0, \alpha = 1$) or the excited state ($\beta = 1, \alpha = 0$) gives the general state as

$$|\psi\rangle_{(\alpha=1)} = \cos\frac{\tau}{2}\,|g\rangle + ie^{i\phi}\sin\frac{\tau}{2}\,|e\rangle\,, \tag{2.12}$$

$$|\psi\rangle_{(\beta=1)} = ie^{-i\phi}\sin\frac{\tau}{2}\,|g\rangle + \cos\frac{\tau}{2}\,|e\rangle\,, \tag{2.13}$$

when $\tau \equiv \int_0^t \Omega(t')\partial t' = \pi$, the state transfers from $|g\rangle \rightleftharpoons |e\rangle$ and the pulses with area of

$\tau = \pi$ are called π-pulses. Also by varying the area of pulse (τ) and the phase of electric field (ϕ) in Eq. (2.13) a general superposition state of the atom can be obtained, starting with the ground state.

2.2 Two-level atom interacting with a thermal bath

In the above sections we considered an ideal system and avoided interactions with environment. Dissipation and decoherence results when a system is interacting with environment. The general Hamiltonian of a system interacting with bath is written as

$$H = H_S + H_B + H_{\text{int}}, \tag{2.14}$$

where H_S and H_B are the system and the bath Hamiltonian and H_{int} is the system and bath interaction. The total evolution of system and bath (environment) in the interaction picture is given by

$$\frac{\partial}{\partial t}\rho(t) = -i[H_I, \rho] \rightarrow \rho(t) = \rho(0) - i\int_0^t [H_I, \rho(s)]\, ds, \tag{2.15}$$

where $\rho(t)$ is the density matrix of system and bath, $\rho(0)$ is the initial state. The system dynamics are obtained by tracing over the bath, denoted as tr_B . On substituting the integral form of Eq. (2.15) back in the differential form gives

$$\frac{\partial}{\partial t}\rho_S = tr_B[H_I, \rho_s(0) \otimes \rho_B(0)] - \int_0^t tr_B[H_I, [H_I, \rho(s)]]\, ds \tag{2.16}$$

since we are interested in the thermal bath, the expectation values of all bath operators vanish i.e. $\langle O_B \rangle = 0$ and the first term is set to zero. We invoke Born approximation by assuming the interaction is very weak and assume that the state of bath remains unchanged. Further we assume $\rho(t)$ shows deviations of order H_I from an uncorrelated state [37]

$$\rho(t) \approx \rho_S(t) \otimes \rho_B + \mathcal{O}(H_I), \tag{2.17}$$

On substituting Eq. (2.17) in Eq. (2.16) and retaining upto second order in H yields

$$\frac{\partial}{\partial t}\rho_S = tr_B[H_I, \rho_s(0) \otimes \rho_B(0)] - \int_0^t tr_B[H_I, [H_I, \rho_S(s) \otimes \rho_B]]\, ds, \tag{2.18}$$

and we can notice that $\rho_S(t)$ depends on the past time $0 \to t$. Since a bath decays quickly compared to the system, the dependency on the past times is quickly lost and we replace $\rho_S(s) \to \rho_S(t)$ to give the Redfield equation

$$\frac{\partial}{\partial t}\rho_S = -\int_0^t tr_B[H_I, [H_I(s), \rho_S(t) \otimes \rho_B]]\, ds. \tag{2.19}$$

On replacing $s = t - s'$ gives

$$\frac{\partial}{\partial t}\rho_S = -\int_0^t tr_B\big[H_I, \big[H_I(t-s'), \rho_S(t) \otimes \rho_B\big]\big]\, ds'. \tag{2.20}$$

and since a system evolves with time scales that are much larger than the bath time scales. We extend the upper limit to infinity under the Markov approximation

$$\frac{\partial}{\partial t}\rho_S = -\int_0^\infty tr_B[H_I, [H_I(t-s), \rho_S(t) \otimes \rho_B]]\, ds, \tag{2.21}$$

Eq. (2.21) is general and valid for any system and bath.

On solving Eq. (2.21) for a two-level system interacting (dipole interaction) with thermal bath at temperature T gives (detailed derivation can be found in [38]) the master equation as

$$\begin{aligned}\frac{\mathrm{d}}{\mathrm{d}t}\rho(t) = \gamma(N+1)\left[\sigma_-\rho(t)\sigma_+ - \frac{1}{2}\sigma_+\sigma_-\rho(t) - \frac{1}{2}\rho(t)\sigma_+\sigma_-\right] \\ +\gamma N\left[\sigma_+\rho(t)\sigma_- - \frac{1}{2}\sigma_-\sigma_+\rho(t) - \frac{1}{2}\rho(t)\sigma_-\sigma_+\right],\end{aligned} \tag{2.22}$$

where $\sigma_+ = |e\rangle\langle g|$, $\sigma_- = |g\rangle\langle e|$ and the decay rate $\gamma = \frac{\omega_{eg}^3 |d_{eg}|^2}{3\pi\epsilon_0\hbar c^3}$[1]. $N = \left[\exp\left\{\frac{\hbar\omega_{eg}}{K_B T}\right\} - 1\right]^{-1}$ the average thermal photon number, where K_B is the Boltzmann constant. Since we typically deal with atomic transitions in the optical transitions or systems at low temperatures the condition $\hbar\omega_{eg} \gg K_B T$ gives $N \to 0$. Then the decay is

[1] The decay rates are written in SI units

simply governed by

$$\frac{\mathrm{d}}{\mathrm{d}t}\rho(t) = \gamma\left[\sigma_-\rho(t)\sigma_+ - \frac{1}{2}\sigma_+\sigma_-\rho(t) - \frac{1}{2}\rho(t)\sigma_+\sigma_-\right]. \tag{2.23}$$

For example the decay of a two-level system on using Eq. (2.23) reads

$$\frac{\mathrm{d}}{\mathrm{d}t}\langle e|\rho|e\rangle \equiv \frac{\mathrm{d}}{\mathrm{d}t}\rho_{ee} = -\gamma\rho_{ee}, \tag{2.24a}$$

$$\frac{\mathrm{d}}{\mathrm{d}t}\langle e|\rho|g\rangle \equiv \frac{\mathrm{d}}{\mathrm{d}t}\rho_{eg} = -\frac{\gamma}{2}\rho_{eg}. \tag{2.24b}$$

Note that the coherence (ρ_{eg}) decays with half the rate of population (ρ_{ee}) and often these decays are added phenomenologically. The the off-diagonal elements of a density matrix can be related to the physical quantity, atomic polarization. Atomic polarization is written as the expectation value of dipole operator

$$\langle \mathbf{P}\rangle = \mathrm{Tr}(\rho\hat{d}), \tag{2.25}$$

where $\hat{d}$ is the dipole operator and for a two-level atom in the interaction picture gives

$$\begin{aligned}\mathrm{Tr}(\rho\hat{d}) &= \mathrm{Tr}\Big[\rho\Big(d_{eg}e^{iH_0t/\hbar}\,|e\rangle\langle g|\,e^{-iH_0t/\hbar} + h.c\Big)\Big],\\ &= \mathrm{Tr}\big[\rho\big(d_{eg}\,|e\rangle\langle g|\,e^{i\omega t} + h.c\big)\big],\\ &= \rho_{ge}d_{eg}e^{i\omega t} + c.c,\end{aligned} \tag{2.26}$$

where $H_0 = \hbar\omega\,|e\rangle\langle e|$ and $d_{ee} = d_{gg} = 0$. On comparing Eq. (2.26) with wave equation of the form

$$\mathbf{P} = 1/2\big(\mathcal{P}(z,t)e^{-i\omega t} + c.c\big), \tag{2.27}$$

gives $\mathcal{P}(z,t) = 2d^*_{eg}\rho_{eg}$.

2.3 Paraxial wave equation in a medium

In the above sections we have discussed two-level atom interacting with constant external electric fields. To study the light propagation through an ensemble of atoms we start by

writing Maxwell equations with source terms

$$\begin{aligned} \boldsymbol{\nabla}\cdot(\epsilon_0\mathbf{E}+\mathbf{P})=0, \qquad & \boldsymbol{\nabla}\times\mathbf{E}=-\frac{\partial\mathbf{B}}{\partial t}, \\ \boldsymbol{\nabla}\cdot\mathbf{B}=0, \qquad & \boldsymbol{\nabla}\times\mathbf{B}=\mu_0\frac{\partial}{\partial t}(\epsilon_0\mathbf{E}+\mathbf{P}), \end{aligned} \tag{2.28}$$

where $\mathbf{P}$ is the atomic polarization. On rearranging Eqs. (2.28) gives [39]

$$\nabla^2\mathbf{E}-\frac{1}{c^2}\frac{\partial^2\mathbf{E}}{\partial t^2}=\mu_0\frac{\partial^2\mathbf{P}}{\partial t^2}. \tag{2.29}$$

We are interested in optical pulses with narrow spectral widths, hence we assume solutions of the form

$$\begin{aligned} \mathbf{E}(\mathbf{r},t)&=\mathrm{Re}\left[\mathcal{E}(\mathbf{r},t)e^{i(\mathbf{k}.\mathbf{r}\pm\omega_0 t)}\right]\hat{e}, \\ \mathbf{P}(\mathbf{r},t)&=\mathrm{Re}\left[\mathcal{P}(\mathbf{r},t)e^{i(\mathbf{k}.\mathbf{r}\pm\omega_0 t)}\right]\hat{e}, \end{aligned} \tag{2.30}$$

where $\mathbf{k}.\mathbf{r}+\omega_0 t$ denotes the forward and the $\mathbf{k}.\mathbf{r}-\omega_0 t$ backward moving waves. ω_0 is mean oscillating frequency and $\mathcal{E}(\mathbf{r},t)$ gives the shape of the envelope. Since we only study isotopic and homogenous mediums, the atomic polarization is assumed to be in the same direction as the electric field and the polarization index ($\hat{e}$) is dropped in further calculations.

On substituting the forward mode solutions Eq. (2.30) in the wave equation gives

$$\nabla^2\mathcal{E}+2i\,\mathbf{k}\cdot\boldsymbol{\nabla}\mathcal{E}+2i\,\frac{\omega_0}{c^2}\frac{\partial\mathcal{E}}{\partial t}-\frac{1}{c^2}\frac{\partial^2\mathcal{E}}{\partial t^2}=-2i\mu_0\omega_0\frac{\partial\mathcal{P}}{\partial t}+\mu_0\frac{\partial^2\mathcal{P}}{\partial t^2}-\omega_0^2\mu_0\mathcal{P}. \tag{2.31}$$

Now we assume the amplitudes to vary slowly in space and time, i.e.

$$\left|\nabla^2\mathcal{E}\right|\ll\left|\mathbf{k}\cdot\boldsymbol{\nabla}\mathcal{E}\right| \qquad\qquad \left|\frac{\partial^2\mathcal{E}}{\partial t^2}\right|\ll\left|\omega_0\frac{\partial\mathcal{E}}{\partial t}\right|\ll\left|\omega_0^2\mathcal{E}\right|. \tag{2.32}$$

The condition $\left|\nabla^2\mathcal{E}\right|\ll\left|\mathbf{k}\cdot\boldsymbol{\nabla}\mathcal{E}\right|$ can be justified by assuming waves which point in a specific direction with negligible spread in the transverse plane. The other condition is well interpreted in the frequency domain. In the frequency domain it gives $|\omega-\omega_0|\ll\omega_0$, i.e. the spectral width is much less than the central frequency. Hence the time condition is well justified for a narrow band optical pulse.

On dropping the higher order terms in Eq. (2.31) and the approximations in Eq. (2.32) yields

$$2i\,\mathbf{k}.\boldsymbol{\nabla}\mathcal{E} + 2i\,\frac{\omega}{c^2}\frac{\partial\mathcal{E}}{\partial t} = -\omega^2\mu_0\mathcal{P}, \tag{2.33}$$

and for one dimension it's simplified as

$$\left(\frac{\partial}{\partial z} + \frac{1}{c}\frac{\partial}{\partial t}\right)\mathcal{E}(z,t) = i\frac{k}{2\epsilon_0}\mathcal{P}(z,t). \tag{2.34}$$

Note that in Eq. (2.30) we considered only the forward mode ($\mathbf{k}.\mathbf{r} - \omega t$) waves. A similar analysis in the backward mode ($\mathbf{k}.\mathbf{r} + \omega t$) gives

$$\left(\frac{\partial}{\partial z} - \frac{1}{c}\frac{\partial}{\partial t}\right)\mathcal{E}(z,t) = i\frac{k}{2\epsilon_0}\mathcal{P}(z,t). \tag{2.35}$$

In a linear isotropic medium one can assume $\mathcal{P} = \epsilon_0\chi\mathcal{E}$ with χ being the electric susceptibility. Also the atomic polarization in terms of density matrix is given by the Eq. (2.27), $\mathcal{P} = 2\mathcal{N}d^*_{eg}\rho_{eg}$. Then the susceptibility is written as

$$\chi = \frac{\mathcal{N}|d_{eg}|^2}{\hbar\Omega\epsilon_0}\rho_{eg}, \tag{2.36}$$

where $\Omega = \dfrac{d_{eg}.\mathcal{E}}{2\hbar}$ is the Rabi frequency. It is clear from the Eq. (2.34-2.36) that dynamics of the system and field are coupled. The susceptibility consists of Rabi frequency and the density matrix elements and in the following chapters this relation is exploited in realizing quantum memories.

The light propagation is given by the Eq. (2.34) and Eq. (2.35). The dynamics of ρ_{eg} can be obtained by solving

$$\frac{\mathrm{d}}{\mathrm{d}t}\rho = -i\hbar[H,\rho] + \mathcal{D}(\rho), \tag{2.37}$$

with $\mathcal{D}(\rho)$ being the dissipator (2.23). Eq's. (2.34)-(2.37) are known as the Maxwell-Bloch equations and most light-matter interaction protocol consists in modelling the Hamiltonian and solving these coupled equations.

2.4 Three-level atom interacting with light

In two-level atoms the light matter interaction results in Rabi oscillations between the ground and the excited states. Adding a third level to the two-level atom gives raise to the interference of probability amplitudes. This interference along with rabi oscillations leads to quantum phenomenon such as EIT, CPT and STIRAP. These phenomena are further extended to realize atom-photon gates and quantum memories protocols.

The procedure for three-level systems is similar to two-level systems. In the following we show the details for a three-level system with lambda configuration. A 'Λ' system Fig. (2.2) consists of an excited and a ground state typically in the optical range and a spin state with long coherence time. The $|e\rangle \leftrightarrow |g\rangle$ transition interacts with a weak probe pulse (Ω_1) and the $|e\rangle \leftrightarrow |s\rangle$ with a strong control field (Ω_2). The transition $|g\rangle \leftrightarrow |s\rangle$ is assumed to be dipole forbidden. The off-resonance between atom and light is denoted by the detunings $\Delta_{1,2}$.

We usually deal with hyperfine transitions of an atom which are denoted by F and m_F. Upon interacting with the light the m_F values of an atom changes, resulting in the change of angular momentum. And only those interactions that conserve the total angular momentum are retained in the Hamiltonian. For example let's assign $m_F = 0$ (1) for the states $|g\rangle$ ($|e\rangle$). Since the transition $|g\rangle \rightarrow |e\rangle$ results in increasing the angular momentum, by the conservation of total angular momentum only a light carrying $1\hbar$ of angular momentum (left circularly polarized) can interact with this transition. Similarly $|g\rangle \leftarrow |e\rangle$ will only emit light with $1\hbar$ unit of angular momentum. Interestingly choosing the right and left circular polarization as the basis vectors makes the dipole matrix elements $\langle\psi_1|\mathbf{d}|\psi_2\rangle$ real [40].

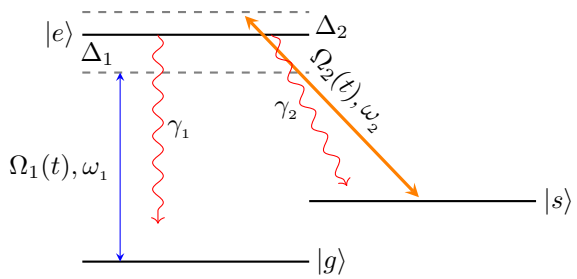

FIGURE 2.2: Three-level Λ system interacting with weak probe light of frequency ω_1 and a strong control field of frequency ω_2.

The Rabi frequencies (Ω) and detunings (Δ) are defined as

$$\begin{aligned} \Omega_1 &= \frac{\mathbf{d}_{eg}\cdot\mathcal{E}_1(z,t)}{2\hbar}, \qquad \Delta_1 = \omega_{eg}-\omega_1, \\ \Omega_2 &= \frac{\mathbf{d}_{es}\cdot\mathcal{E}_2(z,t)}{2\hbar}, \qquad \Delta_2 = \omega_{es}-\omega_2, \end{aligned} \tag{2.38}$$

and following the same prescription as in Sec. (2.1). The Hamiltonian in the rotating wave approximation is written as

$$H = \hbar\omega_{eg}\,|e\rangle\langle e| + \hbar\omega_{sg}\,|s\rangle\langle s| - \hbar\big(\Omega_1\,e^{-i\omega_1 t}\,|e\rangle\langle g| + \Omega_2\,e^{-i\omega_2 t}\,|e\rangle\langle s| + h.c\big). \tag{2.39}$$

Note that the cross terms $\Omega_1\,|e\rangle\langle s|$ and $\Omega_2\,|e\rangle\langle g|$ are dropped, as the transitions $|e\rangle$-$|s\rangle$ and $|e\rangle$-$|g\rangle$ are assumed to satisfy opposite selection rules i.e. $\mathbf{d}_{es}\cdot\mathcal{E}_1(z,t) = \mathbf{d}_{eg}\cdot\mathcal{E}_2(z,t) = 0$. Defining $H_0 = \hbar\omega_1\,|e\rangle\langle e| + \hbar(\omega_1-\omega_2)\,|s\rangle\langle s|$ the Hamiltonian in the interaction picture reads

$$H = \hbar\Delta_1\sigma_{ee} + \hbar(\Delta_1-\Delta_2)\sigma_{ss} - \hbar[\Omega_1(t)\sigma_{eg} + \Omega_2(t)\,\sigma_{es} + h.c], \tag{2.40}$$

where $\sigma_{ij} = |i\rangle\langle j|$. This Hamiltonian describes the dipole interaction of a three-level atom with light. In the following sections we use this to study the quantum phenomenon called EIT and a protocol named STIRAP.

2.4.1 Stimulated Raman adiabatic passage

The Stimulated Raman adiabatic passage (STIRAP) is a technique to coherently control the state of a two-level atom using an excited state. The Hamiltonian for Λ-system can be simplified under the two-photon resonance condition ($\Delta_1 = \Delta_2$) to give

$$H = \hbar\begin{bmatrix} 0 & 0 & -\Omega_1^*(t) \\ 0 & 0 & -\Omega_2^*(t) \\ -\Omega_1(t) & -\Omega_2(t) & \Delta \end{bmatrix}, \tag{2.41}$$

The eigenvalues are given as

$$\omega^0 = 0, \qquad \omega^{\pm} = \frac{1}{2}\left[\Delta \pm \sqrt{\Delta^2 + 4\Big(|\Omega_2|^2 + |\Omega_1|^2\Big)}\right], \tag{2.42}$$

and the corresponding eigenvectors are

$$|D\rangle = \cos\theta(t)\,|g\rangle - \sin\theta(t)\,|s\rangle\,, \tag{2.43a}$$

$$|+\rangle = \sin\theta(t)\sin\phi\,|g\rangle + \cos\theta(t)\sin\phi\,|s\rangle + \cos\phi\,|e\rangle\,, \tag{2.43b}$$

$$|-\rangle = \sin\theta(t)\cos\phi\,|g\rangle + \cos\theta(t)\cos\phi\,|s\rangle - \sin\phi\,|e\rangle\,, \tag{2.43c}$$

here $\tan\theta(t) = \dfrac{\Omega_1}{\Omega_2}$ and $\tan\phi = \sqrt{\left|\dfrac{\omega^-}{\omega^+}\right|}$. The state $|D\rangle$ is the called dark state and is immune to spontaneous decay as there is no contribution from the excited state. Thus by adiabatically changing the dark state any superposition state between $|g\rangle$ and $|s\rangle$ can be achieved. The adiabaticity condition is obtained as (see Sec. A.1)[41]

$$\left|\langle \pm|\dot{H}|D\rangle\right| \ll \Omega|\omega^{\pm} - \omega^{0}|, \qquad \Rightarrow \qquad \left|\frac{\Omega_1\dot{\Omega}_2 - \Omega_2\dot{\Omega}_1}{\Omega^2}\right| \ll |\omega^{\pm}|, \tag{2.44}$$

where $\Omega = \sqrt{\Omega_1^2 + \Omega_2^2}$.

STIRAP and Eq. (2.13) are prominently used to perform unitary rotations on a qubit with high fidelities. The pulse envelopes can be of any shape as long as $\partial\Omega_{(1,2)}/\partial t$ are slow enough to satisfy the Eq. (2.44). Typical STIRAP lasts for ~ 1 μs and high fidelities can only be obtained for long pulse durations. To improve time durations without compromising fidelities, a shortcut to STIRAP known as stimulated Raman shortcut-to-adiabatic passage (STIRSAP) are proposed [42, 43]. In STIRSAP the time required is reduced to 10 ns as compared to ~ 1 μs.

2.4.2 Adiabatic elimination of a three-level atom

Adiabatic elimination is similar to STIRAP, where a dipole forbidden transition $|g\rangle \leftrightarrow |s\rangle$ can be accessed via a third common level. Since $|g\rangle$ and $|s\rangle$ are stable states such a qubit will be coherent and immune to spontaneous emission. The general state for a three-level system is written as

$$|\psi\rangle = c_g(t)\,|g\rangle + c_s(t)\,|s\rangle + c_e(t)\,|e\rangle\,, \tag{2.45}$$

The Schrödinger equation with the Eq. (2.41) gives

$$i\dot{c}_e = \Delta c_e - (\Omega_1 c_g + \Omega_2 c_s), \qquad i\dot{c}_g = \Omega_1^* c_e, \qquad i\dot{c}_s = \Omega_2^* c_e. \tag{2.46}$$

If the detuning is greater than Rabi frequencies and decay rates ($\Delta \gg \Omega_{1,2}$) then it is reasonable to assume that excitation's are very less and we set $\dot{c}_e = 0$. Then c_e is eliminated to obtain

$$i\dot{c}_g = -1/\Delta(|\Omega_1|^2 c_g + \Omega_1^*\Omega_2 c_s), \qquad i\dot{c}_s = -1/\Delta(\Omega_1\Omega_2^* c_g + |\Omega_2|^2 c_s). \tag{2.47}$$

On comparing these equations with two-level atom equations (2.8), gives an equivalent two-dimensional Hamiltonian of the form

$$H_{ae} = -\frac{\hbar}{\Delta}\begin{bmatrix} |\Omega_1|^2 & \Omega_1^*\Omega_2 \\ \Omega_1\Omega_2^* & |\Omega_2|^2 \end{bmatrix}. \tag{2.48}$$

The eigenvalues and vectors are given as

$$E_{_D} = 0, \qquad |D\rangle = \cos\theta\,|g\rangle - \sin\theta\,|s\rangle\,, \tag{2.49a}$$

$$E_{_B} = -\frac{|\Omega_1|^2 + |\Omega_2|^2}{\Delta}, \qquad |B\rangle = \sin\theta\,|g\rangle + \cos\theta\,|s\rangle\,, \tag{2.49b}$$

with $\tan\theta = \dfrac{\Omega_1}{\Omega_2}$. $|D\rangle$ and $|B\rangle$ are called dark and bright states[2].

Thus when the detuning is large adiabatic elimination results in an effective two-level system even when the transition is dipole forbidden. Although it seems that a decay free qubit can be created with adiabatic elimination, losses are always present due to the imperfect adiabaticity.

2.4.3 Electromagnetically induced transparency (EIT)

In the above sections we only studied the Hamiltonian of a three-level system. Here we will solve density matrix evolution of three-level system under a strong control pulse and a weak probe light. The spontaneous emission in a Λ-system is included similar to that of

[2]The transitions under two-photon resonance are called Raman-transitions and with large detunings they are known as off-resonant Raman transitions.

a two-level system. The dissipator for the two transitions is given by Eq. (2.23)

$$\frac{\mathrm{d}\rho}{\mathrm{d}t} = \gamma_1\left[\hat{\sigma}_{gg}\rho_{ee}(t) - \frac{1}{2}\hat{\sigma}_{ee}\rho(t) - \frac{1}{2}\rho(t)\hat{\sigma}_{ee}\right] + \gamma_2\left[\hat{\sigma}_{ss}\rho_{ee}(t) - \frac{1}{2}\hat{\sigma}_{ee}\rho(t) - \frac{1}{2}\rho(t)\hat{\sigma}_{ee}\right] \quad (2.50)$$

where $\gamma_1 = \frac{\omega_{eg}^3|d_{eg}|^2}{3\pi\epsilon_0\hbar c^3}$ and $\gamma_2 = \frac{\omega_{es}^3|d_{es}|^2}{3\pi\epsilon_0\hbar c^3}$. The complete density matrix equations for the Λ-type atom with the Hamiltonian Eq. (2.40) and Eq. (2.50) reads [36]

$$\begin{aligned}
\dot{\rho}_{ee} &= -(\gamma_1+\gamma_2)\rho_{ee} + i\Omega_1\rho_{ge} - i\Omega_1^*\rho_{eg} + i\Omega_2\rho_{se} - i\Omega_2^*\rho_{es},\\
\dot{\rho}_{ss} &= \gamma_2\rho_{ee} + i\Omega_2^*\rho_{es} - i\Omega_2\rho_{se},\\
\dot{\rho}_{gs} &= i(\Delta_2-\Delta_1)\rho_{gs} + i\Omega_1^*\rho_{es} - i\Omega_2\rho_{ge},\\
\dot{\rho}_{se} &= -\left[\frac{1}{2}(\gamma_1+\gamma_2) - i\Delta_2\right]\rho_{se} - i\Omega_1^*\rho_{sg} - i\Omega_2^*(\rho_{ss}-\rho_{ee}),\\
\dot{\rho}_{ge} &= -\left[\frac{1}{2}(\gamma_1+\gamma_2) - i\Delta_1\right]\rho_{ge} - i\Omega_2^*\rho_{gs} - i\Omega_1^*(1-2\rho_{ee}-\rho_{ss}),
\end{aligned} \quad (2.51)$$

where ρ_{gg} is eliminated using the trace condition. Now the weak probe ($\Omega_1 \ll \Omega_2$) light allows us to perform two approximations (i) We retain density matrix terms only to the first order in Ω_1. (ii) $\rho_{gg} \approx 1$, i.e. due to low intensity of the probe, atoms are assumed to be in the ground state. With these two approximations and a resonant control field ($\Delta_2 = 0$), Eqs. (2.51) are written as

$$\dot{\rho}_{gs} = -i\Delta_1\rho_{gs} - i\Omega_2\rho_{ge}, \quad (2.52a)$$

$$\dot{\rho}_{ge} = -(\gamma_1 - i\Delta_1)\rho_{ge} - i\Omega_2^*\rho_{gs} - i\Omega_1^*, \quad (2.52b)$$

where $\gamma_{12} = (\gamma_1+\gamma_2)/2$. The steady state solution of ρ_{eg}, obtained by setting $\dot{\rho} = 0$ yields the expression for susceptibility

$$\chi \equiv \frac{\mathcal{N}|d_{eg}|^2}{\epsilon_0\hbar}\rho_{eg} = \frac{\mathcal{N}|d_{eg}|^2}{\epsilon_0\hbar}\frac{i}{(\gamma_1 + i\Delta_1) - i\frac{|\Omega_2|^2}{\Delta_1}}, \quad (2.53)$$

the imaginary part of χ gives the absorption of the medium and the refractive index given by the slope of the real part of χ. From Fig. 2.3 we can see a dip in the absorption around resonance. This reduction in the absorption of the probe light due to a strong control pulse is know as electromagnetically induced transparency (EIT) [44]. Complete transparency occurs at zero detuning and the width of transparency window increases with increase in the control pulse strength. In Fig. 2.3 we can notice two regimes weak limit

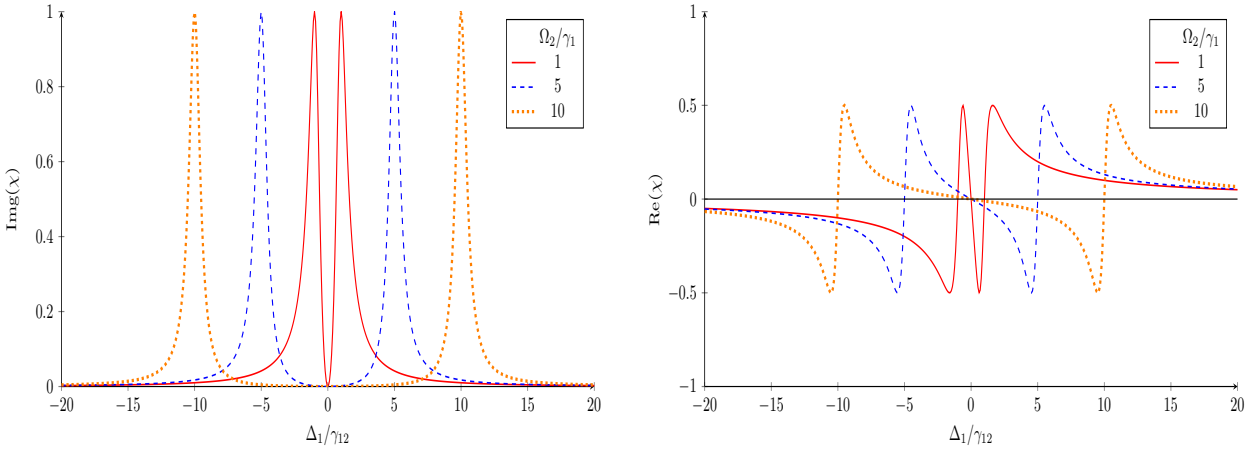

FIGURE 2.3: (a) Imaginary and (b) real parts of χ in the units $\frac{\mathcal{N}|d_{eg}|^2}{\epsilon_0\hbar\gamma_1}$ for different control field strengths (Ω_2/γ_1)

($\Omega_2 \approx \gamma$) and the strong limit ($\Omega_2 \gg \gamma$). In the weak limit, the transparency is due to quantum interference of amplitudes. The transition amplitudes between $|g\rangle$-$|e\rangle$ and $|e\rangle$-$|s\rangle$ destructively interfere to make the atom transparent around the resonance of the probe pulse. The strong limit can be understood using the Autler–Townes effect, see Sec. 2.1. Due to the strong control pulse, the bare atomic states $|e\rangle$ and $|s\rangle$ are dressed in to $|+\rangle$ and $|-\rangle$ with an energy separation of $2\Omega_2$[3] and the probe pulse scans these transitions to give two separated peaks.

Remarks: Notice that EIT is a steady state phenomenon and distinct from saturation effects, where atoms are pumped to other levels to see dips in absorption profile. In EIT, even with most atoms being in ground state ($\rho_{gg} \approx 1$) we observe a dip in the absorption at resonance. CPT (Coherent population trapping) is another interesting steady state phenomenon closely related to EIT [45, 46].

2.5 Heisenberg-Langevin approach

Here we discuss the operator formalism to study the light-matter interactions. This formalism is particularly convenient, when the probe light is quantized or when the atoms are trapped inside optical cavities.

[3]Occasionally Ω is defined as $d \cdot \mathcal{E}/\hbar$ giving width of Ω

Consider a system interacting with bath. The total Hamiltonian of system and bath can be written as

$$H = H_{\text{sys}} + H_B + H_I \tag{2.54a}$$

$$H_B = \hbar \int_{-\infty}^{\infty} d\omega\ \omega b^\dagger(\omega) b(\omega), \tag{2.54b}$$

$$H_I = i\hbar \int_{-\infty}^{\infty} d\omega K(\omega)[b^\dagger(\omega)\hat{a} - b(\omega)\hat{a}^\dagger], \tag{2.54c}$$

where $\hat{b}(\omega)$ and $\hat{a}$ denotes the annihilation operator for the bath and the system. H_{sys} and H_B are free Hamiltonians of the system and the bath. H_I denotes the interaction Hamiltonian between the system and the bath. Here $K(\omega)$ is the interaction strength between the system and the bath. By using these Hamiltonians in Eq. (2.54), we can write the time evolution for the field operators $b(\omega)$ as

$$\dot{b}(\omega) = -i\omega b(\omega) + K(\omega)\hat{a}, \tag{2.55}$$

which yields

$$b(\omega) = e^{-i\omega(t-t_0)} b_0(\omega) + K(\omega) \int_{t_0}^{t} e^{-i\omega(t-t')} \hat{a}(t') dt'. \tag{2.56}$$

Here b_0 is the field mode at time $t = t_0$ and can be considered as the input field mode. The decay rate (κ) is related to the two-point correlation as $\kappa = \left\langle \hat{b}^\dagger(t)\hat{b}(0) \right\rangle = K^2(\omega)$ [38]. We also assume that state of bath is stationary, i.e. $[\rho_B, H_B] = 0$, this makes the decay rates $K(\omega)$ constant [38]. Hence we set $K(\omega) = \sqrt{\kappa}$, this approximation in Langevin theory is know as the first Markov approximation [47]. Now we can define the total input mode $b_{\text{in}}(t)$ which is the total electromagnetic field interacting with the system.

$$b_{\text{in}}(t) = \int d\omega e^{-i\omega(t-t_0)} b_0(\omega). \tag{2.57}$$

similarly one can define an output electric field mode by considering the time reversal in the dynamical equations. The evolution of a general system operator $\hat{\sigma}$ is written as

$$\dot{\hat{\sigma}} = -\frac{i}{\hbar}[\hat{\sigma}, H] + \int d\omega\ \kappa \Big(b^\dagger(\omega)[\hat{a}, \hat{\sigma}] - b(\omega)[\hat{a}^\dagger, \hat{\sigma}] \Big), \tag{2.58}$$

and on using Eq. (2.56) and Eq. (2.57) in the Eq. (2.58) gives the evolution of a system operator as [47]

$$\frac{\mathrm{d}}{\mathrm{d}t}\hat{\sigma} = -i/\hbar\,[\hat{\sigma}, H] - \left[\hat{\sigma}, \hat{a}^\dagger\right]\left(\frac{\kappa}{2}\hat{a} + \sqrt{\kappa}\hat{b}_{\mathrm{in}}\right) + \left(\frac{\kappa}{2}\hat{a}^\dagger + \sqrt{\kappa}\hat{b}_{\mathrm{in}}^\dagger\right)\left[\hat{\sigma}, \hat{a}\right], \tag{2.59}$$

where κ is decay rate. A similar equation is derived with output modes

$$\frac{\mathrm{d}}{\mathrm{d}t}\hat{\sigma} = -i/\hbar\,[\hat{\sigma}, H] - \left[\hat{\sigma}, \hat{a}^\dagger\right]\left(-\frac{\kappa}{2}\hat{a} + \sqrt{\kappa}\hat{b}_{\mathrm{out}}\right) + \left(-\frac{\kappa}{2}\hat{a}^\dagger + \sqrt{\kappa}\hat{b}_{\mathrm{out}}^\dagger\right)\left[\hat{\sigma}, \hat{a}\right], \tag{2.60}$$

with $\hat{\sigma} = \hat{a}$ in Eqs. (2.59) and (2.60) gives the relation between the input and output modes

$$\hat{b}_{\mathrm{out}} - \hat{b}_{\mathrm{in}} = \sqrt{\kappa}\hat{a}. \tag{2.61}$$

For a two-level atom interacting with bath, we replace $\hat{a} \to \hat{\sigma}_{ge}$ in Eq. (2.59) and denote the bath operator $\hat{b}_{\mathrm{in}}$ by f. The Langevin equations for a two-level atom are written as

$$\frac{\mathrm{d}}{\mathrm{d}t}\hat{\sigma} = -i/\hbar\,[\hat{\sigma}, H] - [\hat{\sigma}, \sigma_{eg}]\left(\frac{\gamma}{2}\sigma_{ge} + \sqrt{\gamma}\hat{f}\right) + \left(\frac{\gamma}{2}\sigma_{eg} + \sqrt{\gamma}\hat{f}^\dagger\right)[\hat{\sigma}, \sigma_{ge}], \tag{2.62}$$

where γ is the decay rate. The equations of motion are written as

$$\frac{\mathrm{d}}{\mathrm{d}t}\hat{\sigma}_{eg} = \underbrace{i\Delta\hat{\sigma}_{eg} + i\Omega(\hat{\sigma}_{ee} - \hat{\sigma}_{gg}) - \frac{\gamma}{2}\hat{\sigma}_{eg}}_{D(\hat{\sigma}_{eg})} + \hat{F}_{eg}, \tag{2.63a}$$

$$\frac{\mathrm{d}}{\mathrm{d}t}\hat{\sigma}_{ee} = \underbrace{i\Omega(\hat{\sigma}_{eg} - \hat{\sigma}_{ge}) - \gamma\hat{\sigma}_{ee}}_{D(\hat{\sigma}_{ee})} + \hat{F}_{ee}. \tag{2.63b}$$

where $\hat{F}_{ab}$ is the bath operator corresponding to $\hat{\sigma}_{ab}$. $D(\sigma)$ is the called the deterministic part of $\hat{\sigma}$ containing all terms besides the noise ($\hat{F}$). From Eq. (2.62) we can notice that a decay is always accompanied by a corresponding bath. Also similar to the density matrix formalism the coherence decays at half the rate of population, see Eq. (2.23).

The two-time correlations between two bath operators can be obtained by using generalized Einstein relation [48, 49].

$$\left\langle \hat{F}_1(t)\hat{F}_2(t')\right\rangle = \delta(t-t')\left\langle D(\hat{\sigma}_1\hat{\sigma}_2) - D(\hat{\sigma}_1)\hat{\sigma}_2 - \hat{\sigma}_1 D(\hat{\sigma}_2)\right\rangle, \tag{2.64}$$

where $D(\hat{\sigma}_n)$ and $\hat{F}_n$ are the deterministic and the noise part of $\hat{\sigma}_n$. E.g. the low intensity approximation $\hat{\sigma}_{gg} = 1$ gives

$$\begin{aligned}\left\langle \hat{F}_{ge}(t)\hat{F}^{\dagger}_{ge}(t')\right\rangle &= \delta(t-t')\left\langle D(\hat{\sigma}_{gg}) - D(\hat{\sigma}_{ge})\hat{\sigma}_{eg} - \hat{\sigma}_{ge}D(\hat{\sigma}_{eg})\right\rangle, \\ &= \delta(t-t')\gamma.\end{aligned} \tag{2.65}$$

N three-level atoms

Now we write the Langevin equations for N three-level atoms with Λ-configuration. The Λ system is same as in Fig. (2.2) and consists of an excited ($|e\rangle$), ground ($|g\rangle$) and a spin state ($|s\rangle$). The $|e\rangle \leftrightarrow |g\rangle$ transition interacts with a weak probe pulse (Ω_1) and the $|e\rangle \leftrightarrow |s\rangle$ with a strong control field (Ω_2). The Hamiltonian for the Λ-system is written as sum of free and interaction parts $H = H_0 + V$

$$H_0 = \int \hbar\omega\hat{a}^{\dagger}(\omega)\hat{a}(\omega)\,d\omega + \hbar\omega_{eg}\sum_{j=1}^{N}\sigma^j_{ee} + \hbar\omega_{sg}\sum_{j=1}^{N}\sigma^j_{ss}, \tag{2.66a}$$

$$V = -g\hbar\sum_{j=1}^{N}\sigma^j_{eg}\mathcal{E}(z) + \text{H.c.} - \hbar\sum_{j=1}^{N}\Omega(z_j,t)e^{-i\omega_2(t-z_j/c)}\,\sigma^j_{es} + h.c, \tag{2.66b}$$

where $g = d_{eg}\sqrt{\omega_1/2\hbar\epsilon_0 V}$ [4] is the coupling constant. $\mathcal{E}(z)$ is the quantized input pulse. $\Omega(z,t)$ is the strong classical control pulse and the summation is over all atoms.

On using Eqs. (2.62)-(2.65) the Langevin equations for the Λ-system are written as (derivation in appendix, Sec. A.3)

$$\left(\frac{\partial}{\partial t} + c\frac{\partial}{\partial z}\right)\tilde{\mathcal{E}} = i\tilde{g}^{*}P, \tag{2.67a}$$

$$\frac{\partial}{\partial t}P = -(\gamma_{ge} + i\Delta)P + i\tilde{g}\tilde{\mathcal{E}} + i\Omega S, \tag{2.67b}$$

$$\frac{\partial}{\partial t}S = -i\Delta S + i\Omega^{*}P, \tag{2.67c}$$

where $\sqrt{N}\tilde{\sigma}_{ge} = P$, $\sqrt{N}\tilde{\sigma}_{gs} = S$ and $\tilde{g} = \sqrt{N}g$. $\Delta = \omega_{eg} - \omega_1$ is the detuning with the input pulse. The above equations can be further simplified by setting $\frac{\partial}{\partial t}P = 0$ under the adiabatic approximation (appendix Sec. A.4). The Eq. (2.67) describe the dynamics of an ensemble of three-level atoms interacting with light. These equations are the starting point of all quantum memory protocols and in the next chapter we solve them under

[4] Here we use g and Ω instead of Ω_1 and Ω_2 to be consistent with the literature.

various physical conditions.

Chapter 3

Quantum Memories

In this chapter we discuss different protocols of photonic quantum memories. Photonic quantum memory is a device capable of storing and re-emitting the photons on demand. Here an input pulse ($\mathcal{E}$) interacts with an ensemble of atoms. Then the absorption and emission of the input pulse are controlled using a control pulse (Ω). In the following we discuss three different memory schemes:

- Quantum memory with EIT.
- Controlled reversible inhomogeneous broadening (CRIB).
- Atomic frequency combs (AFC).

A typical quantum memory uses either one of these techniques or slight variations of them.

In all of the above protocols an ensemble of atoms with $|g\rangle$, $|e\rangle$ and $|s\rangle$ in Λ-configuration is used, see Fig. 2.2. The mean frequency of input pulse (ω_1) is tuned to the $|e\rangle$-$|g\rangle$ transition. The $|e\rangle$-$|s\rangle$ is tuned to the mean frequency of a control pulse. Once the input pulse is converted into an atomic excitation. A control pulse is used to transfer the excitation to the long lived spin state ($|s\rangle$). After the storage time a second control-pulse is used to retrieve the input. The storage time will be limited by the life time of the spin state. Since most quantum memories use a Λ-type atom we rewrite the Langevin equations in the interaction picture Eq. (2.67)

$$\left(\frac{\partial}{\partial t} + c\frac{\partial}{\partial z}\right)\mathcal{E} = ig^* P, \tag{3.1a}$$

$$\frac{\partial}{\partial t}P = -(\gamma_{ge} + i\Delta)P + ig\mathcal{E} + i\Omega S, \tag{3.1b}$$

$$\frac{\partial}{\partial t}S = -i\Delta S + i\Omega^* P, \tag{3.1c}$$

where $g = d_{eg}\sqrt{\mathcal{N}\omega_1/2\hbar\epsilon_0}$ with $\mathcal{N}$ begin atomic number density. $\Delta = \omega_{eg} - \omega_1$ is the detuning with the input pulse. $\sqrt{N}\sigma_{ge} = P$, $\sqrt{N}\sigma_{gs} = S$.

The operators P and S (with $\sigma_{gg} \approx 1$) satisfy relations similar to electric field Eq. (A.28)

$$\Big[P(t,z), P^\dagger(t,z')\Big] = \Big[S(t,z), S^\dagger(t,z')\Big] = \frac{N}{\eta(z)}\delta(z-z'). \tag{3.2}$$

Thus quantum memory protocols can be understood as mapping of the electric field modes to atomic modes. An electric field excitation is transferred to P-modes through absorption. Then for longer storage times, the excitation is mapped from P-mode to S-modes using a control pulse. Then a second control pulse maps back the excitation from the S-mode to P-mode. Finally the P-mode decays, leaving the excitation back in the electric field mode.

3.1 Quantum memory with EIT

In EIT Sec. 2.4.3, The $|e\rangle$-$|g\rangle$ transition of a Λ system is made transparent around the resonance frequency (ω_{eg}), by driving the $|e\rangle$-$|s\rangle$ transition with a strong control pulse. The width of the EIT-dip near the resonance is obtained by Taylor expansion of the susceptibility Eq. (2.53)

$$\chi = \frac{\mathcal{N}|d_{eg}|^2}{\epsilon_0\hbar|\Omega|^2}\left[-\Delta + i\Delta^2\frac{\gamma_{ge}}{|\Omega|^2} + O(\Delta^3)\right], \tag{3.3}$$

where $\Delta = \omega_{eg} - \omega_1$ is the detuning between atom and the input pulse. Then the transmittance is written as [50]

$$T = \exp\{-kL\mathrm{Im}(\chi)\} \approx \exp\{-\Delta^2/\bar{\omega}_{tr}^2\}, \tag{3.4}$$

where $k = \omega_1/c$ and L is the length of the medium. The width of the dip is defined as

$$\bar{\omega}_{tr} = \sqrt{\frac{2\epsilon_0\hbar|\Omega|^4}{kL\mathcal{N}|d_{eg}|^2\gamma_{ge}}} = \sqrt{\frac{|\Omega|^4 c}{g^2 L\gamma_{ge}}} = \frac{|\Omega|^2}{\sqrt{\mathcal{O}}\gamma_{ge}}, \tag{3.5}$$

here $\mathcal{O} = \dfrac{g^2 L}{c\gamma_{ge}}$ is called the optical depth.

In EIT the region with the low absorption also corresponds to high refractive index (derivative of the Re χ). Thus when an input pulse width $(1/\tau_p)$ is smaller than the transmittance width. The pulse velocity is reduced with negligible absorption [51, 52, 53]. Also an atomic system can be transferred from a ground state to a long lived spin states, by adiabatically following the dark-state, see Sec. 2.4.1. Then by integrating EIT and adiabatic transfer of population, one can freeze the light pulse in an ensemble of atoms. The stopped light can be remitted by adiabatically moving from the spin state to the ground state, hence EIT can be used as a viable quantum memory.

Consider N number of Λ-atoms interacting with a resonant ($\Delta = 0$) input pulse. The dynamical equations for the field and the atomic polarization reads Eq. (3.1)

$$\left(\frac{\partial}{\partial t} + c\frac{\partial}{\partial z}\right)\mathcal{E} = \frac{g}{\Omega^*}\frac{\partial}{\partial t}S, \tag{3.6a}$$

$$\frac{\partial}{\partial t}P = -\gamma_{ge}P + ig\mathcal{E} + i\Omega S, \tag{3.6b}$$

where $P = -i/\Omega\frac{\partial}{\partial t}S$ is used. Then Eq. (3.6b) gives

$$\begin{aligned} S &= -\frac{\tilde{g}\mathcal{E}}{\Omega} - \frac{i}{\Omega}\left(\frac{\partial}{\partial t} + \gamma_{ge}\right)\left(-\frac{i}{\Omega^*}\frac{\partial}{\partial t}S\right), \\ &= -\frac{i}{\Omega}\left[\frac{\partial}{\partial t}\left(-i/\Omega^*\frac{\partial}{\partial t}S\right) + \gamma_{ge}(-i/\Omega^*\frac{\partial}{\partial t}S) - ig\mathcal{E}\right]. \end{aligned} \tag{3.7}$$

Assuming that $\Omega(t, z)$ changes slowly [54, 53] derivatives of S are dropped to give

$$\left(\frac{\partial}{\partial t} + c\frac{\partial}{\partial z}\right)\mathcal{E} = \frac{g^2}{\Omega^*}\frac{\partial}{\partial t}\frac{\mathcal{E}(z,t)}{\Omega}. \tag{3.8}$$

If the control pulse is time independent $\Omega(t, z) = \Omega(z)$ then the transformation $t' \to t - z/v_g$ gives

$$\mathcal{E}(z,t) = \mathcal{E}\left(0, t - \int_0^z \frac{dz'}{v_g(z')}\right), \tag{3.9}$$

with the group velocity

$$v_g = \frac{c}{1 + g^2/|\Omega|^2} \tag{3.10}$$

Then the delay (τ_d) can be defined as

$$\tau_d = (1/c - 1/v_g)L = \mathcal{O}\frac{\gamma}{|\Omega|^2}, \tag{3.11}$$

and along with the condition $1/\tau_p < \bar{\omega}_{tr}$ gives

$$\tau_d/\tau_p < \sqrt{\mathcal{O}}, \tag{3.12}$$

hence high optical depths are required to see any noticeable storage times. Requiring optical depths is a major draw back for EIT protocols. This reduction in velocity was observed in the Rubidium vapour cells . The velocity of a light pulse was reduced to 8m/s with a delay of 13 ms [55].

Until now we discussed only the velocity reduction by considering driving pulses of the form $\Omega(z)$. In the following we include the time dependency in Ω. Then by adiabatically controlling the $\Omega(t)$, we show that a light pulse can be completely stopped and re-accelerated.

Defining new operators of the form [50]

$$\Psi = \cos\theta\,\mathcal{E}(z,t) - \sin\theta S(z,t), \tag{3.13a}$$

$$\Phi = \sin\theta\,\mathcal{E}(z,t) + \cos\theta S(z,t), \tag{3.13b}$$

where the mixing angle is defined as

$$\tan^2\theta(t) = \frac{g^2}{|\Omega(t)|^2}. \tag{3.14}$$

Similar to S and P, Ψ and Φ also satisfy bosonic relations

$$\left[\Psi(z,t), \Psi^\dagger(z',t)\right] = \left[\Phi(z,t), \Phi^\dagger(z',t)\right] = L\delta(z-z'), \tag{3.15}$$

with L being the length of the medium. Moreover the dark states can be created from vacuum state by

$$|n_k\rangle = \frac{1}{\sqrt{n!}}(\Psi_k^\dagger)^n\,|0\rangle\,, \tag{3.16}$$

similarly Φ gives the bright states. Since a combination of field and spin gives Ψ (Φ) generates dark (bright) states, these quasi-particles are called dark (bright)-state polaritons. Now we rewrite the dynamical equations Eq. (3.6) in terms of polaritons to give

$$\left(\frac{\partial}{\partial t}+c\frac{\partial}{\partial z}\right)(\cos\theta\Psi+\sin\theta\Phi)=\tan\theta\Big[-\sin\theta\dot{\Psi}+\cos\theta\dot{\Phi}-\dot{\theta}(\cos\theta\Psi+\sin\theta\Phi)\Big], \quad (3.17)$$

on separating Ψ and Φ gives

$$\left(\frac{\partial}{\partial t}+c\cos^2\theta\frac{\partial}{\partial z}\right)\Psi=-\dot{\theta}\Phi-\sin\theta\cos\theta\ c\ \frac{\partial\Phi}{\partial z}. \quad (3.18)$$

Similarly writing Eq. (3.7) in the polariton basis gives

$$\Phi=\frac{\sin\theta}{g^2}\left(\frac{\partial}{\partial t}+\gamma\right)\left(\tan\theta\frac{\partial}{\partial t}\right)[\sin\theta\Psi-\cos\theta\Phi], \quad (3.19)$$

Normalizing time with $t'=t/\tau_p$ and retaining to lowest order in $(g\tau_p)^{-1}$ results in $\Phi\approx 0$. Then Eq. (3.18) on applying the transformations

$$d\tau=\cos^2\theta(t)\,dt, \qquad z'\to z-c\tau \quad (3.20)$$

gives

$$\Psi(z,t)=\Psi\left(z-c\int_0^t\cos^2\theta(t')\,dt'\right). \quad (3.21)$$

On comparing the above with $\Psi(z-vt)$, it's clear that polariton is not effected by propagation.

In the strong field regime ($\Omega\gg\tilde{g}\to\theta\approx 0$) the polariton becomes completely photonic, i.e. $\Psi=\mathcal{E}$, with propagation velocity of c. In the weak field regime ($\tilde{g}\gg\Omega\to\theta\approx\pi/2$) the field-modes are completely mapped to spin-modes ($\Psi=S$) with zero propagation velocity. Thus by adiabatically rotating the mixing angle, the the electric field is stored and retrieved in a controlled fashion. Here the adiabaticity condition translates to

$$\frac{\gamma_{ge}}{\Omega^2\tau_p}\ll 1\Rightarrow 1/\tau_p\ll\bar{\omega}_{tr} \quad (3.22)$$

Hence the only condition required for storage and retrieval of light is that EIT-window contains all the input light frequencies.

Experiments The Λ-type levels required for EIT are usually obtained in the hyperfine structure (D-transitions) of the Caesium (Cs) and Rubidium (Rb) atoms, with the transition energies in the infrared range [56, 57, 58, 56, 59]. EIT type memories are demonstrated in systems such as warm atomic vapours cold atoms and Bose-Einstein condensates (BEC) [60, 61, 62] .

In warm atomic vapours, atomic gas cells are maintained at temperatures $300-350$K and storage times upto micro seconds are achieved using Cs [56] and Rb atoms [57, 58, 56, 59]. The measured efficiencies for atomic vapours are in the range $10\% - 15\%$. In cold atom ensembles, few atoms ($\sim 10^6$) are trapped using a magneto-optical trap (MOT) and similar to atomic vapour cells the storage times $\sim 1\mu s$ are demonstrated using Rb atoms [63, 64, 65, 66, 67, 20]. An efficiency of $\sim 85\%$ is achieved using MOT traps [20]. In BEC, atoms are cooled down to low temperatures and storages times around few milli-seconds has been achieved using Rb atoms [60, 61] and Na atoms [62]. The measured efficiency for the BEC are in the range $\sim 50\%$. EIT-memory at temperature 4K and storage times ~ 1 min is demonstrated in rare earth-ion-doped crystal (REIC) [68].

3.2 Controlled reversible inhomogeneous broadening

The basic principle behind the CRIB based quantum memory is as follows: a light pulse is first absorbed in an ensemble of atoms. Once the light is absorbed, the excited atoms start to develop a time-dependent phase due to the free evolution. These accumulated phases are eliminated by inverting the detuning between the light and the atomic transition, resulting in the coherent emission of the light pulse [69]. Hence, one can store light in a controlled way in the atomic ensemble. For example, consider an ensemble of atoms with N number of Λ-type atoms, a single photon interacting with the $|e\rangle$-$|g\rangle$ transition can be completely absorbed if it's broadening is larger than the width of input pulse. The state after the absorption is written as

$$|\psi\rangle = \sum_{j=1}^{N} c_j \, |\{e_j\}\rangle \tag{3.23}$$

where $|\{e_j\}\rangle = |g_1, g_2, ...e_j..g_n\rangle$ with j being atom number. Since the medium is inhomogeneous broadened the mean frequency (ω_{eg}) of the atom shifts and we denote this shift by δ_j. For time scales much less than the inhomogeneous broadening, the state $|\psi\rangle$ evolves due to the free Hamiltonian and the states is given as

$$|\psi\rangle = \sum_{j=1}^{N} e^{-i(\omega_{eg}+\delta_j^+)\tau} |\{e_j\}\rangle \tag{3.24}$$

At time $t = \tau$, a π-pulse (2.1.1) is applied between the transition $|e\rangle$-$|s\rangle$ and the state is written as [70]

$$|\psi\rangle = \sum_{j=1}^{N} c_j e^{-i(\omega_{eg}+\delta_j^+)\tau} |\{s_j\}\rangle\,, \tag{3.25}$$

where $|\{s_j\}\rangle = |g_1, g_2, ...s_j..g_n\rangle$. After the storage time T_s another π-pulse is applied to give

$$|\psi\rangle = e^{-i\omega_{eg}(t+\tau)} \sum_{j=1}^{N} c_j e^{-i\delta_j^+\tau} e^{-i\delta_j^- t} e^{-i\omega_{sg}^j T_s} |\{e_j\}\rangle\,, \tag{3.26}$$

where δ_j^- denotes shifts after the second π-pulse. Then ω_{sg}^j term can be drooped assuming a small in-homogeneous broadening for the transition $|e\rangle$-$|s\rangle$. If $\delta_+ = -\delta_-$ then at time τ after the second pulse, phases due to inhomogeneous broadening cancel to give the initial state. Hence due to this rephasing, a photon emission is expected leaving the atom in the initial state. The condition $\delta_+ = -\delta_-$ is achieved using variety of techniques e.g., in atomic gases this amounts to sending the π-pulses in opposite directions [71], in solid state systems δ's are reversed by switching the polarity of the electrodes [72] and in Gradient echo memories (GEM) schemes δ's are reversed by switching the sign of the electric field gradient from positive to negative [73, 22].

In the following we give details for CRIB. We begin by splitting the atomic polarization (σ_{ge}) into forward and backward mode

$$\sigma_{ge}(z,t) = \sigma_f(z,t)e^{i\omega z/c} + \sigma_b(z,t)e^{-i\omega z/c}, \tag{3.27}$$

where the forward and backward mode differ by a position dependent phase $e^{(-2i\omega z/c)}$. Then the equations for the forward mode are given by Eq. (3.1)

$$\frac{\partial}{\partial t}\sigma_f(z,t) = -i\Delta\sigma_f + id_{eg}E_f(z,t), \tag{3.28a}$$

$$\left(\frac{\partial}{\partial t} + c\frac{\partial}{\partial z}\right)E_f(z,t) = i\beta\int_{-\infty}^{\infty} G(\Delta)\sigma_f(z,t)\,d\Delta, \tag{3.28b}$$

where $\beta = g^2N/d_{eg}$ and $G(\Delta)$ is normalized spectral distribution for the inhomogeneous broadening. The backward mode equations are similarly given as:

$$\frac{\partial}{\partial t}\sigma_b(z,t) = -i\Delta\sigma_b + id_{eg}E_b(z,t), \tag{3.28c}$$

$$\left(\frac{\partial}{\partial t} - c\frac{\partial}{\partial z}\right)E_b(z,t) = i\beta\int_{-\infty}^{\infty} G(\Delta)\sigma_b(z,t)\,d\Delta. \tag{3.28d}$$

where for convenience we assume that a initial Δ_0 is broadened by Δ' to give $\Delta = \Delta_0 + \Delta'$, hence we write $G(\Delta) = G(\Delta_0).G(\Delta')$ [74].

The essence of CRIB lies in the inherent symmetry of the dynamical equations Eq. (3.28a-3.28d) the transformation $\Delta \to -\Delta$ in the backward mode is equivalent to the transformation $t \to -t$ and $\mathcal{E}_f(z,t) \to -\mathcal{E}_f(z,-t)$ in the forward mode. Hence if we can reverse the detuning and apply the position dependent phase factor, backward mode can evolve like a time reversal copy of forward mode.

For convenience we split the time scale from $-\infty$ to 0 for absorption and 0 to ∞ for emission. We further split the emission into backward mode and forward mode. At $t = 0$ we assume the light is absorbed and the non-absorbed part of light has left the medium. Then we apply control pulses to shift the excitation from excited state to the spin state and vice versa. After the application of control pulses and phase shifts, the remission is studied in the time $0 \to \infty$.

3.2.1 Absorption in CRIB

Assuming that absorption happens in forward mode the equations are modified as

$$\left(\frac{\partial}{\partial t} + c\frac{\partial}{\partial z}\right)E_f^{in}(z,t) = i\beta\int_{-\infty}^{\infty}\sigma_f(z,t)\;G(\Delta_0)G'(\Delta')\,d\Delta_0 d\Delta', \tag{3.29a}$$

$$\frac{\partial}{\partial t}\sigma_f(z,t) = -i(\Delta_0 + \Delta')\sigma_f + id_{eg}E_f(z,t), \tag{3.29b}$$

where $G(\Delta_0)$ and $G'(\Delta')$ are the initial and broadened distributions. On solving Eq. (3.29b) with initial condition $\sigma_f(z, -\infty, \Delta_0, \Delta') = 0$ gives

$$\sigma_f(z,t) = id_{eg} \int_{-\infty}^{t} e^{-i(\Delta'+\Delta_0)(t-s)} E_f(z,s)\, ds, \tag{3.30}$$

since absorption happens in negative times. Fourier transform for input can be defined as

$$\mathcal{E}_f(z,\omega) = \int_{-\infty}^{0} e^{i\omega t} E_f(z,t)\, dt, \tag{3.31}$$

applying Fourier transform on Eq. (3.29a) and Eq. (3.30) gives (Appendix Sec. B)

$$\left[\frac{\partial}{\partial z} - \frac{i\omega}{c} + \kappa H(\omega)\right] \mathcal{E}_f(z,\omega) = 0, \tag{3.32}$$

with

$$H(\omega) \equiv \int_0^\infty dx\, e^{i\omega x} \int_{-\infty}^{\infty} G(\Delta_0) G'(\Delta') e^{-i(\Delta'+\Delta_0)x}\, d\Delta_0 d\Delta', \qquad \kappa \equiv \frac{|g|^2 N}{c}, \tag{3.33a}$$

Then the solution of absorption is written as (3.32)

$$E_f(z,\omega) = E_f(0,\omega)\, e^{i\omega z/c}\, e^{-\kappa H(\omega) z}. \tag{3.34}$$

3.2.2 Backward mode in CRIB

At $t = 0$ we assume that absorption is completed . The phase shift $\exp(-2i\omega_0 z/c)$ is applied. The detuning is reversed, i.e. $\Delta_0 + \Delta' \to \Delta_0 - \Delta'$ to couple to backward mode. Then the equations for the backward mode are obtained to be

$$\left(\frac{\partial}{\partial t} - c\frac{\partial}{\partial z}\right) E_b^{in}(z,t) = i\beta \int_{-\infty}^{\infty} \sigma_b(z,t)\; G(\Delta_0) G'(\Delta')\, d\Delta_0 d\Delta', \tag{3.35a}$$

$$\frac{\partial}{\partial t}\sigma_b(z,t) = -i(\Delta_0 - \Delta')\sigma_b + id_{eg} E_b(z,t), \tag{3.35b}$$

The initial condition for backward mode is taken to be endpoint of the absorption

$$\sigma_b(z,0) = \sigma_f(z,0) = id_{eg} \int_{-\infty}^{0} e^{i(\Delta'+\Delta_0)s} \mathcal{E}_f(z,s)\, ds = id\mathcal{E}_f(z, \Delta' + \Delta_0). \tag{3.36}$$

On solving Eq. (3.35b) with the above initial condition gives

$$\sigma_b(z,t) = \sigma(z,0,\Delta_0,\Delta')e^{i(\Delta_0-\Delta')t} + id\int_{-\infty}^{t} e^{-i(\Delta'-\Delta_0)(t-s)}\mathcal{E}_b(z,s)\,ds. \tag{3.37}$$

Then the solution, assuming a narrow atomic distribution $G(\Delta_0) = \delta(\Delta_0)$ is obtained as, derivation in Sec. B

$$E_b(0,t) = -\frac{\gamma}{2\pi}\left(1-e^{-\alpha L}\right)\int_{-\gamma/2}^{\gamma/2} E_f(0,-\omega)(1/\gamma)e^{i\omega t}\,d\omega, \tag{3.38}$$

where $\alpha = \kappa 2\pi/\gamma$. To ensure the complete absorption input pulse width ($\bar{\omega}_{in}$) has to be smaller than broadening width (γ). Then the integral in Eq. (3.38) can be treated as Fourier transform and the final output is given as

$$E_b(0,t) = -\left(1-e^{-\alpha L}\right)E_f(0,-t). \tag{3.39}$$

Defining efficiency of the form

$$\eta \equiv \frac{\int \left|E^{\text{out}}(t)\right|^2 dt}{\int \left|E^{\text{in}}(t)\right|^2 dt}. \tag{3.40}$$

gives

$$\eta_b = (1-e^{-\alpha L})^2. \tag{3.41}$$

3.2.3 Forward mode in CRIB

At $t = 0$ the absorption is completed and all the unabsorbed light has left the medium. Then if we reverse the detunings, but without applying the phase shift $\exp(-2i\omega_0 z/c)$, the light will continue to propagate in the forward direction. On using the same arguments as in absorption and back scattering gives (Appendix Sec. B)

$$E_f(L,\omega) = -\kappa L E_f(0,-\omega)G'(-\omega) \times \frac{\sin(\omega L/c)}{\omega L/c} \times \exp\left(-\frac{\alpha L}{2}\right), \tag{3.42}$$

and assuming that input pulse width ($\bar{\omega}_{in}$) is smaller than c/L the output in the forward mode is given as

$$E_f(L,t) = -\alpha L\, e^{-\alpha L/2}E_f(0,-t), \tag{3.43}$$

where αL is the optical depth and in both cases the input pulse emits the medium without any distortions and the efficiency is given as

$$\eta_f = (\alpha L)^2 e^{-\alpha L}. \tag{3.44}$$

In Fig. 3.1 we plot the forward and the backward efficiencies, Eqs. (3.44) and (3.41). we can notice that the forward mode efficiency peaks at 54% and the back ward mode scattering results in 100% efficiency.

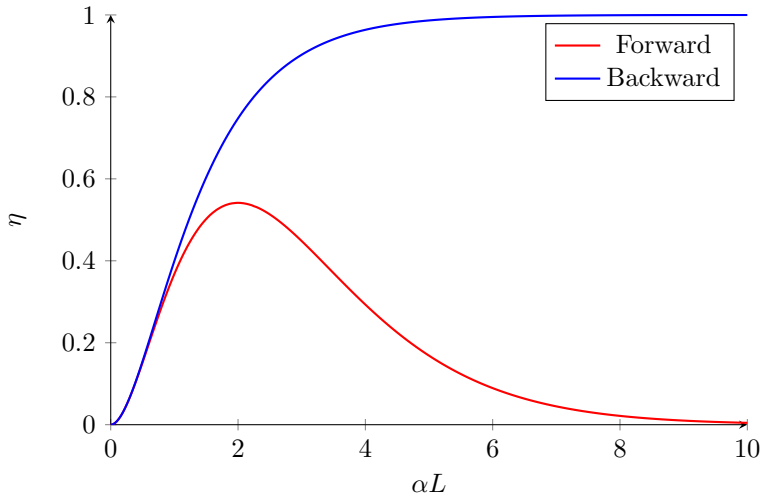

FIGURE 3.1: Efficiencies for the forward and backward scattering. The efficiency in the backward mode goes to 100% unlike in the forward which peaks at 54%, at $\alpha L = 2$

Experiments CRIB-Memories are typically realized in REIC e.g. doping Eu^{3+} ions in Y_2SiO_5 gives a Λ-type atom with transition frequencies in the optical range (579.87nm) [72]. This system has been used to demonstrate the CRIB quantum memory at low temperatures (4k). CRIB at telecommunication wavelengths is realized at 2.6K [75]. CRIB has been experimentally demonstrated with with 15% efficiency by doping Pr^{3+} ions in Y_2SiO_5 [21]. Another protocol known as gradient echo mechanism GEM is theoretically equivalent to CRIB and an efficiency of $\sim 87\%$ is demonstrated using Rb atoms [22].

3.3 Atomic frequency combs

Quantum memory using Atomic Frequency Combs (AFC) [76] is very similar to CRIB. In CRIB the re-phasing of the phases is achieved by reversing the detunings, whereas in

AFC the re-phasing is achieved using a frequency comb. The AFCs are typically consist of rare-earth ions doped in crystals that have optical transition between the ground state $|g\rangle$ and the excited state $|e\rangle$ [76, 28]. This transition has a narrow homogeneous bandwidth γ and a large inhomogeneous bandwidth Γ ($\Gamma \gg \gamma$). The transition $|g\rangle$-$|e\rangle$ is spectrally shaped such that the atomic density function consists of a series of equispaced narrow peaks (teeth), with spacing Δ, resulting in a comb like structure in frequency modes, Fig. 3.2.

$$n(\delta) = \frac{\Delta}{\sqrt{2\pi}\gamma\Gamma} e^{-\frac{\delta^2}{2\Gamma^2}} \sum_{n=-\infty}^{\infty} e^{-\frac{(\delta - n\Delta)^2}{2\gamma^2}}, \tag{3.45a}$$

and in time domain $\int_{-\infty}^{\infty} \eta(\delta) e^{-i\delta t}\, d\delta$ yields

$$n(t) = \frac{2\pi}{\Delta} \sum_{n=-\infty}^{\infty} e^{-\left(t - n\frac{2\pi}{\Delta}\right)^2 \frac{\Gamma^2}{2}} e^{-\left(n\frac{2\pi}{\Delta}\right)^2 \frac{\gamma^2}{2}}, \tag{3.45b}$$

where $\delta = \omega_L - \omega_A$ is the detuning, Γ is comb width. Δ and γ are the peak separation and peak width. Assuming that a incoming photon with a width much wider than peak separation but narrower than comb width, i.e. $\Gamma \gg \gamma_p \gg \Delta$ is interacting with $|e\rangle - |g\rangle$ transition. Formally the state of the AFC, after absorbing a single photon, can be written as

$$|\Psi\rangle_{\text{AFC}} = \sum_{j=1}^{M} \left(c_j e^{i\delta_j t} |\{e_j\}\rangle \prod_{k \neq j} |\{g_k\}\rangle \right). \tag{3.46}$$

Here $|\{g_j\}\rangle \equiv \left|g_1 g_2 ... g_{N_j}\right\rangle_j$ and $|\{e_j\}\rangle \equiv \sum_n \alpha_n \left|g_1 ... e_2 ... g_{N_j}\right\rangle_j$ represents the ground and collective single-excitation state of all the atoms with detuning δ_j, respectively, and the c_j's represent the absorption coefficient of each tooth in the comb. The coefficients α_n characterize the absorption by individual atoms. The photon emission probability $P(t)$ from this setup is proportional to

$$P(t) \propto |\langle G| S_- |\Psi\rangle_{\text{AFC}}|^2, \tag{3.47}$$

where $S_- = \sum_j |\{g_j\}\rangle \langle\{e_j\}|$ is the step down operator and $|G\rangle = \prod_k |\{g_k\}\rangle$ is the collective ground state of the ensemble. Here the sum is over all the teeth. If the comb has narrow

peaks ($\Delta \gg \gamma$) then δ_j can be approximated with $j\Delta$ and the probability of emission is given as

$$P(t) \propto \left| \sum_{j=1}^{M} c_j e^{ij\Delta t} \right|^2, \tag{3.48}$$

hence the probability re-phases with a time period of $2\pi/\Delta$[1] to give coherent photon-echo Fig. 3.2. This echo was demonstrated in REIC by doping Nd^{3+} into YVO_4 crystal and the comb is prepared through frequency-selective optical pumping [77]. After the optical pumping the transition $|e\rangle$-$|g\rangle$ is shaped into a comb structure with $\Delta = 4$MHz. Then this AFC is interacted with weak pulses to observe the echo at 250ns [77].

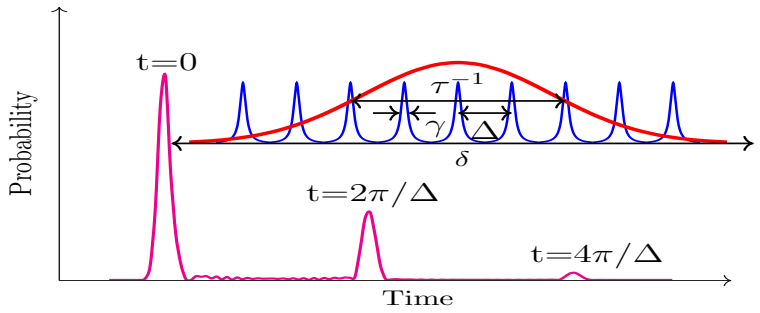

FIGURE 3.2: Electric field output from an AFC. Here the first peak at time $t = 0$ shows the probability (intensity) of the unabsorbed light. We observe photon-echo at time interval of $2\pi/\Delta$. In the inset, we show the spectrum of the AFC. The teeth in the AFC have width γ and are separated by Δ. Here, $\Gamma = N\Delta$ is the width of the comb for N number of teeth, δ is the detuning, and τ is the temporal width of input laser pulse.

In the following, we present a complete description of AFC and show the photon echoes occur at $2\pi/\Delta$. Since the only difference between the CRIB and the AFC is the spectral function, i.e., $G(\Delta)$ for CRIB and $n(\delta)$ for AFC the equations remain same. The equation for the forward and backward modes in AFC reads

$$\frac{\partial}{\partial t}\sigma_f(z,t) = -i\delta\sigma_f + id_{eg}E_f(z,t), \tag{3.49a}$$

$$\left(\frac{\partial}{\partial t} + c\frac{\partial}{\partial z}\right)E_f(z,t) = i\beta\int_{-\infty}^{\infty} n(\delta)\sigma_f(z,t)\,d\delta \tag{3.49b}$$

[1] To see compare $P(t)$ with Fourier series formulae.

where $n(\delta)$ is normalized spectral distribution. The backward mode equations are similarly given as:

$$\frac{\partial}{\partial t}\sigma_b(z,t) = -i\delta\sigma_b + id_{eg}E_b(z,t) \tag{3.49c}$$

$$\left(\frac{\partial}{\partial t} - c\frac{\partial}{\partial z}\right)E_b(z,t) = i\beta\int_{-\infty}^{\infty} n(\delta)\sigma_b(z,t)\,d\delta \tag{3.49d}$$

3.3.1 Absorption in AFC

Absorption is described by forward mode equations. Solving Eq. (3.49a) with the initial condition $\sigma_f(z,-\infty) = 0$, gives

$$\sigma_f(z,t,\delta) = id_{eg}e^{-i\delta t}\int_{-\infty}^{t} e^{i\delta t'}E_f(z,t')\,dt', \tag{3.50}$$

and substituting in Eq. (3.49b), gives

$$\begin{aligned}\left(\frac{\partial}{\partial t} + c\frac{\partial}{\partial z}\right)E_f(z,t) &= -d_{eg}\beta\int_{\infty}^{\infty} n(\delta)e^{-i\delta t}\,d\delta\int_{\infty}^{t} e^{i\delta t'}E_f(z,t')\,dt',\\ &= -d_{eg}\beta\int_{\infty}^{t} n(t-t')E_f(z,t')\,dt'.\end{aligned} \tag{3.51}$$

Since absorption is of time scales τ_p (width of input pulse) for $\tau_p \ll 2\pi/\Delta$ only the central tooth of Eq. (3.45b) contributes and hence can be approximated as

$$n(t-t') = e^{-(t-t')^2\Gamma^2/2}, \tag{3.52}$$

further $\tau_p\Gamma \gg 1$, thus $n(t-t')$ acts like a Dirac delta. Then Eq. (3.51) is given as

$$\left(\frac{\partial}{\partial t} + c\frac{\partial}{\partial z}\right)E_f(z,t) = -\frac{d_{eg}\beta}{2}E_f(z,t), \tag{3.53}$$

with the transformation $t' = t - z/c$ it transforms to

$$\frac{\partial}{\partial z}E_f(z,t') = -\frac{\tilde{\alpha}}{2}E_f(z,t'), \tag{3.54}$$

if $\tau_p \gg L/c$ then t' can be replaced with t and the solution is given as

$$E_f(z,t) = E_f(0,t)e^{-\tilde{\alpha}z/2}. \tag{3.55}$$

3.3.2 Backward mode in AFC

After absorption the excitation is shifted to a long lived spin state by applying a π-pulse and a second π-pulse will bring the excitation back to the excited state. The atomic polarization after absorption, i.e. at $t = 0$ is given by

$$\sigma_f(z,0,\delta) = \sigma_b(z,0,\delta) = id_{eg}\int_{-\infty}^{0} e^{i\delta t'} E_f(z,t')\,dt'. \tag{3.56}$$

Solving the Eq. 3.49c with 3.56 gives

$$\sigma_b(z,t,\delta) = id_{eg}e^{-i\delta t}\left(\int_{-\infty}^{0} e^{i\delta t'} E_f(z,t')\,dt' + \int_{0}^{t} e^{i\delta t'} E_b(z,t')\,dt'\right), \tag{3.57}$$

substituting this in Eq. 3.49d gives

$$\left(\frac{\partial}{\partial t} - c\frac{\partial}{\partial z}\right)E_b(z,t) = -\beta\left(\int_{-\infty}^{0} n(t-t')E_f(z,t')\,dt' + \int_{0}^{t} n(t-t')E_b(z,t')\,dt'\right), \tag{3.58}$$

using the same arguments as in absorption it can be simplified as

$$\frac{\partial}{\partial z}E_b(z,t) = \tilde{\alpha}\int_{-\infty}^{0} n(t-t')E_f(z,t')\,dt' + \tilde{\alpha}\int_{0}^{t} n(t-t')E_b(z,t')\,dt', \tag{3.59}$$

and further using $n(t-t') = \delta(t-t')$ gives

$$\frac{\partial}{\partial z}E_b(z,t) - \frac{\tilde{\alpha}}{2}E_b(z,t) = \tilde{\alpha}E_f\left(z, t - \frac{2\pi}{\Delta}\right)e^{-\left(\frac{2\pi}{\Delta}\right)^2\frac{\gamma^2}{2}}. \tag{3.60}$$

Since we are interested in first-echo the summation over peaks is dropped and solving for $E_b(z,t)$ gives

$$\begin{aligned} E_b(z,t) &= \tilde{\alpha}e^{-\left(\frac{2\pi}{\Delta}\right)^2\frac{\gamma^2}{2}} e^{\frac{\tilde{\alpha}z}{2}} \int_{L}^{z} e^{-\frac{\tilde{\alpha}z'}{2}} E_f\left(z', t - \frac{n2\pi}{\Delta}\right) dz', \\ &= \tilde{\alpha}e^{-\left(\frac{2\pi}{\Delta}\right)^2\frac{\gamma^2}{2}} E_f\left(0, t - \frac{2\pi}{\Delta}\right) \quad e^{\frac{\tilde{\alpha}z}{2}} \int_{L}^{z} e^{-\tilde{\alpha},z'}\,dz'. \end{aligned} \tag{3.61}$$

The output in the backward mode given as

$$E_b(0,t) = \tilde{\alpha}e^{-\left(\frac{2\pi}{\Delta}\right)^2\frac{\gamma^2}{2}} E_f\left(0, t - \frac{2\pi}{\Delta}\right)\int_{L}^{0} e^{-\tilde{\alpha}z'}\,dz', \tag{3.62}$$

and the efficiency of first echo is defined as the ratio of the total amount of light coming out in the first echo (at time $t = 2\pi/\Delta$) and the total input intensity, i.e.,

$$\eta_b = \frac{\int_{\pi/\Delta}^{3\pi/\Delta} |E_b(0,t)|^2\, dt}{\int |E_f(0,t)|^2\, dt} = e^{-\left(\frac{2\pi\gamma}{\Delta}\right)^2} (1 - e^{-\tilde{\alpha}L})^2 \tag{3.63}$$

which shows that efficiency is controlled by both finesse (Δ/γ) and the absorption ($\tilde{\alpha}$). The dependence over the absorption can be avoided by placing the AFC in a cavity making the efficiency limited only by the finesse [28].

3.3.3 Forward mode in AFC

In the forward mode the Eq. (3.59) changes to

$$\frac{\partial}{\partial z} E_f(z,t) = -\tilde{\alpha} \int_{-\infty}^{0} \eta(t-t') E_f(z,t')\, dt' - \tilde{\alpha} \int_{0}^{t} \eta(t-t') E_f(z,t')\, dt', \tag{3.64}$$

using same arguments in backward-mode and solving for $E_f(z,t)$ gives

$$E_f(z,t) = -\tilde{\alpha} e^{-\left(\frac{2\pi}{\Delta}\right)^2 \frac{\gamma^2}{2}} E_f\left(0, t - \frac{2\pi}{\Delta}\right) e^{-\frac{\tilde{\alpha} z}{2}} \int_0^z dz', \tag{3.65}$$

The output in the forward-mode is given as

$$E_f(L,t) = -e^{-\left(\frac{2\pi}{\Delta}\right)^2 \frac{\gamma^2}{2}} E_f\left(0, t - \frac{2\pi}{\Delta}\right) \quad \tilde{\alpha} L\, e^{-\frac{\tilde{\alpha} L}{2}}, \tag{3.66}$$

and the efficiency of first-echo, is written as

$$\eta_f = e^{-\left(\frac{2\pi\gamma}{\Delta}\right)^2} (\tilde{\alpha}L)^2 e^{-\tilde{\alpha}L}. \tag{3.67}$$

It is clear from the output equations that time for first-echo depends only on the teeth separation of AFC and in the limit $\Delta \gg \gamma$ AFC approaches to CRIB memories also the excitation at $t < 2\pi/\Delta$ can be transferred to a long lived spin-state for better storage times.

AFC are very robust in multi-mode storing, i.e. storing series of temporally separate

pulses. The shortest duration of each pulse is limited by $\tau_p \sim 1/(N\Delta)$ and total duration of input pulse is limited by $2\pi/\Delta$, hence the total number of stored modes is limited only by the number of tooth (N). Thus by adding more peaks on can in principle store any number of multi-modes.

Experiments Similar to CRIB, AFC-memories are tradtitonally performed in REIC at low temperatures $(< 5)K$. AFC in hot atomic vapours is proposed in [78].

In [28] Pr^{3+} ions are doped in Y_2SiO_5 crystal and the $|e\rangle$-$|g\rangle$ transitions is reshaped into a AFC with comb spacing 250 KHz, thus giving an echo time of 4 μs. The echo time is increased to 20 μs by applying the control pulses and shifting the excitation to a spin state. The total efficiency of the protocol is measured to be $\sim 3\%$. In a similar experiment [23] an AFC with comb spacing 660 KHz is obtained, giving an echo time of 1.5 μs and an efficiency of $\sim 10\%$.

Chapter 4

Intra-atomic frequency comb (I-AFC)

In the previous chapter we discussed how quantum memories allows for controlled and reversible transfer of the quantum information between the photonic and the matter systems. In all these quantum memories the incoming photon interacts with a carefully designed spectrum of the atomic ensemble. By controlling the shape and the characteristics of the spectrum one can store and retrieve photons from the ensemble.

Implementing AFC in an ensemble (in the usual way) relies on the frequencies of different atoms being stable relative to each other. This can be achieved in solids to some reasonable approximation at sufficiently low temperature. Here we study a frequency comb (FC) constructed by putting together multiple transitions between ground and excited state Fig. 4.1. The multiple transitions are obtained by splitting the hyper fine structure of an atom using an external magnetic field.

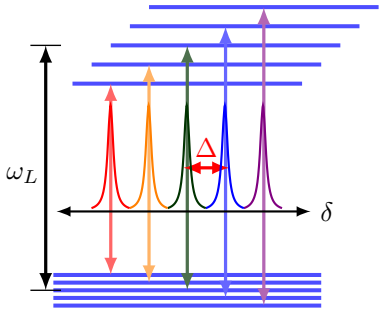

FIGURE 4.1: Multiple ground and excited states of an atom with different allowed transitions. The mean transition frequency is ω_L. The spacing between different transitions is Δ however this need not be same. Therefore, the spectrum forms a non-uniform AFC.

Since each atom consists the FC we call it intra-atomic frequency comb (I-AFC) [79]. The spacing between the different transition frequencies is controlled by applying external magnetic field.

In order to show that the I-AFC can be used for photonic quantum memories, we study the interaction of light with an AFC and show that photon-echo occurs from an ensemble of such atoms. The typical echo times in AFC are ~ 1 ns and are controlled by the spacing of the comb Δ . To achieve long storage time one can transfer the excitation from the excited states to spin states by applying π pulses.

The I-AFC exists in every atom hence it can be used alone or in ensemble to realize efficient quantum memories. Since the FC is constructed from different transitions of individual atoms. An Important advantage of the proposed scheme is that the spacing between different teeth (Δ) of the FC is controlled by the external magnetic field. Therefore, the spacing of the comb can be controlled by varying the magnetic field which can influence the efficiency and the photon-echo time of the quantum memory.

In the following section we start by realizing I-AFC in an atom. Then we discuss the light of interaction with the I-AFC.

4.1 Transitions and amplitudes in Zeeman effect

The Hamiltonian of the atom in the presence of an external magnetic field can be written as

$$H = H_{_0} + H_{\text{hfs}} + H_{_B} \tag{4.1}$$

where $H_{_0}$ gives the fine structure (FS) of the atom and adding the interaction of nuclear spin with electron spin lifts the degeneracy in the FS to result in hyper fine structure (HFS). Adding $H_{_B}$ further splits the HFS into Zeeman levels. When strength of the magnetic field is adjusted this splitting can result in transitions with spacing much greater than the width of transitions. Since we are interested in the splitting of fine structure, the following notation is introduced

$$H' = H_{\text{hfs}} + H_{_B} \tag{4.2}$$

where H' can be seen as correction to H_0. The hyperfine correction due to nuclear spin interaction is given as [40]

$$H_{\text{hfs}} = A(\mathbf{I}\cdot\mathbf{J}) = \frac{A}{2}(F^2 - I^2 - J^2), \tag{4.3}$$

where A is the hyperfine structure constant. The interaction due to magnetic field is written as

$$H_B = -(\hat{\mu}_{\mathbf{J}} + \hat{\mu}_{\mathbf{I}})\cdot\mathbf{B} = (g_J\mu_B J_z - g_I\mu_N I_z)B, \tag{4.4}$$

where μ_B and μ_N are the Bohr and nuclear magneton. The Lande g-factor (g_J) is given by

$$g_J = 1 + \frac{J(J+1) + S(S+1) - L(L+1)}{2J(J+1)}. \tag{4.5}$$

whereas g_I differs form atom to atom, for example $g_I = 0.7369$ from Cesium and $g_I = 0.54108$ for Rubidum atom [40].

To calculate the perturbed states and energies we solve

$$H' |\xi_n\rangle = E_n |\xi_n\rangle , \tag{4.6}$$

then the transition dipole strength is given as $\langle\xi_m|\mathbf{d}|\xi_n\rangle$. In the next chapter we solve Eq. (4.6) for Cesium and Rubidium atoms to construct I-AFC.

4.2 I-AFC interacting with light: a toy model

We start with a toy model with a single ground state and N number of degenerate excited states (Fig. 4.2b). The excited states are chosen such that the transitions are possible only between the ground state and the excited states and the transitions are forbidden among excited states. The mean transition frequency is ω_L, and the spacing between different transitions is considered to be Δ; hence, the transition spectrum for this atom will resemble an AFC. The question is whether a photon-echo can be observed in this ensemble in order to be eligible for quantum memory.

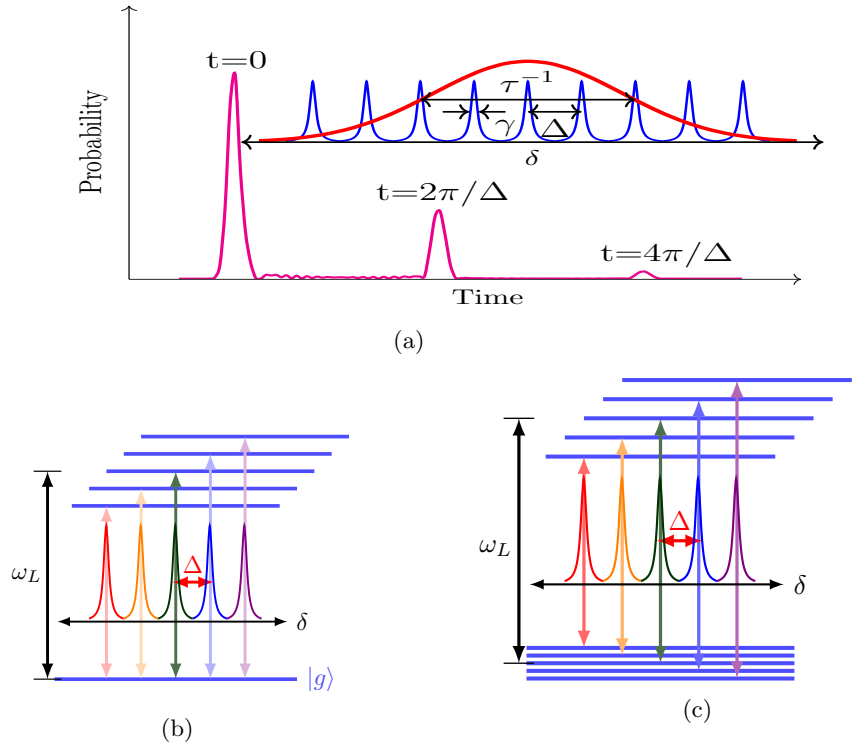

FIGURE 4.2: (a) Electric field output from an AFC. Here the first peak at time $t = 0$ shows the probability (intensity) of the unabsorbed light. Numerical calculations show a photon-echo at time interval of $2\pi/\Delta$. In the inset, we show the spectrum of the AFC. The teeth in the AFC have width γ and are separated by Δ. Here, $\Gamma = N\Delta$ is the width of the comb for N number of teeth, δ is the detuning, and τ is the temporal width of input laser pulse. (b) An atom with a single ground state and multiple degenerate excited states. The degeneracy between the excited states is lifted by applying external magnetic field. ω_L is the mean transition frequency between the ground and the excited states and $\Delta \ll \omega_L$ is the spacing between different transitions. Each of the transition has a natural line-width γ. Hence, the transition spectrum of this atom forms an AFC. (c) Here we consider multiple ground and excited states with different allowed transitions. The mean transition frequency is ω_L; however, the spacing between different transitions need not be same. Therefore, the spectrum forms a non-uniform AFC.

The Hamiltonian for this atom in the presence of electromagnetic field reads

$$H_s = \sum_{n=1}^{N} \hbar\omega_{n0} \left|n\right\rangle\!\left\langle n\right| - \frac{\mathcal{E}(z,t)\, d}{2} \sum_{n=1}^{N} (\left|n\right\rangle\!\left\langle 0\right| e^{i\omega_L t} + h.c) \tag{4.7}$$

and in the interaction picture the operator is transformed as $e^{iH_0 t}\ (H_s - H_0)\ e^{-iH_0 t}$ and with $H_0 = \hbar\omega_L \left|n\right\rangle\!\left\langle n\right|$ Eq. (4.7) gives

$$H = \sum_{n=1}^{N} \hbar\delta_n \left|n\right\rangle\!\left\langle n\right| - \frac{\mathcal{E}(z,t)\, d}{2} \sum_{n=1}^{N} (\left|n\right\rangle\!\left\langle 0\right| + \left|0\right\rangle\!\left\langle n\right|) \tag{4.8}$$

where δ_n is the detuning between the mean frequency ω_L of light and the frequency of the n-th excited state

If the state of the atom at time t is given as the superposition of all the states, i.e., $|\psi(t)\rangle = \sum_{n=0}^{N} c_n(t)\,|n\rangle$, then the dynamical equation in terms of the coefficients $c_n(t)$ reads

$$\dot{c}_n = \frac{id}{2\hbar}\mathcal{E}(z,t)c_0 - i\delta_n c_n, \quad \dot{c}_0 = \frac{id}{2\hbar}\mathcal{E}(z,t)\sum_{n=1}^{N} c_n(t). \tag{4.9}$$

The interaction between the photon and the atom is weak. Hence, the probability of finding the atom in the ground state is almost unity, i.e, $|c_0|^2 \simeq 1$. Therefore,

$$c_n(t) = \frac{id}{2\hbar}e^{-i\delta_n t}\int_{-\infty}^{t} e^{i\delta_n t'}\mathcal{E}(z,t')\,dt'. \tag{4.10}$$

For a Gaussian input, i.e., electric field of the form $\mathcal{E}(z,t) = \mathcal{E}_0 \exp\left(-t^2/2\tau^2\right)$ with the temporal width $\tau \ll t$ Eq. (4.10) yields

$$c_n(t) = \frac{i\Omega}{2}\frac{\sqrt{\pi}}{\bar{\omega}}\exp\left[-(\delta_n\tau)^2/2 - i\delta_n t\right],$$

where $\Omega = \dfrac{d\mathcal{E}_0}{\hbar}$.

Since we have assumed equispaced excited states we can write $\delta_n = \delta_0 + n\Delta$ for some constant δ_0. The photon emission probability $P(t)$ (for forward propagation) for this atomic system can be redefined as

$$P(t) = |\,\langle 0|\,s_-\,|\psi(t)\rangle\,|^2 = \left|\frac{i\Omega}{2}\frac{\sqrt{\pi}}{\bar{\omega}}\sum_{n=1}^{N} e^{-int\Delta}\right|^2, \tag{4.11}$$

where $s_- = \sum_n |0\rangle\langle n|$ and the sum is over all the states in the excited level. Here we have assumed that $\bar{\omega} = \tau^{-1} \gg \Delta$ which implies that $\exp\left[-(n\Delta)^2/2\bar{\omega}^2\right] \to 1$. Clearly, Eq. (4.11) results in a photon-echo at $t = 2\pi/\Delta$ when the probability of the photon emission is maximum , see Fig. 4.2.

4.3 I-AFC

In the above toy model we qualitatively showed that an I-AFC will re-phase with a time period of $2\pi/\Delta$, nonetheless the wave propagation through I-AFC is avoided for simplicity. To understand the dynamics in realistic settings, we consider a multi level atom with n excited states $|e_n\rangle$ and m ground states $|g_m\rangle$. Then the free hamiltonian is written as

$$H_f = \sum_{n=1}^{N_e} \hbar\omega_n^e \, |e_n\rangle\langle e_n| + \sum_{m=1}^{N_g} \hbar\omega_m^g \, |g_m\rangle\langle g_m| \tag{4.12}$$

and the dipole interaction is given as

$$H_{\text{int}} = \sum_{n=1}^{N_e} -\frac{\mathcal{E}(z,t)}{2}\left(\sum_{n,m} d_{nm} \, |e_n\rangle\langle g_m| \, e^{-i\omega_L t} + H.C\right) \tag{4.13}$$

where d_{nm} is the transition dipole moment between $|e_n\rangle$ and $|g_m\rangle$. Here we are assuming that the transition among the ground states and among the excited states is forbidden. Therefore, $d_{nn'} = d_{mm'} = 0$. The Hamiltonian in the interaction picture can be calculated with $H_0 = \sum_{n=1}^{N_e} \hbar\omega_L \, |e_n\rangle\langle e_n|$ gives

$$H_I = \sum_{n=1}^{N_e} \hbar(\omega_n^e - \omega_L) \, |e_n\rangle\langle e_n| + \sum_{n=1}^{N_g} \hbar\omega_n^g \, |g_n\rangle\langle g_n| - \frac{\mathcal{E}(z,t)}{2}\left(\sum_{n,m} d_{nm} \, |e_n\rangle\langle g_m| + H.C\right), \tag{4.14}$$

we assume that the number of atoms in the ensemble is much larger than the average number of photons in the light pulse, therefore, the population is assumed to be in the ground state, i.e., $\sum_m \rho_{mm} \simeq 1$ and $\rho_{nn} \simeq \rho_{nn'} \simeq \rho_{mm'} \simeq 0$ but $\rho_{nm} \neq 0$. This yields the dynamical equation for the coherence [79]

$$\frac{\partial \rho_{nm}(z,t)}{\partial t} + \left(i\delta_{nm} + \frac{\gamma}{2}\right)\rho_{nm}(z,t) = \frac{i d_{nm}}{2\hbar}\rho_{mm} \, \mathcal{E}(z,t). \tag{4.15}$$

where $\delta_{nm} = [(\omega_n^e - \omega_m^g) - \omega_L]$ is the detuning between the transition $|e_n\rangle \leftrightarrow |g_m\rangle$ and the mean frequency of the laser light and γ is spontaneous decay rate of the transition. Using the definition for the atomic polarization Eq. (2.27).

$$\mathcal{P}(z,t) = 2\mathcal{N} \sum_{n,m} d_{nm}^* \rho_{nm}, \tag{4.16}$$

and taking Fourier transform of Eq. (4.15) we can arrive at the equations

$$\tilde{\rho}_{nm}(z,\omega) = \frac{id_{nm}\,\rho_{mm}}{2\hbar}\frac{\tilde{\mathcal{E}}(z,\omega)}{i(\delta_{nm}+\omega)+\gamma/2}, \tag{4.17}$$

$$\mathcal{P}(z,\omega) = 2\mathcal{N}\sum_{n,m}\frac{i|d_{nm}|^2\rho_{mm}}{2\hbar}\frac{\tilde{\mathcal{E}}(z,\omega)}{\gamma/2+i(\delta_{nm}+\omega)}, \tag{4.18}$$

and propagation equation for $\tilde{\mathcal{E}}(z,\omega)$

$$\left(\frac{\partial}{\partial z}+\frac{i\omega}{c}\right)\tilde{\mathcal{E}}(z,\omega) = \frac{i\omega_L}{2\epsilon_0 c}\mathcal{P}(z,\omega). \tag{4.19}$$

From here it is straight forward to solve for $\tilde{\mathcal{E}}(z,\omega)$ which reads

$$\tilde{\mathcal{E}}(z,\omega) = \tilde{\mathcal{E}}(0,\omega)e^{-\mathcal{D}z} \tag{4.20}$$

where $\mathcal{D}$ is defined as

$$\mathcal{D} = \frac{\mathcal{N}\omega_L}{2\hbar\epsilon c}\sum_n\frac{|d_n|^2}{\gamma/2+i(\delta_n+\omega)}+\frac{i\omega}{c}, \tag{4.21}$$

here the absorption coefficient of a transition is defined as $\mathcal{C}_n = \frac{|d_n|^2\mathcal{N}\omega_L}{2\hbar\epsilon c}$. Clearly the first term in $\mathcal{D}$ is a comb where the Lorentzian distributions in ω are placed at δ_n. The second term results in a position dependent phase where $\omega/c = k$. Inverse Fourier transform of $\tilde{\mathcal{E}}(z,\omega)$ gives the output in the time domain. For example in Fig. 4.3 we solve Eq. (4.20) with an ideal comb spacing of $\Delta = 300$ MHz and we can see that the echo-time is $2\pi/\Delta$. Since in a ideal comb the echo is obtained at $2\pi/\Delta$ we characterize the quality of the quantum memory by efficiency η and fidelity $\mathfrak{F}$

$$\eta = \frac{\int_{\pi/\Delta}^{3\pi/\Delta}|\mathcal{E}(L,t)|^2\,dt}{\int|\mathcal{E}(0,t)|^2\,dt}, \quad \mathfrak{F} = \frac{\left|\int_{\pi/\Delta}^{3\pi/\Delta}\mathcal{E}^*(0,t-2\pi/\Delta)\;\mathcal{E}(L,t)\,dt\right|^2}{\int|\mathcal{E}(0,t-2\pi/\Delta)|^2\,dt\;\int_{\pi/\Delta}^{3\pi/\Delta}|\mathcal{E}(L,t)|^2\,dt}. \tag{4.22}$$

Theoretically, similar to AFC the maximum efficiency that can be achieved with an I-AFC between $|e\rangle$-$|g\rangle$ is $< 54\%$ [76]. To store the excitation for a long time the excitation we construct another frequency comb between the transition $|e\rangle$-$|s\rangle$. Then the excitation is transferred to a long-lived spin state ($|s\rangle$) by applying a π pulse, before the first echo. This excitation can be retrieved at a later time by applying another π-pulse which transfers the

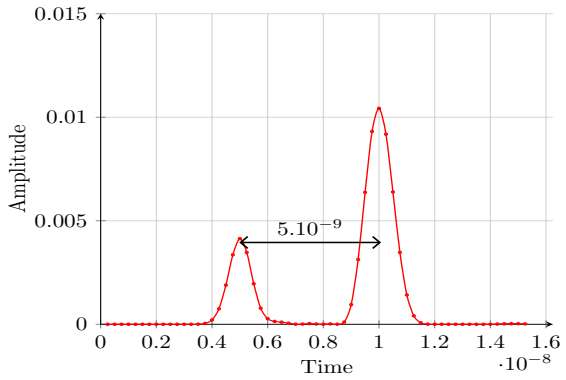

FIGURE 4.3: Photon echo with the parameters $\Delta = 200$ MHz, $\gamma = 5$ MHz and $gz = 50$ MHz.

excitation from the spin state to the excited state from where we can observe a photon echo at time $2\pi/\Delta$ [28]. In this scenario the efficiency of the photon echo of I-AFC can approach $\sim 100\%$ [76, 79].

Chapter 5

Randomness in I-AFC

One of the limitation of the I-AFC is that the frequency combs obtained in natural atomic systems are not always uniform. The non-uniformity can be due to unequal absorption or due to unequal spacing between different hyperfine states. This may severely affect the storage quality i.e., the quality of the quantum memory, forcing us to choose the atomic systems which have almost uniform frequency combs. Further, the temperature of the atomic ensemble and the local fluctuations in the electric and magnetic fields can cause fluctuations in various parameters of the frequency comb. For example, the stray electric field can shift the frequency comb. Therefore, random fluctuations in the electric field can give rise to broadening of the transition lines. Similarly, fluctuating magnetic field can affect the spacing between different transitions.

Here we study the effect of various environmental factors on I-AFC based quantum memory. The effect of the environment is incorporated as random fluctuations and non-uniformity in the parameters such as comb spacing and the optical depth, of the frequency comb. Since, fluctuating environment affects the absorption, the line width, and the mean frequency of the transition, we study the effect of fluctuation in these quantities without considering any specific model for the environment. The effect of random fluctuations in the absorption and the comb spacing is incorporated by introducing randomness in the said parameters stochastically and then the macroscopic polarization is obtained by averaging over the fluctuations.

In the following sections we show the effect of temperature on I-AFC. We further study the effect of non-uniformity and local fluctuations on the efficiency of I-AFC based quantum memory. As an example, we also consider the I-AFC in the Cesium (Cs) and

Rubidium (Rb) atoms.

5.1 Doppler broadening

An atom moving with velocity $\boldsymbol{v}$ experiences a change of frequency of the incoming light from ω_L to $\omega_L + \boldsymbol{k}\cdot\boldsymbol{v}$, where $\boldsymbol{k}$ is the wave vector of the incoming light such that $|\boldsymbol{k}| = \omega_L/c$. This will modify the detuning of a given transition from δ to $\delta + \boldsymbol{k}\cdot\boldsymbol{v}$. In the I-AFC system, this frequency shift results in the following expression for the atomic polarization Eq. (4.18) [79]:

$$\mathcal{P}(z,\omega,\boldsymbol{v}) = 2\mathcal{N}\sum_n \frac{i|d_n|^2}{2\hbar}\frac{\tilde{\mathcal{E}}(z,\omega)}{\gamma/2 + i(\delta_n + \boldsymbol{k}\cdot\boldsymbol{v} + \omega)}. \tag{5.1}$$

The velocity of an atom in thermal equilibrium at temperature T is governed by the Maxwell-Boltzmann distribution $p(\boldsymbol{v}) \equiv p_v \propto \exp\left(-mv^2/2k_BT\right)$. Thus, the effects of temperature can be incorporated in the atomic polarization by averaging the polarization over the velocity distribution p_v [35]. Here m is the mass of the atom and k_B is the Boltzmann constant. Since, only the velocity component along the direction of propagation of light contributes to the Doppler shift, we consider the velocity only along the z-axis, i.e., $\boldsymbol{v} = v\hat{z}$. The average macroscopic polarization is given as

$$\mathcal{P}(z,\omega) = \int \mathcal{P}(z,\omega,v)\; p_v\; dv,. \tag{5.2}$$

In order to solve for the atomic polarization analytically, we replace the Gaussian probability distribution with a corresponding Lorentzian of the form $L_v = \dfrac{a}{\pi(a^2+v^2)}$ where the width $a \propto \sqrt{\dfrac{2k_BT}{m}}$ [80]. On replacing $p_v \to L_v$ Eq. (5.2) gives

$$\mathcal{P}(z,\omega,T) = \tilde{\mathcal{E}}(z,\omega)\sum_n \frac{\mathcal{N}}{\hbar}\frac{i|d_n|^2}{\gamma/2 + ka + i(\delta_n + \omega)}, \tag{5.3}$$

which shows that the natural broadening is increased due to the thermal velocity distribution. Then the output electric field at temperature T is written as

$$\tilde{\mathcal{E}}(z,\omega) = \tilde{\mathcal{E}}(0,\omega)e^{-\mathcal{D}z} \tag{5.4}$$

where

$$\mathcal{D} = \sum_n \frac{i\gamma\alpha_n}{\gamma/2 + ka + i(\delta_n + \omega)}, \qquad \alpha_n = \frac{\mathcal{N}\rho_{nn}|d_n|^2\omega_L}{2\hbar\epsilon c\gamma}. \tag{5.5}$$

where $\alpha_n L$ gives optical depth of n^{th} transition.

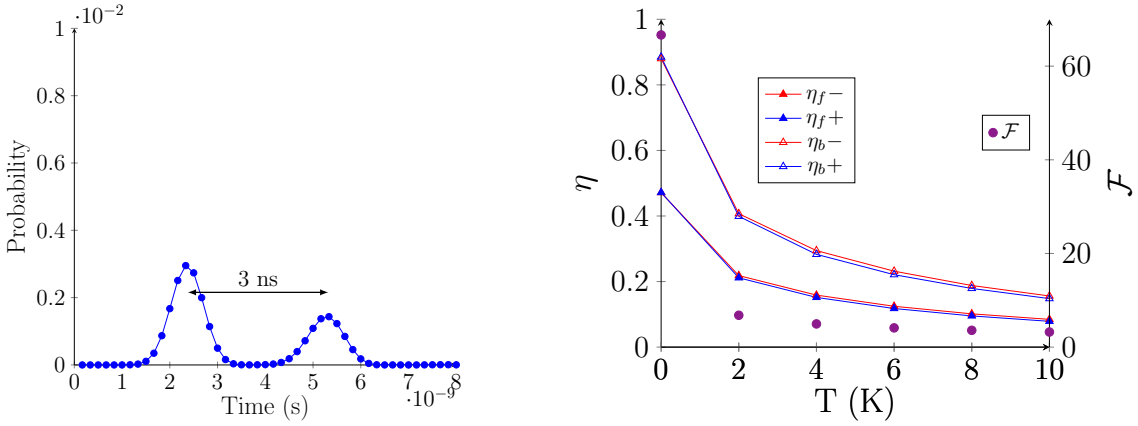

(a) (b)

FIGURE 5.1: (a) Here we show the photon-echo from an I-AFC ensemble at temperature T = 10K. The echo occurs at 3ns after the absorption. (b) Due to the Doppler broadening the efficiency of the quantum storage decrease as we increase the temperature. Here we show the relation between the efficiency of the storage for the forwards and backward modes and the Finesse of the I-AFC as a function of temperature.

In Fig. (5.1a) we plot the photon-echo at temperature $T = 10$K and in Fig. 5.1b we present the efficiencies of the forward and backward propagation as a function of temperature. Fig. 5.1b shows that the I-AFC based quantum memory can be useful for temperatures as high as 10K. We can also see increase in efficiency with finesse ($\mathcal{F}$), here we define $\mathcal{F} = \Delta/(\gamma + 2ka)$ where the comb spacing (Δ) is obtained by inverting the echo time.

Since in a ideal comb the echo is obtained at $2\pi/\Delta$ we characterize the quality of the quantum memory by efficiency η and fidelity $\mathfrak{F}$

$$\eta = \frac{\int_{\pi/\Delta}^{3\pi/\Delta} |\mathcal{E}(L,t)|^2\, dt}{\int |\mathcal{E}(0,t)|^2\, dt}, \quad \mathfrak{F} = \frac{\left|\int_{\pi/\Delta}^{3\pi/\Delta} \mathcal{E}^*(0, t - 2\pi/\Delta)\ \mathcal{E}(L,t)\, dt\right|^2}{\int |\mathcal{E}(0,t-2\pi/\Delta)|^2\, dt \ \int_{\pi/\Delta}^{3\pi/\Delta} |\mathcal{E}(L,t)|^2\, dt}. \tag{5.6}$$

A general fluctuation in I-AFC can be broadly classified into :

- **Random and non-uniform comb spacing**: In random comb spacing we shift

the mean frequency of the I-AFC by the random number ζ with probability $P(\zeta) \propto \exp\Big[-\zeta^2/(2\sigma_\zeta^2)\Big]$. In non-uniform comb spacing, the individual peaks of I-AFC are shifted randomly but there is no fluctuations in the mean frequencies.

- **Random and non-uniform optical depth**: In random optical depths we shift the amplitudes of the peaks by the random number ζ with probability $P(\zeta) \propto \exp\Big[-\zeta^2/(2\sigma_\zeta^2)\Big]$. In non-uniform optical depths, the individual peaks heights are shifted randomly.

The random effects are incorporated in the macroscopic polarization by averaging over the fluctuating polarization with a random parameter ζ which occurs with probability distribution $P(\zeta)$. The formal expression for the average polarization reads

$$\mathcal{P}(\omega) = \tilde{\mathcal{E}}(\omega) \int \mathcal{D}(\omega, \zeta)\ P(\zeta)\ d\zeta. \tag{5.7}$$

For the purpose of calculations, we consider an I-AFC with a total of seven teeth at temperature $T = 10$ K and light pulse with Gaussian spectrum of the following form:

$$\tilde{\mathcal{E}}(0, \omega) = \exp\left[-\frac{\omega^2}{2(2\Delta)^2}\right], \tag{5.8}$$

where Δ is the average comb spacing. The total spectral width of the photon is chosen in such a way that it covers all the seven peaks of the frequency comb.

5.2 Random comb spacing

Although, the spacing between different hyperfine energy levels is predominately determined by the applied external magnetic field, the spin-orbit coupling and interactions with the nuclear spins can result in non-uniform spacing between these energy levels. This non-uniformity can make a frequency comb unusable for purpose of quantum memory. Furthermore, when we dope these atoms in some dielectrics, or due to stray electric and magnetic fields, there can be fluctuations in the mean frequencies of different transitions. In this section, we address the effect of these adversaries on the efficiency of the I-AFC based quantum memory.

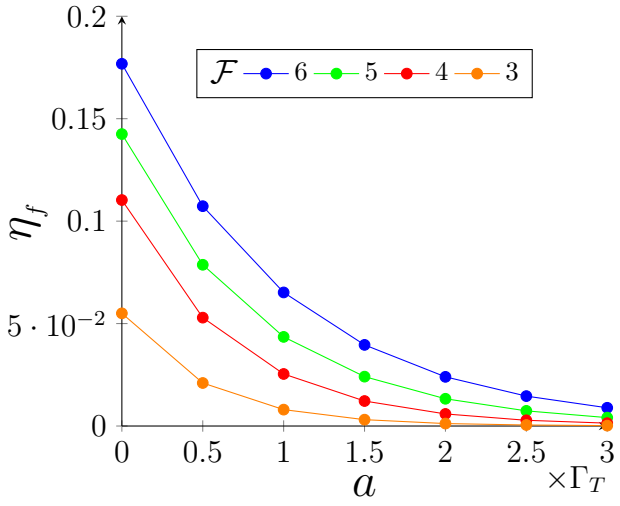

FIGURE 5.2: Here we have plotted the efficiencies as a function of the fluctuation strength a of the comb spacing and for various values of the finesse $\mathcal{F} = \Delta/(\gamma + 2\Gamma_T)$. We have chosen the optical depth $\alpha L = 30$, tooth width $\gamma = 5$MHz and the calculations are done at temperature $T = 10$K. From here we can see that although the efficiency is decreasing as we increase the randomness, the efficiencies are significant even at fluctuations of the order of Doppler broadening Γ_T.

We start with fluctuations in the comb spacing, which is introduced by shifting the comb spacing by a random number ζ with probability $P(\zeta) \propto \exp\left[-\zeta^2/(2\sigma_\zeta^2)\right]$. Here we have assumed the probability distribution to be Gaussian with width σ_ζ. In this scenario, the propagator $\mathcal{D}$ reads

$$\mathcal{D}(\omega, \zeta) = \sum_{n=-3}^{3} \frac{\gamma\alpha_n}{\gamma/2 + \Gamma_T + i(n\Delta + \zeta + \omega)} + \frac{i\omega}{c}. \tag{5.9}$$

Following the approach given in Eq. (5.7) the averaged propagator is written as

$$\mathcal{D}(\omega) = \sum_{n=-3}^{3} \frac{\gamma\alpha_n}{\gamma/2 + \Gamma_T + a + i(n\Delta + \omega)} + \frac{i\omega}{c}, \tag{5.10}$$

where $2a \propto \sigma_\zeta$ is the FWHM of the probability distribution. Eq. (5.10) shows that a general randomness in the comb spacing increases the broadening similar to the Doppler broadening.

In Fig. 5.2 we plot the forward efficiencies as a function of width a for different values of finesse $\mathcal{F}$. Here Γ_T ($\sim 5 \times 10^7$) $\gg \gamma$ ($\sim 5 \times 10^6$) thus making the Doppler broadening dominant over natural broadening and we take the randomness a as a multiple of the Doppler width Γ_T. We observe that the efficiency drops with increasing

randomness. However, increasing the finesse results in higher efficiency; hence, the effect of the fluctuating comb spacing can be mitigated by applying stronger magnetic field. Interestingly, the effect of random fluctuations on the Fidelity between the input and output states is negligible. This is because the random fluctuations in the comb spacing effectively increases the tooth width which does not affect the phases in the outcome electric field.

5.3 Non-uniform comb spacing

Here, we consider the case when the frequency comb is not uniform but there is no fluctuations in the mean frequencies. For such systems the propagator $\mathcal{D}$ can be written as

$$\mathcal{D} = \sum_{n=-3}^{3} \frac{\gamma\alpha_n}{\gamma/2 + \Gamma_T + i(\delta_n + \omega)} + \frac{i\omega}{c}. \tag{5.11}$$

For simplicity, we can assume the frequency δ_n of each of the tooth as a deviation from a average position, i.e., $\delta_n = n\Delta + \zeta_n$, where ζ_n is fixed and sampled randomly from the set $[-a\Gamma_T, a\Gamma_T]$. We use the standard deviation in the mean frequency of each of the tooth of the frequency comb as the measure for the non-uniformity in the frequency comb. The standard deviation can be calculated using the following expression

$$\sigma_\Delta^2 = \frac{1}{N-1} \sum_{n=-3}^{3} (\zeta_n^2 - \langle\zeta\rangle^2), \tag{5.12}$$

where N is the number of teeth.

In Figs. 5.3a and 5.3b we plot the numerically optimized efficiencies as a function of standard deviation in comb spacing for different finesse. Since multiple non-uniform combs can have the same value of the standard deviation σ_Δ, we can have a band of efficiencies for the same σ_Δ. We see that this band broadens with the standard deviation σ_Δ which itself is a function of a. An interesting finding of this plot is that occasionally large σ_Δ can result in higher efficiencies than the perfectly uniform combs. In other words, the uniform combs are not optimum for efficient quantum memory. Although there is no obvious explanation for this increase in the efficiency, we noticed that for some of these

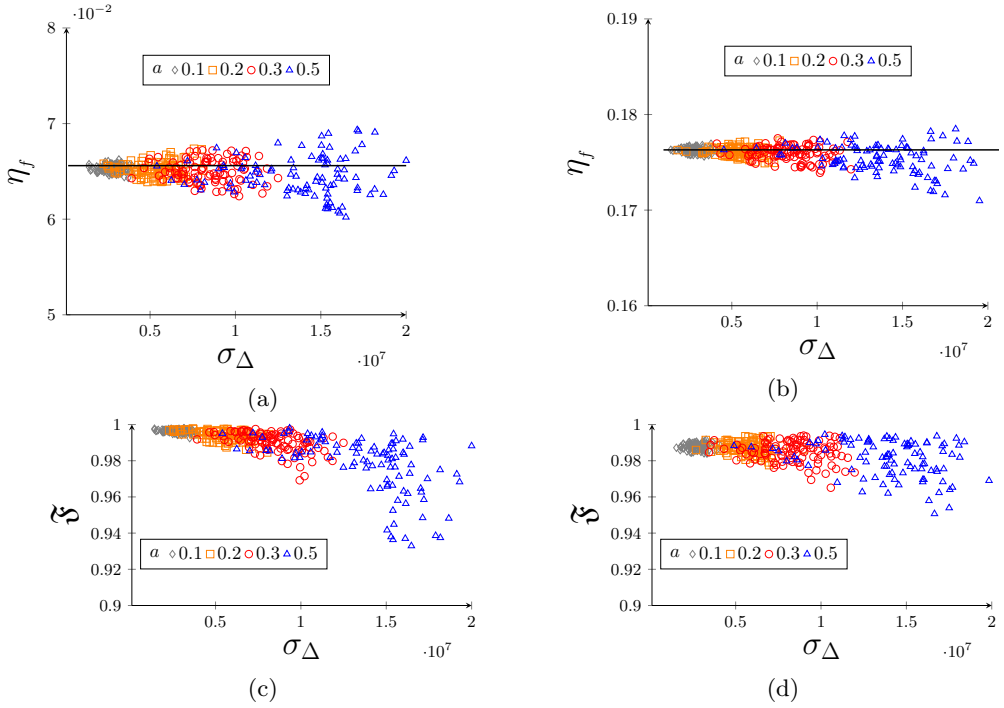

FIGURE 5.3: In a and b we plot the efficiency for non-uniform comb with no fluctuations in the tooth-spacing. Here the non-uniformity is quantified by the standard deviation σ_Δ of mean frequency of each of the tooth in the frequency comb. We have set $\mathcal{F} = 3$, $\alpha L = 18$ for Fig. a and $\mathcal{F} = 6$, $\alpha L = 30$ for Fig. b, and the dashed line represents efficiency for the uniform comb. In c and d we plot the corresponding fidelities for the figures a and b.

cases the average finesse is also larger than the ideal comb. Larger finesses is known to improved efficiency. For example, if we choose fluctuations from the set $[0, a\Gamma_T]$ for the teeth that are on the right side of the center of the frequency comb and from the set $[-a\Gamma_T, 0]$ for the teeth on the left of the center such that the comb is symmetric about the center, we always observe an improved efficiency. In Figs. 5.3c and 5.3d we plot the fidelity as a function of σ_Δ. Unlike the efficiency, the variation in the fidelity is not too severe.

5.4 Random and non-uniform optical depths

The optical depth of various teeth in I-AFC in natural atoms is non-uniform in general. The non-equal transition probability between different atomic states is one of the biggest contributor to such non-uniformity. This can be further exaggerated by random environmental effects. In this section we study the effect of non-uniform optical depth and

fluctuation therein of different teeth of the I-AFC on the efficiency of the quantum memory. Similar to Sec. 5.2, we incorporate the fluctuating optical depth in I-AFC dynamics by adding randomness in the propagator $\mathcal{D}$ as follows

$$\mathcal{D} = \sum_n \frac{(\gamma\alpha_n + \zeta_n)}{\gamma/2 + \Gamma_T + i(n\Delta + \omega)} + \frac{i\omega}{c}, \tag{5.13}$$

where ζ_n determine the fluctuations in the optical depth and it occurs with probability $P(\zeta) \propto \exp\left[-\zeta^2/2\sigma_\zeta^2\right]$. The average propagator can be calculated by taking average of Eq. (5.13) with the probability function $P(\zeta)$. Since the probability is an even function of ζ, from Eq. (5.7) we can see that the randomness has no effect on the optical depths. This shows that the fluctuating optical depths do not affect the efficiency of the quantum memory.

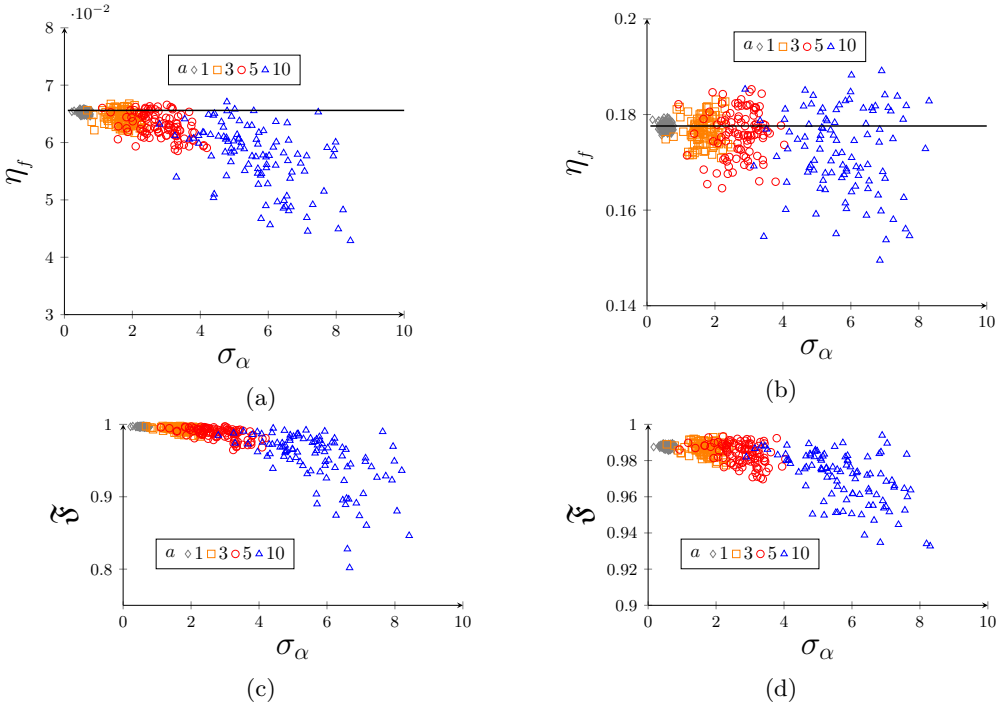

FIGURE 5.4: In a ($\mathcal{F} = 3$, $\alpha L = 18$) and b ($\mathcal{F} = 6$, $\alpha L = 30$) we plot efficiency and standard deviation of optical depths over 100 trails where dashed line represents efficiency with zero randomness. In c and d we plot the corresponding fidelities.

However, the non-uniform optical depth without fluctuations can result in the lower quality of the memory. In this case, the propagator for such systems is defined by Eq. (5.13) but there is no probability distribution over ζ. But ζ_n is sampled from the set $[-a, a]$. The non-uniformity of the comb is quantified by the standard deviation which is defined as $\sigma_\alpha^2 = 1/(N-1)\sum_{n=-3}^{3}(\zeta_n^2 - \langle\zeta\rangle^2)$ for N number of teeth.

In Fig. 5.4 we plot the efficiency and the fidelity as a function of standard deviation in optical depth for different finesse. The calculations are done at temperature $T = 10$K. The results for non-uniform optical depth are qualitatively similar to the one we got for non-uniform comb spacing. In this case also we see the non-uniform comb occasionally yield more efficient quantum memory as oppose to uniform comb. This might be because of the occasional average increase in the absorption strength of the frequency comb.

This shows that the fluctuations in different parameters in the I-AFC affect the quality of the photon storage differently. The fluctuations in the absorption in different teeth of the comb, i.e., non-uniformity in the height of the teeth has negligible effect on the efficiency. Whereas the fluctuations in the comb spacing has significant effect. Fortunately, this adverse effect can be mitigated by increasing the finesse of the frequency comb, which can be done by increasing the external magnetic field. Similarly, the fidelity between the input and the output states is robust against the fluctuation in the absorption and the comb spacing. Furthermore, we showed that the non-uniform frequency combs without any fluctuations in the comb parameters can also yield efficient quantum memory. Since the intra-atomic frequency combs found in natural atomic systems are often non-uniform, our results suggest that a large class of these systems can be used for I-AFC based efficient quantum memory.

5.5 Cesium and Rubidium

TABLE 5.1: Transition energies and amplitudes in Cs atom

Transitions in MHz	Detuning δ_n	Amplitude $(\lvert d_n\rvert^2)$ in $(ea_o)^2$
1467.76	-1105.29	0.0119
1871.67	-701.379	0.021
2237.08	-335.975	0.0283
2573.05	0	0.0346
2885.59	312.539	0.04
3178.89	605.845	0.0447
3320.06	747.013	0.0135

(a)

Transitions in MHz	Detuning δ_n	Amplitude $(\lvert d_n\rvert^2)$ in $(ea_o)^2$
7242.76	-931.6	0.0164
7427.04	-747.317	0.0319
7815.46	-358.897	0.0245
8174.36	0	0.0183
8509.73	335.368	0.0129
8825.77	651.409	0.0081
9125.56	951.205	0.0039

(b)

TABLE 5.2: I-AFC in Cesium atom. (a) Transition frequencies and amplitudes for the selection rule $\Delta M_F = -1$. (b) Transition frequencies and amplitudes for the selection rule $\Delta M_F = 1$.

TABLE 5.3: Transition energies and amplitudes in Rb atom

Transitions in MHz	Detuning δ_n	Amplitude $(\lvert d_n\rvert^2)$ in $(ea_o)^2$
865.724	-990.228	0.292681
1160.27	-695.684	0.284192
1486.25	-369.705	0.275183
1855.95	0.	0.265686
2225.03	369.075	0.0975561
2292.66	436.708	0.256044
2852.87	996.919	0.248483

(a)

Transitions in MHz	Detuning δ_n	Amplitude $(\lvert d_n\rvert^2)$ in $(ea_o)^2$
-2359.16	-996.92	0.248479
-1798.95	-436.708	0.256039
-1362.24	0	0.265682
-992.536	369.705	0.27518
-666.557	695.683	0.28419

(b)

TABLE 5.4: I-AFC in Rubidium. (a) Transition frequencies and amplitudes for the selection rule $\Delta M_F = -1$. (b) Transition frequencies and amplitudes for the selection rule $\Delta M_F = 1$.

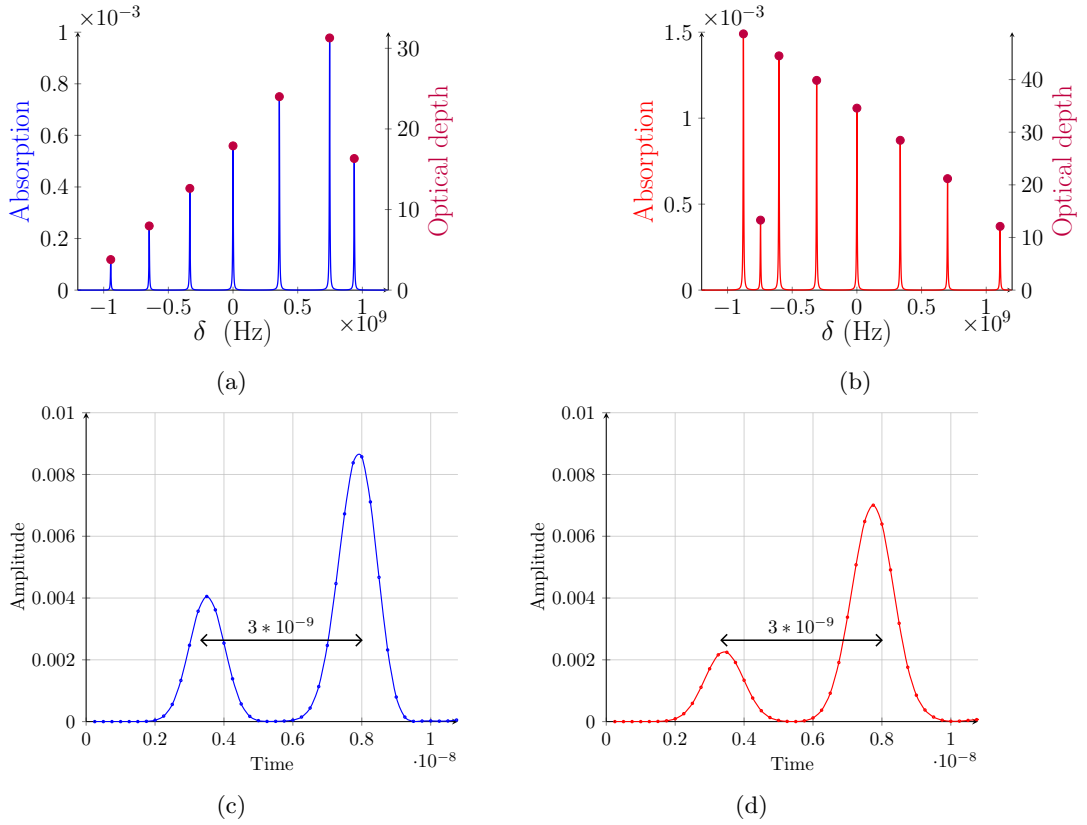

FIGURE 5.5: Non-Uniform AFC and the photon-echo in Cs atom at magnetic field $B = 0.1$T. (a), (b): Numerically calculated absorption and optical-depths for various transitions for $\Delta m = +1$ and $\Delta m = -1$. Here the x-axis is the detuning with respect to the incoming light and y-axis is the value of the absorption for various transitions. The solid circles represent the optical depth corresponding to each transition, length of the vapour cloud cell $L = 5cm$ (c), (d): The photon echo observed in Cs atoms for $\Delta m = \pm 1$ transitions.

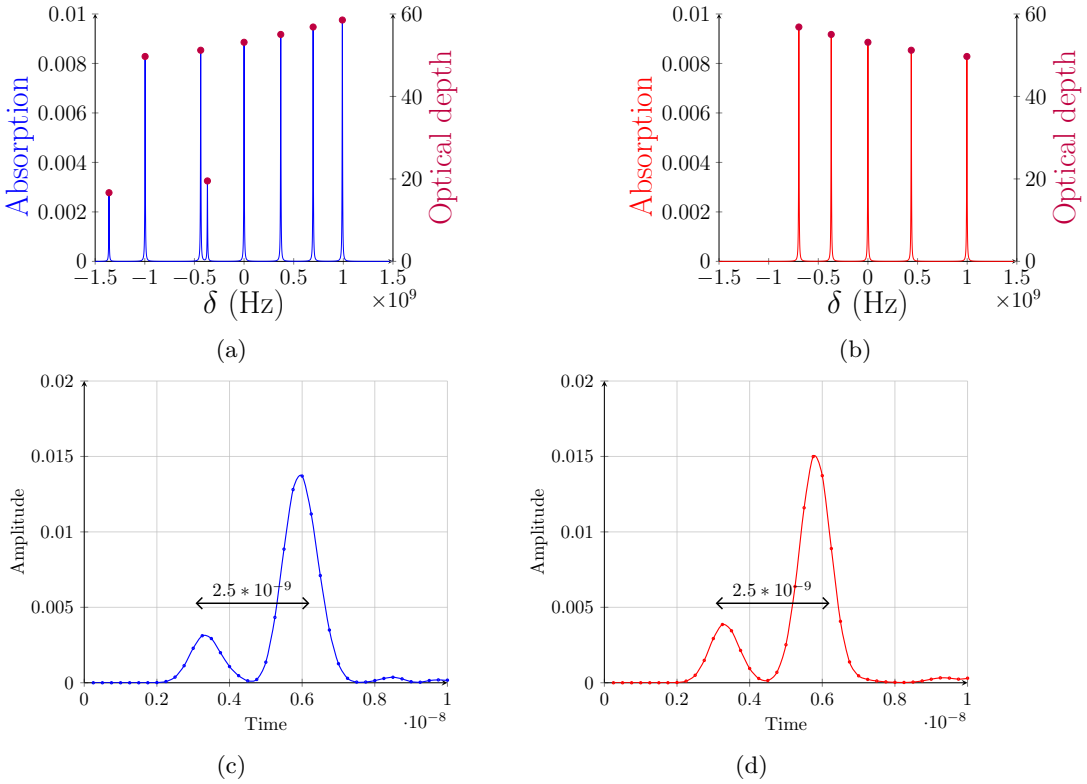

FIGURE 5.6: Non-Uniform AFC and the photon-echo in Rb atom at magnetic field $B = 0.15$T. (a), (b): Numerically calculated absorption and optical-depths for various transitions for $\Delta m = +1$ and $\Delta m = -1$. (c), (d): The photon echo observed in Cs atoms for $\Delta m = \pm 1$ transitions.

Now we discuss a physical example of I-AFC in Cs and Rb atoms. We show that, despite the non-uniformity and fluctuations in the frequency combs, both Cs and Rb atomic ensembles can provide a robust and efficient I-AFC We construct an I-AFC in Cs and Rb atoms and show that they results in echoes similar to an ideal I-AFC. We start by picking an optical transition in the atom, then we apply magnetic field interaction to split the degeneracy in hyper-fine levels. Magnetic fields strengths of $B \sim 0.1T$ in Cs and Rb atoms give I-AFC with comb spacing $\Delta = 300$MHz and $\Delta = 400$MHz. Hence the echo times $(2\pi/\Delta)$ for Cs and Rb are expected to be ~ 3ns and ~ 2.5ns.

To obtain the energy corrections and the transition amplitudes we solve the eigenvalue equation Eq. (4.6) (see appendix). On solving the equation for Cs gives the Table. 5.2 and for Rb gives the Table. 5.4. We arrange the transitions based on their selection rules i.e. $\Delta M_F = \pm 1$.

On comparing the Eq. (4.18) with the atomic polarization ($\mathcal{P} = \epsilon_0 \chi \mathcal{E}$) gives the susceptibility χ as

$$\chi = \sum_n \frac{\mathcal{N}\rho_{nn}|d_n|^2}{\hbar\epsilon_0} \frac{1}{\gamma/2 + i(\delta_n + \omega)}, \qquad \alpha_n = \frac{\mathcal{N}|d_n|^2 \omega_L L}{\hbar\epsilon_0 c\gamma}. \tag{5.14}$$

here α_n is the optical depth of a transition. The working temperatures for I-AFC are $\sim$ 10K hence $\frac{K_B T}{2\hbar} \sim$ 1THZ. The energy gap among the ground state levels, with 0.1T of external magnetic field is $\sim$ 1GHZ. Since the thermal energy is much higher than the ground state energies, all the ground states will be equally populated i.e. $\rho_{nn} \approx 1/N_g$ with N_g being number of levels. We also redefine $\mathcal{N} \to \mathcal{N}/N_g$.

The absorption of the I-AFC is given by Img(χ_e). On using the transitions and amplitudes from the Tables. 5.2 and 5.4 gives the absorption profiles of Cs and Rb, see Figs. 5.5 and 5.6. The dynamics of electric field is governed by the Eq. (4.20) with $\mathcal{D}$ containing the comb structure. We numerically solve Eq. (4.20) with the detunings and amplitudes from the Cs and Rb tables. We also set $\mathcal{N} = 10^{18} m^{-3}$ and $\gamma = 5$ MHz [81]. From Figs. 5.5 and 5.6 and we can notice that an echo is obtained at $2\pi/\Delta$ for 3 ns and 2.5 ns. Optimized efficiencies upto 50% are obtained in Cs and Rb by varying the width of the input pulse. Its interesting to notice that the Cs and Rb I-AFC's though being non-uniform in strength and spacing produces an echo similar to ideal case with equal detunings. Unlike in AFC the I-AFC doesn't require combs with large number of peaks, for example even 5-peaks can result in efficient echoes.

5.5.1 Randomness in Cesium atom I-AFC

In real system such as Cesium (Cs) and Rubidium (Rb) atoms, the comb spacing (controlled by external magnetic field) and the absorption coefficient of each of the tooth can be non-uniform. Furthermore, local fluctuations in the electric or magnetic fields can give rise to fluctuations in the teeth spacing and variation in the height of each teeth of the frequency comb. These factors can result in non-optimum quality of the quantum memory. Here we consider randomness in the comb spacing and optical depths of the I-AFC in Cesium, since I-AFC in Rb is similar to Cs we except the same results in Rb atom also.

At temperature $10K$ and magnetic field $B = 0.1\ T$ the maximum efficiency we can

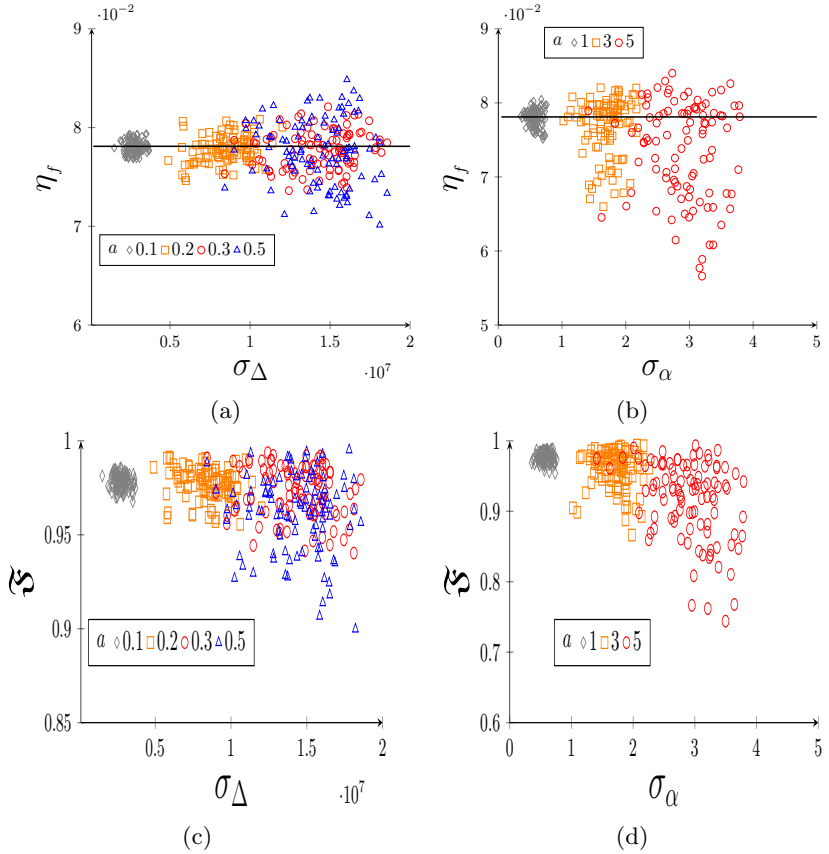

FIGURE 5.7: The non-uniformities in comb spacing and optical depths are quantified by the standard deviations σ_Δ and σ_d. The dashed line represents efficiency for the uniform comb. In Fig. (a) and (b) and we plot efficiency of Cesium atom I-AFC at magnetic field strength $B = 0.1T$. In (c) and (d) we polt the corresponding fidelities.

achieve in this system is $\eta_f \approx 7.8\%$. In Figs. 5.7a and 5.7c we plot the optimized efficiency and the fidelity in Cs I-AFC as a function of σ_Δ upon introducing the fluctuations in the comb. We have set $\mathcal{F} = 3$ and $\alpha L = 18$ and observe that with the increase in the randomness the band for the fidelity as well as efficiency broadens and in some cases the efficiency can reach upto 8.5%. In Figs. 5.7b and 5.7d we plot the efficiency and fidelity in Cesium atom as a function of σ_α. Here we have chosen ($\mathcal{F} = 3, \alpha L = 18$), temperature to be 10K, and external magnetic field 0.1T. As expected, the efficiency and the fidelity in Cs atoms are robust against a large fluctuation in α.

Part-II

Atom-cavity systems

Chapter 6

An introduction to atom-cavity interactions

In the previous chapters we focused on light-matter interactions with light being a classical wave and system being a ensemble of atoms. The atomic system is assumed to be isotropic and linear and the quantization of the light played no significant role in the dynamics. Here we study light matter interactions where the matter is reduced to an individual atom and the light is quantized.

Since the interaction with single atom and a photon is weak, atoms are trapped inside high finesse cavities to improve the interaction strengths. The inclusion of cavity typically results in stronger interactions and atomic emission directed in to the cavity mode. Increase in the interaction strength is obvious as the photon now can bounce multiple times before leaking out of the cavity. The single direction of emission is due to the change in the density of bath modes and by adjusting the cavity parameters, an atom can be made to emit predominately into the cavity mode, with negligible emission into other directions.

In the following discussion we will start with a two-level atom interacting with a cavity mode and then we study input output relation which in principle gives dynamics of any general atom cavity system. Then we obtain steady state solutions for atom cavity system which will be important to realize atom-photon gates. We then study the ladder structure of atom-cavity which helps in intuitive understanding of photon blockade and single photon generation. Then single photon generation using cavity-STIRAP is briefly discussed.

6.1 Two level atom interacting with cavity

The simplest atom-cavity setup consists of a two-level system interacting with a cavity. Although cavities have been realized in variety of systems, for simplicity we consider a Fabry-perot cavity with one partially transmitting mirror and the other with full reflection, Fig. 8.2. The Hamiltonian for the atom-cavity system is written as [82]

$$\begin{aligned} H &= H_{\text{atom}} + H_{\text{cavity}} + H_{\text{interaction}} \\ &= \hbar\omega_0\hat{\sigma}_{ee} + \hbar\omega_c\hat{a}^\dagger\hat{a} - \hbar g(\hat{a}\sigma_{eg} + \hat{a}^\dagger\sigma_{ge}), \end{aligned} \tag{6.1}$$

where ω_0 and ω_c are the frequencies of the atom and the cavity. $\hat{a}$ is the annihilation operator of cavity and $\hat{\sigma}_{ge}$ is step down operator of the atom. The coupling constant is $g = d_{eg}\sqrt{\frac{\omega_c}{2\hbar\epsilon_0 V}}$ with V being the mode volume and d_{eg} dipole matrix element. Hamiltonian of the form Eq. (6.1) has been realized in superconducting qubits, NV-centers, quantum dots, atomic systems, ion-traps and optomechanical systems [83]. The cavities also evolved from the conventional Fabry-perot to optical nano fibres and photonic crystal wave guides [84].

In Chapter. 2 we discussed the operator approach to include decay of the system. Although we discussed interaction of the system with one degree of freedom (bath), it is straight forward to generalize for multiple baths e.g. the evolution equation for a two level system interacting with a leaky cavity and the thermal bath is written as Eq. (2.62)

$$\begin{aligned} \frac{\partial}{\partial t}\hat{A} = -i\Big[\hat{A}, H\Big] - \Big[\hat{A}, \hat{a}^\dagger\Big]\Big(\frac{\kappa}{2}\hat{a} + \sqrt{\kappa}\hat{a}_{\text{in}}\Big) - \Big(\frac{\kappa}{2}\hat{a}^\dagger + \sqrt{\kappa}\hat{a}^\dagger_{\text{in}}\Big)\Big[\hat{A}, \hat{a}\Big] \\ - \Big[\hat{A}, \sigma_+\Big]\Big(\frac{\gamma}{2}\sigma_- + \sqrt{\gamma}\hat{f}\Big) + \Big(\frac{\gamma}{2}\sigma_+ + \sqrt{\gamma}\hat{f}^\dagger\Big)\Big[\hat{A}, \sigma_-\Big], \end{aligned} \tag{6.2}$$

here $\hat{A}$ is any general system operator. κ and γ are the decay rates of the cavity and the atom. $\hat{a}_{\text{in,out}}$ represents the input and output operators Eq. (2.61) . Note that in the atomic decay we drop the noise $\hat{f}$ as we typically deal with optical frequencies ($\hbar\omega_0 \gg K_B T$) all the thermal excitations are neglected, see Eq. (A.34) and the discussion following it.

Then on using the Hamiltonian Eq. (6.1) in Eq. (6.2) results in the dynamical equations as

$$\frac{\partial\hat{a}}{\partial t} = -\Big[i(\omega_c - \omega_p) + \frac{\kappa}{2}\Big]\hat{a} + ig\sigma_{ge} - \sqrt{\kappa}\hat{a}_{\text{in}}, \tag{6.3a}$$

$$\frac{\partial \hat{\sigma}_{ge}}{\partial t} = -\Big[i(\omega_0 - \omega_p) + \frac{\gamma}{2}\Big]\hat{\sigma}_{ge} + ig\hat{a}(\hat{\sigma}_{gg} - \hat{\sigma}_{ee}), \tag{6.3b}$$

$$\frac{\partial \hat{\sigma}_{gg}}{\partial t} = \gamma\hat{\sigma}_{gg} + ig\Big[-\hat{a}\hat{\sigma}_{eg} + \hat{a}^\dagger\hat{\sigma}_{ge}\Big], \tag{6.3c}$$

where ω_p is mean frequency of the input light. Also note that substituting $g\hat{a} \to \Omega$ in Eqs. (6.3b) and (6.3c) will give Langevin equations (2.63) for two-level atom interacting with a classical light.

The complete dynamics of an atom-cavity system are given by Eq. (6.3) and Eq. (6.2). Nevertheless, a general analytical solution is difficult hence we confine ourselves to a narrow band input fields. Then the steady state solutions are sufficient to describe the dynamics [85, 86]. The steady state solution are obtained by setting $\frac{\partial}{\partial t}\hat{\sigma}_{ge} = \frac{\partial}{\partial t}\hat{a} = 0$ and since we typically use weak coherent pulses ($\langle \hat{a}^\dagger_{\text{in}}\hat{a}_{\text{in}}\rangle \sim 1$) hence we assume that atom stays in ground state and approximate $\hat{\sigma}_{gg} - \hat{\sigma}_{ee} \simeq 1$ [87]. Then Eqs. (6.3) yields the reflection coefficient r which is given by

$$r = \frac{\hat{a}_{\text{out}}}{\hat{a}_{\text{in}}} = \frac{[i(\omega_c - \omega_p) - \kappa/2][i(\omega_0 - \omega_p) + \gamma/2] + g^2}{[i(\omega_c - \omega_p) + \kappa/2][i(\omega_0 - \omega_p) + \gamma/2] + g^2}, \tag{6.4}$$

and under the resonant condition $\omega_c = \omega_p = \omega_0$ Eq. (6.4) simplifies to

$$r = \frac{-\kappa\gamma/4 + g^2}{\kappa\gamma/4 + g^2}. \tag{6.5}$$

When the atom is not interacting with the cavity $g = 0$,hence $r = -1$ and in the strong limit $g^2 \gg \kappa\gamma$ gives $r = 1$. Thus atom-cavity setup acts as non linear mirror where the phase of the light is controlled by the interaction strength. This will be exploited in Chapter. 7 to realize atom-photon gates using atom-cavity setups.

6.2 Ladder structure of the atom-cavity system

Energy spectrum of atom-cavity system can be a useful tool in modelling and obtaining a qualitative picture of the atom-cavity systems. Particularly this can be useful when the decay of the atom-cavity setup is very less, i.e. $g \gg (\kappa, \gamma)$ and it doesn't involve solving Langevin equations for complete dynamics. To study the energy levels of atom-cavity

setup we start by writing the Hamiltonian Eq. (6.1) in the interaction picture

$$H_I = e^{iH_0 t}(H - H_0)e^{-iH_0 t} = \hbar\Delta\,|e\rangle\langle e| - \hbar g(\hat{a}\sigma_{eg} + \hat{a}^\dagger\sigma_{ge}), \tag{6.6}$$

where $H_0 = \omega_c(|e\rangle\langle e| + \hat{a}^\dagger\hat{a})$ and $\Delta = \omega_0 - \omega_c$ is the atom-cavity detuning. Writing the Hamiltonian Eq. (6.6) in the excitation preserving basis $\{|e, n-1\rangle\,,\ |g, n\rangle\}$ gives the eigenvalues as

$$H_I = \begin{pmatrix} \Delta & g\sqrt{n} \\ g\sqrt{n} & 0 \end{pmatrix} \Rightarrow \quad |\pm\rangle = \frac{1}{\sqrt{|E_\pm/\Delta|^2 + 1}} \begin{pmatrix} E_\pm/\Delta \\ 1 \end{pmatrix}, \quad E_\pm = \frac{1}{2}\Big(\Delta \pm \sqrt{\Delta^2 + 4g^2 n}\Big). \tag{6.7}$$

Note that the H_I is block diagonal in the basis $\{|e, n-1\rangle\,,\ |g, n\rangle\}$. The n^{th} splitting on resonance is given as $2g\sqrt{n}$. From Fig. 6.1 we can see that ladder structure is anharmonic, i.e. the the energy gap between $|+, n\rangle$ and $|-, n\rangle$ is non linear and increases with n. Also note that semi-classical light-matter interaction would have given a linear splitting of $2g$. Thus atom cavity setup renders a non-linear system where the fock-number gives the anharmonic splitting . When an external light interacts with this system it is shown to have applications ranging from single photon generators, single atom quantum memories , quantum gates, Non demolition bell state measurements [83] and generation of cat-states [26].

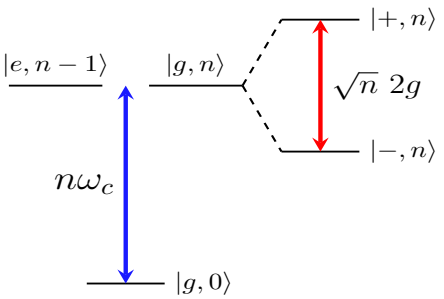

FIGURE 6.1: Non-linear splitting of a two level system interacting with cavity mode. The atom frequency is assumed to be on resonance with the cavity i.e. $\omega_0 = \omega_c$.

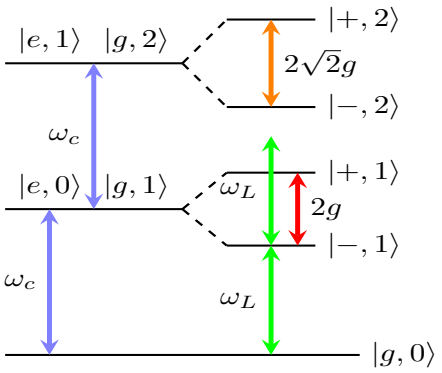

FIGURE 6.2: Ladder for the photon blockade. ω_c is cavity frequency, ω_L is the frequency of light and g is the coupling strength.

6.3 Photon blockade

A natural consequence of anharmonic splitting is the effect of photon blockade [88, 89]. This can be understood by simply drawing the ladder structure for the atom-cavity system see Fig. 6.2. An input light with the frequency $\omega_L = \omega_c - g$ will be resonant with $|-,1\rangle$ and drives the transition

$$|g,0\rangle \overset{\omega_L=\omega_c-g}{\Longleftrightarrow} |-,1\rangle \tag{6.8}$$

and the next nearest transitions are $|+,1\rangle$ and $|-,2\rangle$ with energies $\omega_c + g$ and $2\omega_c - \sqrt{2}g$. Since we have assumed resonance between input light and $|g,0\rangle$-$|-,1\rangle$ the input light can have frequencies of the form $\omega_L = n(\omega_c - g)$ with n being a positive integer. Then the detunings for the levels $|+,1\rangle$ and $|-,2\rangle$ are given as $2g$ and $(2-\sqrt{2})g$. Thus when g is very high, the presence of a photon in the cavity mode will suppress the second and higher excitations, this is known as photon blockade. Note we have avoided the decay of the atom-cavity setup and the ladder structure is valid in the regime $g \gg \kappa, \gamma$.

Photon blockade can also be used to generate single photons. Assuming a perfect blockade the relevant states are written as

$$|-,1\rangle = \frac{1}{\sqrt{2}}(|g,1\rangle - |e,0\rangle) \text{ and } |g,0\rangle\,, \tag{6.9}$$

and the excitation and decay of the atom-cavity setup resulting in the single photon generation can be written as

$$|g,0\rangle \overset{\omega_L}{\Longleftrightarrow} \frac{1}{\sqrt{2}}(|g,1\rangle - |e,0\rangle) \qquad\qquad |g,1\rangle \overset{\kappa}{\rightarrow} |g,0\rangle \tag{6.10}$$

here κ is the decay rate of the cavity. Note that the blockade picture is valid only when atom-cavity interaction is the strongest and the interaction with the input light is weak.

Single photon blockade was verified by trapping a single Caesium and Rubidium atoms in the regime $g \gg (\kappa, \gamma)$ [88, 89]. In a typical blockade experiment a weak coherent pulse resonant with $|-,1\rangle$ is incident upon the cavity. Then the light leaking from the cavity is detected and the coincidence counts are recorded to see the presence of higher excitations.

6.3.1 n-photon blockade

The n-photon blockade in principle can be generated by driving the transition

$$|g,0\rangle \overset{\omega_c - g/\sqrt{n}}{\longleftrightarrow} |-,n\rangle\,. \tag{6.11}$$

This has been experimentally demonstrated upto $n = 2$ [89]. A single atom can only absorb energy in the units of ω_L. Hence the n^{th} excitation can be achieved using light of frequency $n\omega_L = n\omega_c - \sqrt{n}g$, but using this frequency can also make the excitation form the $n-1$ manifold significant. Moreover to increase the population in the n-th manifold stronger driving fields are required but using driving strengths $\sim (g, \kappa)$ can destroy the ladder structure. Thus making it challenging to achieve an ideal n-photon blockade.

6.4 Cavity-STIRAP

Here we discuss STIRAP in cavity systems Fig. 6.3, we have a Λ-type atom with ground ($|g\rangle$), excited ($|e\rangle$) and spin ($|s\rangle$) states. The ($|e\rangle - |g\rangle$) is driven by the cavity mode and the transition ($|e\rangle - |s\rangle$) is driven by a classical light . The advantage of cavity-STIRAP[1] is that it can be implemented in a single atom and hence can be used to generate single photons deterministically. The Hamiltonian for a Λ-system interacting with cavity and

[1] This is also known as virtual-STIRAP

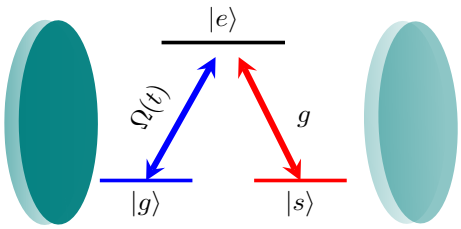

FIGURE 6.3: Three-level atom interacting with the cavity mode and a classical pulse. The transition $|e\rangle$-$|g\rangle$ is driven by the classical pulse Ω and the $|e\rangle$-$|s\rangle$ is driven by the cavity mode with strength g.

classical pulse is written as

$$H = \omega_c \hat{a}^\dagger \hat{a} + \omega_{eg} |e\rangle\langle e| + \omega_{sg} |s\rangle\langle s| + g(\hat{a}\sigma_{eg} + \hat{a}^\dagger \sigma_{ge}) + \Omega(\sigma_{es} e^{-i\omega_L t} + \sigma_{se} e^{i\omega_L t}) \tag{6.12}$$

where g and Ω represent the cavity and classical interaction strength and with $H_0 = \omega_c \hat{a}^\dagger \hat{a} + \omega_c |e\rangle\langle e| + (\omega_c - \omega_L) |s\rangle\langle s|$ the Hamiltonian in the interaction picture is obtained by $e^{iH_0 t} H e^{-iH_0 t}$, reads

$$H = \Delta_c |e\rangle\langle e| + (\Delta_c - \Delta_L) |s\rangle\langle s| + g(\hat{a}\sigma_{eg} + \hat{a}^\dagger \sigma_{ge}) + \Omega(\sigma_{es} + \sigma_{se}) \tag{6.13}$$

where $\Delta_c = \omega_{eg} - \omega_c$ and $\Delta_L = \omega_{es} - \omega_L$. Writing the Hamiltonian in the excitation conserving basis $|g, n+1\rangle, |s, n\rangle, |e, n\rangle$ along with the condition $\Delta_c = \Delta_L$ gives

$$H = \hbar \begin{bmatrix} 0 & 0 & \sqrt{n+1}g \\ 0 & 0 & \Omega \\ \sqrt{n+1}g & \Omega & \Delta \end{bmatrix} \tag{6.14}$$

The eigenvalues are given as

$$\omega^0 = 0, \qquad \omega^\pm = \frac{1}{2}\left[\Delta \pm \sqrt{\Delta^2 + 4\Big(|\Omega|^2 + g^2(n+1)\Big)}\right], \tag{6.15}$$

and the corresponding eigenvectors are

$$|D\rangle = \cos\theta(t) |g, n+1\rangle - \sin\theta(t) |s, n\rangle, \tag{6.16a}$$

$$|+\rangle = \sin\theta(t)\sin\phi |g, n+1\rangle + \cos\theta(t)\sin\phi |s, n\rangle + \cos\phi |e, n\rangle, \tag{6.16b}$$

$$|-\rangle = \sin\theta(t)\cos\phi |g, n+1\rangle + \cos\theta(t)\cos\phi |s, n\rangle - \sin\phi |e, n\rangle, \tag{6.16c}$$

here $\tan\theta(t) = \frac{g\sqrt{n+1}}{\Omega}$ and $\tan\phi = \sqrt{\left|\frac{\omega^-}{\omega^+}\right|}$. With no photons in the cavity $n = 0$, the dark state is written as

$$|D\rangle = \cos\theta(t)\,|g,1\rangle - \sin\theta(t)\,|s,0\rangle\,, \tag{6.17}$$

thus by adiabatically following the dark state a single photon can be deterministically generated [90, 91] i.e.

$$|s,0\rangle \xrightarrow{STIRAP} |g,1\rangle \xrightarrow{\kappa} |g,0\rangle\,, \tag{6.18}$$

where κ the decay rate of the cavity. Here $\theta(t)$ is controlled by varying the pulse envelopes, the pulses can be of any shape as long as they satisfy adiabaticity condition, see Sec. 2.4.1. Apart from single photon generation, a general unitary rotation can be performed on the atomic states $|g\rangle$ and $|s\rangle$ by adjusting the $\theta(t)$. Also STIRAP is used for a variety of applications, e.g., generation of many-particle entangled states, two qubit atom-gates and adiabatic implementation of Grover's quantum search algorithm [92].

Chapter 7

Atom-photon gates and its applications.

In the previous chapter we have seen how the general dynamics of atom-cavity are obtained. In this chapter, we show the realization of two qubit atom-photon gates in atom-cavity systems. A typical atom-cavity system is driven in two important regimes [93, 82, 94]. The bad cavity regime ($\kappa \gg g^2/\kappa \gg \gamma$) where the decay of the cavity mode (κ) is predominant than atom-cavity coupling (g) and atomic decay rate (γ). Since cavity decay is much larger than coherent coupling, photon in this regime quickly leaks out of the cavity. Contrary to bad cavity regime is the strong coupling regime ($g \gg \kappa, \gamma$) where the coherent emission and absorption of photon is dominant than the decay i.e. the cavity-atom system undergoes coherent Rabi oscillations before the photon leaks out [95].

When a weak input pulse with a narrow frequency range interacts with atom-cavity system. The system is expected to saturate quickly and attain the steady state[85, 86]. We rewrite the steady state solution Eq. (6.5) :

$$\frac{\hat{a}_{\text{out}}}{\hat{a}_{\text{in}}} = r = \frac{-\kappa\gamma/4 + g^2}{\kappa\gamma/4 + g^2}. \tag{7.1}$$

If the atom-cavity system is decoupled, then $g = 0$ which gives $r = -1$ i.e. the photon enters and leaves the cavity with a phase difference of π. If the atom-cavity is strongly coupled i.e. $g \gg \gamma, \kappa$ yields $r = 1$ thus the photon enters and leaves the cavity without any phase. $r = 1$ can also be achieved by $g \gg \sqrt{\gamma\kappa}$ even in the bad-cavity regime i.e. $\kappa \gg g, \gamma$ which is typically explored in rare earth ions to perform non-demolition measurements [86], photon-atom gates [96] and to create entanglement in Nitrogen-vacancy centres [85].

In this chapter, we discuss the controlled atom-photon gates and their applications in creating cat-states and analysing GHZ-sates. We also study the swap operation between atom-photon using atom-cavity setup.

7.1 Controlled operations between atom and photon.

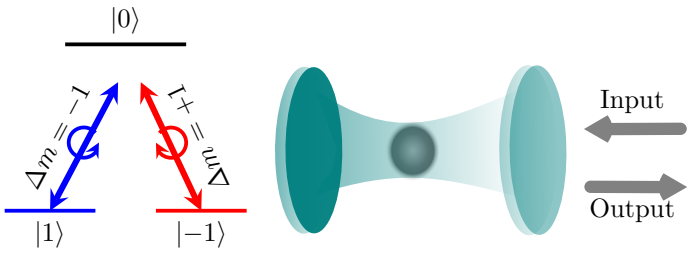

FIGURE 7.1: Three level system interacting with cavity mode of right polarization.

A general quantum operation on two qubits can be performed by local unitary operations on the qubits and a controlled operation of the form

$$C_{x,y,z} = \begin{pmatrix} I & 0 \\ 0 & \sigma_{x,y,z} \end{pmatrix}, \tag{7.2}$$

The local unitary operations on atoms can be implemented using STIRAP techniques, Sec. 6.4. However, the controlled operation between atom and photons is not that trivial. To implement two-qubit controlled gates between atom and photons. We consider a three level Λ-system with two ground states ($|-1\rangle$ $|1\rangle$) and an excited state ($|0\rangle$) Fig. 7.1. The two ground states are chosen to satisfy opposite selection rules i.e.

$$|-1\rangle \rightarrow |0\rangle \Rightarrow \Delta m = +1, \tag{7.3}$$

$$|1\rangle \rightarrow |0\rangle \Rightarrow \Delta m = -1, \tag{7.4}$$

and the transitions $\Delta m = \pm 1$ interact with light carrying $\pm 1\hbar$ unit of angular momentum and for the rest of thesis we denote left (right) circular polarization with $+1(-1)\hbar$ unit of angular momentum.

We also assume the cavity mode to be right circularly polarized, see Fig. 7.1. Since the cavity is right circular polarized, the transition $|-1\rangle - |0\rangle$ ($\Delta m = 1$) is always decoupled

i.e. $g = 0$ in Eq. (7.1) and hence irrespective of photon polarization it will reflect with a π-phase. Also the transition $|1\rangle - |0\rangle$ ($\Delta m = -1$) will not interact with the left circular polarization due to selection rule mismatch. The transformation after reflection is given as

$$|R\rangle|-1\rangle \rightarrow -|R\rangle|-1\rangle, \quad |L\rangle|-1\rangle \rightarrow -|L\rangle|-1\rangle, \quad |L\rangle|1\rangle \rightarrow -|L\rangle|1\rangle, \tag{7.5}$$

but the transition $|1\rangle - |0\rangle$ will interact with $|R\rangle$ to give

$$|R\rangle|1\rangle \rightarrow |R\rangle|1\rangle, \tag{7.6}$$

thus the transformation in the basis $\{|L\ -1\rangle, |L\ 1\rangle, |R\ -1\rangle, |R\ 1\rangle\}$ can be written as

$$C_z = \left(\begin{array}{cc|cc} 1 & 0 & \multicolumn{2}{c}{\multirow{2}{*}{0}} \\ 0 & 1 & & \\ \hline \multicolumn{2}{c|}{\multirow{2}{*}{0}} & 1 & 0 \\ & & 0 & -1 \end{array}\right), \tag{7.7}$$

The C_x gate can be realized by performing Hadamard operation on the atomic system. An efficient unitary on atomic states can be achieved by the optimized-STIRAP techniques where the excited state $|0\rangle$ is adiabatically eliminated [97, 98] and has been experimentally verified with a time scale of $\sim$ 1ms [99]. Consider a unitary acting on $|\pm 1\rangle$ states of the atom

$$U_A(\theta) = \frac{1}{\sqrt{2}}\begin{pmatrix} 1 & e^{i\theta} \\ -e^{-i\theta} & 1 \end{pmatrix} \quad \Rightarrow \quad \begin{aligned} |\theta\rangle_a &\equiv \frac{1}{\sqrt{2}}(|-1\rangle + e^{i\theta}|1\rangle), \\ |\bar{\theta}\rangle_a &\equiv \frac{1}{\sqrt{2}}(-e^{-i\theta}|-1\rangle + |1\rangle), \end{aligned} \tag{7.8}$$

and reflecting the photon off the cavity results in

$$\begin{aligned} |L\rangle|\theta\rangle_a &\rightarrow -|L\rangle|\theta\rangle_a, \\ |L\rangle|\bar{\theta}\rangle_a &\rightarrow -|L\rangle|\bar{\theta}\rangle_a, \\ |R\rangle|\theta\rangle_a &\rightarrow e^{i\theta}|R\rangle|\bar{\theta}\rangle_a, \\ |R\rangle|\bar{\theta}\rangle_a &\rightarrow e^{-i\theta}|L\rangle|\theta\rangle_a, \end{aligned} \qquad C = -\left(\begin{array}{cc|cc} 1 & 0 & \multicolumn{2}{c}{\multirow{2}{*}{0}} \\ 0 & 1 & & \\ \hline \multicolumn{2}{c|}{\multirow{2}{*}{0}} & 0 & -e^{-i\theta} \\ & & -e^{i\theta} & 0 \end{array}\right) \tag{7.9}$$

where $\theta = \pi$ gives C_x operation and $\theta = -\pi/2$ gives C_y operation. Hence a general two-qubit operation can be performed by simply reflecting photons off the cavity and

implementing the STIRAP protocol on the atom. In the following sections we use the controlled operations in atom-cavity setups to generate optical cat-states and implement a GHZ-state analyser.

7.2 Creating Cat-states

An interesting application of atom-photon gates is the generation of optical cat-states. Here we assume that the cavity can sustain only right circular polarization. The coherent and cat-states are defined as:

$$|\alpha\rangle = e^{-\frac{|\alpha|^2}{2}} \sum \frac{\alpha^n}{\sqrt{n!}} |n\rangle \,, \tag{7.10}$$

$$|cat_{\pm}\rangle = \mathcal{N}_{\pm}(|\alpha\rangle \pm |-\alpha\rangle). \tag{7.11}$$

where $\mathcal{N}_{\pm} = [2(1 \pm e^{-2|\alpha|^2})]^{-1/2}$ is the normalization constant. On using Eq. (7.5) the transformation on coherent state is written as

$$\begin{aligned} |1\rangle |\alpha_R\rangle &\rightarrow |1\rangle \left(e^{-\frac{|\alpha|^2}{2}} \sum \frac{\alpha^n}{\sqrt{n!}} |n_R\rangle \right) \rightarrow |1\rangle |\alpha_R\rangle \,, \\ |-1\rangle |\alpha_R\rangle &\rightarrow |-1\rangle \left(e^{-\frac{|\alpha|^2}{2}} \sum \frac{\alpha^n (-1)^n}{\sqrt{n!}} |n_R\rangle \right) \rightarrow |-1\rangle |-\alpha_R\rangle \,, \end{aligned} \tag{7.12}$$

Starting the atom in the superposition state $\frac{1}{\sqrt{2}}(|1\rangle + |-1\rangle)$ and reflecting a coherent state $|\alpha_R\rangle$ off the cavity results in

$$\frac{1}{\sqrt{2}}(|1\rangle + |-1\rangle) \otimes |\alpha_R\rangle \xrightarrow[\text{off cavity}]{\text{reflection}} \frac{1}{\sqrt{2}}(|1\rangle |\alpha_R\rangle + |-1\rangle |-\alpha_R\rangle), \tag{7.13}$$

then a Hadamard operation

$$H = \frac{1}{\sqrt{2}} \begin{pmatrix} 1 & 1 \\ 1 & -1 \end{pmatrix}, \tag{7.14}$$

on the atom gives

$$\frac{1}{\sqrt{2}}(|1\rangle |\alpha\rangle + |-1\rangle |-\alpha\rangle) \rightarrow \frac{1}{\sqrt{2}}[|1\rangle (|\alpha\rangle + |-\alpha\rangle) + |-1\rangle (|\alpha\rangle - |-\alpha\rangle)], \tag{7.15}$$

and finally a measurement on the atom will project the photons to one off the cat states. This technique was demonstrated by trapping a single rubidium atom in a cavity. Although this process is deterministic and efficient, coherent pulses with $\alpha = 1.4$ are used and further increase in the strength reduced the fidelity of cat-states [26].

7.3 Swap operation between atom and photon

The swap is a unitary operation that maps the state of system A to system B. This can be a useful tool when the state preparation is easier in one of the system e.g. it's easier to prepare the polarization states than to prepare superposition of atomic states. Hence with an efficient swap operation one can map the polarization to the atomic superposition.

The swap can be realized by combining controlled operation and local unitary operations but this will result in a swap operation with low gate fidelity. Here we study atom-cavity system where the swap operation is realized between the atomic state and the incoming photon. We use the similar setup as in Fig. 7.1 but the cavity mode is set to interact with both the transitions and we work in the bad-cavity regime $\kappa \gg g^2/\kappa \gg \gamma$. $\Gamma = g^2/\kappa$, is the decay in to the cavity mode and since it's higher than the spontaneous decay of the atom, we can approximate the Hamiltonian for Fig. 7.1 to [32, 100, 101]

$$H = (\omega_0 - \omega_c)\,|0\rangle\langle 0| + \sum_{p=\{R,L\}} \int \omega \hat{a}_p^\dagger(\omega)\hat{a}_p(\omega) + i\sqrt{\Gamma}[\hat{a}_p(\omega)\sigma_p^\dagger - \hat{a}_p^\dagger(\omega)\sigma_p]\; d\omega. \tag{7.16}$$

Here all frequencies are scaled relative to cavity frequency, i.e. $\omega \to \omega - \omega_c$. $\hat{a}_{R,L}$ represent the cavity operators for right and left circular polarizations and $\sigma_{_L} = |-1\rangle\langle 0|$, $\sigma_{_R} = |1\rangle\langle 0|$ represent the atomic operators. Then the Hamiltonian in the interaction picture is written as

$$H_I = \sum_{p=\{R,L\}} i\sqrt{\Gamma} \int [\hat{a}_p(\omega)\sigma_p^\dagger e^{-i(\omega-\delta)t} - \hat{a}_p^\dagger(\omega)\sigma_p e^{i(\omega-\delta)t}]\; d\omega, \tag{7.17}$$

where $\delta = \omega_0 - \omega_c$ is the atom cavity detuning and we assume that cavity and atom are in resonance and set $\delta = 0$. To realize the swap operation, we solve the evolution of the basis states $\{|R,1\rangle, |L,-1\rangle, |R,-1\rangle, |L,1\rangle\}$ with the Hamiltonian in Eq. (7.17). The evolution of the states $|R,-1\rangle, |L,1\rangle$ is trivial as they the light will not interact due to the mismatch in selection rules, see Eq. (7.3). The evolution for the states $|R,1\rangle$ and $|L,-1\rangle$

is identical, due to the symmetry in the Hamiltonian. To obtain the evolution of the state $|R,1\rangle$ ($|L,-1\rangle$) we consider a state of the form [100, 101]

$$|\Psi(t)\rangle = \int f_R(\omega,t)\hat{a}_R^\dagger \, d\omega \, |0\rangle\,|1\rangle + \int f_L(\omega,t)\hat{a}_L^\dagger \, d\omega \, |0\rangle\,|-1\rangle + f_0(t)\,|0\rangle\,|0\rangle\,. \tag{7.18}$$

After modelling the Hamiltonian, ideally we should proceed with Langevin equations for the dynamics but we can afford to drop the decay mechanisms assuming that the system is saturated quickly [102]. Then the system dynamics are given by

$$i\frac{\partial}{\partial t}\,|\Psi\rangle = H_I\,|\Psi\rangle\,, \tag{7.19}$$

where we set $\hbar = 1$ On solving the Eq. (7.19) with the initial state

$$|\Psi(-\infty)\rangle \equiv |R,1\rangle = \int f_{\text{inp}}(\omega,-\infty)\ \hat{a}_R^\dagger \, d\omega \, |0\rangle\,|1\rangle\,, \tag{7.20}$$

yields the steady state solution as (see Appendix D)

$$\begin{aligned} |\Psi(\infty)\rangle =& \frac{-i\Delta}{\Gamma - i\Delta}\int f_{\text{inp}}(\omega,-\infty)\hat{a}_R^\dagger \, d\omega \, |0\rangle\,|1\rangle + \qquad (7.21)\\ & \frac{-\Gamma}{\Gamma - i\Delta}\int f_{\text{inp}}(\omega,-\infty)\hat{a}_L^\dagger \, d\omega \, |0\rangle\,|-1\rangle \\ =& \frac{-i\Delta}{\Gamma - i\Delta}\,|R\rangle\,|1\rangle + \frac{-\Gamma}{\Gamma - i\Delta}\,|L\rangle\,|-1\rangle\,, \qquad (7.22) \end{aligned}$$

here $f_{\text{inp}}(\omega,-\infty)$ is the pulse shape of the photon before entering the cavity. Hence the complete transformation in the basis $\{|R-1\rangle\,,|R1\rangle\,,|L-1\rangle\,,|L1\rangle\}$ is written as [32]

$$\mathbb{S} = \begin{pmatrix} 1 & 0 & 0 & 0 \\ 0 & a & b & 0 \\ 0 & b & a & 0 \\ 0 & 0 & 0 & 1 \end{pmatrix}, \qquad \begin{aligned} a &\equiv \frac{-i}{(\Gamma/\Delta) - i}, \\ b &\equiv \frac{-1}{1 - i(\Delta/\Gamma)}, \end{aligned} \tag{7.23}$$

here $\Gamma = g^2/\kappa$ and $\Delta = \omega_0 - \omega_p$, is the detuning between atom and the photon. The weak swap operation Eq. (7.23) will approximate to an strong swap operation followed by $\sigma_z \otimes \sigma_z$, only under resonance i.e. $\Delta = 0$. Also the following useful relations for a and b

are trivial to verify

$$a - b = 1, \qquad |a|^2 + |b|^2 = 1, \qquad ab^* + a^* b = 0. \tag{7.24}$$

7.4 Non-destructive GHZ state analyser

An atom-photon gate can also be utilized to perform a photon-photon gate [103]. In particular by realizing a C_x operation on two photons we show one can also perform a deterministic and non-destructive measurement on N-photons GHZ states. The most general N-photon GHZ basis $\{|\psi\rangle_{p_1,p_2,\cdots,p_N}\}$ is written as [104]

$$|\psi\rangle_{p_1,\cdots,p_N} = \frac{1}{\sqrt{2}}\big(\,|p_1,p_2,\cdots,p_N\rangle \pm |\bar{p}_1,\bar{p}_2,\cdots,\bar{p}_N\rangle\,\big), \tag{7.25}$$

$$= C_{N,N-1}C_{N-1,N-2}\cdots C_{2,1}H\,|p_1,p_2,\cdots,p_N\rangle\,, \tag{7.26}$$

where $|p_m\rangle \in \{|R\rangle, |L\rangle\}$, $\big|\bar{R}\big\rangle = |L\rangle$ and $\big|\bar{L}\big\rangle = |R\rangle$. The operator H is the Hadamard operator and $C_{i,j}$ is the C_x operation between i-th and j-th system. Note that the two-photon Bell states are the special examples of GHZ states when $N = 2$.

The C_x operation between photons can be realized with atom-photon gates and local unitary rotations on photons and atoms Fig. 7.2

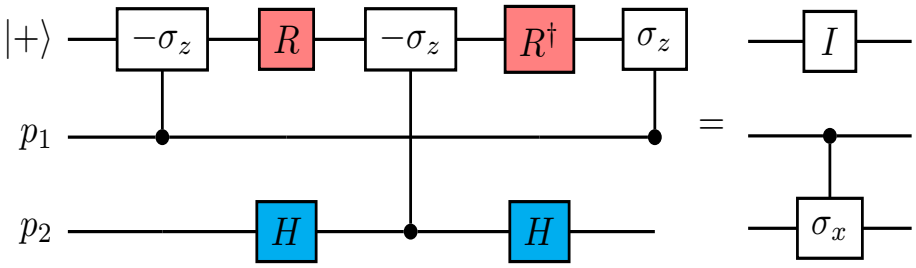

FIGURE 7.2: C_x operation on two photons: The atom is prepared in an initial state $|+\rangle$. Then the first photon $|p_1\rangle$ (control) is reflected of the cavity. Then a rotation is performed on the the atom. Next on the second photon $|p_2\rangle$ (target) we apply Hadamard operations before and after the reflection from the cavity. Then a second rotation to is applied on the atom. Then the first photons is reflected to complete the C_x operation.

Thus using C_x operation on two photon in a N-photon GHZ state we can convert it into a product of single photon state and (N-1)-photon GHZ state. Repeating this step $N-1$ times followed by a Hadamard operation on the last photon we can convert the GHZ

state $|\psi\rangle_{\mathbf{p}}$ to $|\mathbf{p}\rangle$ in Eq. (7.26). The set of orthogonal states $\{|\mathbf{p}\rangle\}$ can be analysed non-destructively by interacting them with an atom-cavity setup [105, 106], Hence, we achieve a non-destructive N-photon GHZ state analyser for delayed photons. Since the process is unitary one can convert product states to GHZ states by reversing the unitary operations. Next we propose an experimental method to realize N-photon GHZ state analyser.

Implementations:

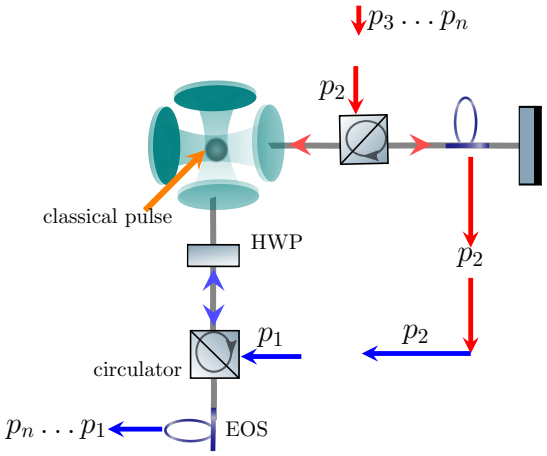

FIGURE 7.3: Atom-cavity setup for the non demolition measurement. HWP stands for half wave plate and in the dashed box is setup for the odd photons.

The experimental protocol is summarized as follows:

- Initially the atom is prepared in the state $|+\rangle$. The state preparation and readout have been performed with high fidelity (99%) [105, 106].
- The first photon $|p_2\rangle$ (control) is reflected of the cavity through a circulator [107] and stored in a delay loop controlled by an electro optical switch (EOS) [108, 109].
- The classical pulses are used to perform the first Hadamard operation on the atom.
- The second photon $|p_1\rangle$ (target) is reflected by the cavity with and a half wave plate (HWP) is placed for the Hadamard operation.
- The second set of classical pulses are sent for the Hadamard operation on the atom.
- The second photon is released from the loop and reflected of the cavity to complete the CNOT operation and the atom is left in the state $|+\rangle$.

The C_x gate between the atom and the photon requires atomic systems with the selection rules $\Delta m = \pm 1$ and cavities with right and left circular polarization's. The selections rules

can be realized in the hyper-fine levels. For this purpose we can choose Cs or ^{87}Rb atoms. In order to make two (or more) photons interact sequentially with an atom, we use a dual cavity configuration where an atom is placed between two optical cavities as in Fig. 7.3. In our proposal, the atom-cavity system is catalytic in nature in the sense that the atom-cavity setup only assists in realizing C_x operation between the two photons, leaving the atomic state unaffected. Therefore, the same atom-cavity setup can be used repeatedly to realize multiple C_x operations between different photons. Hence only one atom-cavity setup is required to transform the GHZ state $|\psi_{\mathbf{p}}\rangle$ to the product state $|\mathbf{p}\rangle$. Since the whole process is unitary, performing the operation in reverse will result in the transformation $|\mathbf{p}\rangle \rightarrow |\psi_{\mathbf{p}}\rangle$.

Chapter 8

Coherent feedback control and QCT

In this chapter, we study the technique of coherent feedback control to improve the fidelity of swap gate, thus making it a useful tool for preparation of atomic states with high fidelities. We also propose an implementation of the protocol Quantum channel transparency (QCT) using two-qubit atom-photon gates.

A practical quantum computer requires preparation, manipulation, and readout of qubits [110]. Some of the promising platforms for quantum computing include trapped ions [3], atom-cavity systems [24, 25], semiconductor qubits [5, 6] and superconducting qubits [1, 2]. Although a practical and scalable quantum computer requires all the three steps implemented with high fidelity [111], here we focus only on the state preparation in atom-cavity setups. A typical preparation scheme starts by initializing the qubit in a known state [112] and then unitary rotations are applied on the qubit to the desired state.

In all the aforementioned platforms the unitary rotations are typically achieved by applying electromagnetic pulses. For high fidelities this demands prior knowledge of the initial state of the system and precise adjustments of frequency, amplitude and phase of the light. This has been experimentally demonstrated in trapped ions[113, 114], atom-cavity setups [115, 116, 117] and superconducting qubits [118].

Another protocol known as STIRAP is used for the state preparation in three level systems (Fig. 8.2) [92]. After the initialization of a qubit in a known state (typically in one of the ground state). The excited state is adiabatically avoided to realize the desired rotation on the qubit. This also requires carefully designed pulses and due to adiabaticity,

high fidelities can only be obtained for long pulse durations. To improve time durations without compromising fidelities, a shortcut to STIRAP known as stimulated Raman shortcut-to-adiabatic passage (STIRSAP) are proposed [42, 43]. Similar to the above techniques these have been implemented in superconducting qubits [119, 120], atomic systems [121] , NV-centers in diamond [122, 123] and ion traps [124]

The swap operation between ancilla and system is another way to initialize a system in a particular state. Once the ancilla is prepared in the desired state, swap can be used to map the ancilla state to the system. The swap is independent of the initial states of the ancilla or the system, hence it doesn't require the initialization of the system in a known state. The swap operation has been demonstrated in atom-cavity setups but only with low fidelities [125] and also requires resonant pulses. In atom-cavity setups the swap operation is realized by the protocol known as single-photon Raman interaction (SPRINT) [126, 125]. In SPRINT a three system is trapped in a cavity. Then weak coherent pulses (with average photons < 1) are reflected off the atom-cavity setup to realize the swap operation. The fidelity for swap operation in SPRINT is measured to be 0.73 [125].

In this work we propose a protocol where the system is coherently controlled with controller single photons to convert a weak swap in to a perfect swap operation. Here the photons are sequentially reflected off an atom-cavity system to realize the swap operation between the photon and the atom. The fidelity of the atomic state can be improved to any desired precision by increasing the number of controller photons. Unlike the existing protocols this technique doesn't require resonant pulses or shaping of the pulse and can be performed without the knowledge of the initial state of the atom.

8.1 Coherent feedback control

In a coherent feedback control formalism, the state of a system is asymptotically pushed towards a target state $|T\rangle \in \mathcal{H}_s$ by sequentially applying weak measurements on the system [31]. Consider a trace-preserving quantum channel \$ described by an n-element set of Kraus operators K_i. If the Kraus operators satisfy the fix-point condition and complete span condition, i.e,

$$K_i |T\rangle = z_i |T\rangle , \tag{8.1}$$

$$\text{span}\{K_i^\dagger |T\rangle\}_{i=0,\ldots,n-1} = \mathcal{H}_s, \tag{8.2}$$

for all $i = 0, \ldots, n-1$ with $z_i \in \mathbb{C}$, then an arbitrary initial state ρ of the system converges to target state $|T\rangle$ under repeated application of the channel \$, i.e., $\$^n(\rho) \to |T\rangle\langle T|$ as $n \to \infty$.

An arbitrary quantum channel \$ can be implemented by a unitary operator U which couples the system to a suitable ancilla system (quantum controller) in initial state $|0\rangle$, such that the resultant action on the system is given by the Kraus operators $\{K_i\}$ upon a projective measurement on the controller in orthonormal basis $\{|i\rangle\}$. Therefore, the coherent feedback control can also be thought of as a sequence of n number of quantum controllers interacting with the system using the same unitary operator U between the system and the individual controllers.

For example, consider a control channel, with the controller state $|x\rangle = 1/\sqrt{2}(|0\rangle + |1\rangle)$ and unitary interaction of the form [31]

$$U = \exp\left[-\frac{i\lambda}{2}(\sigma_y \otimes \sigma_y + \sigma_z \otimes \sigma_z)\right], \tag{8.3}$$

where $\lambda = \mathbb{R}$. Then the Kraus operators $\{K_i = \langle i| U |x\rangle_c\}_i$ satisfy the conditions (8.1) and (8.2) with $|x\rangle$ as the target state. The target state is achieved irrespective of the initial state of the system and when $\lambda = \pi/2$, the target state is reached in a single iteration. Another protocol for coherent feedback control is using the weak swap gate [31]

$$U = \exp[-i\lambda S], \tag{8.4}$$

where $\lambda = \mathbb{R}$ and $S = 1/2(\mathbb{I} + \sum_{j\in\{x,y,z\}} \sigma_j \otimes \sigma_j)$ is the swap operation. Here the Kraus operators $\{K_i = \langle i| U |T\rangle\}_i$ satisfy the conditions (8.1) and (8.2), with $|T\rangle$ begin the state of the ancilla. Hence repeated application of the weak swap will converge the system state to the target state $|T\rangle$.

8.2 Coherent control with atom-cavity setup

Here we implement the coherent feedback control using a atom-cavity setup. The coherent channel, with unitary operation as in Eq. (8.3) can be written as

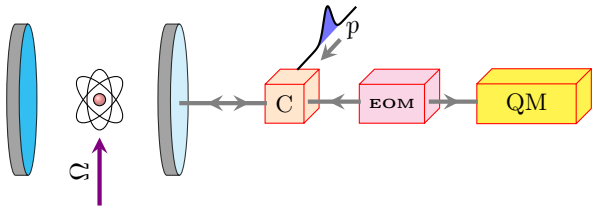

FIGURE 8.1: Coherent control with atom-cavity setup. The atom consists the same structure in Fig. 7.1. The photon (p) is initialised in the target state $|T\rangle = 1/\sqrt{2}(|L\rangle + |R\rangle)$. The photon interaction with the atom-cavity setup results in C_z operation and the C_y is realized by implementing a local unitary on the atom . After this the photon is stored in a quantum memory until the local unitary operations $U_{a,p}$ are performed. Then the photon is re-emitted by the quantum memory to perform the second C_y operation. The circulator (C) is used to orient the photon with the cavity axis. Electro-optical-modulator (EOM) is used to perform unitary operations on photons. The classical pulses (Ω) are used in the STIRAP protocols, to perform unitary rotations on the atom.

$$\begin{aligned} U &= \exp\left[-\frac{i\lambda}{2}(\sigma_y \otimes \sigma_y + \sigma_z \otimes \sigma_z)\right], \\ U &= C_y(U_p \otimes U_a)C_y, \end{aligned} \tag{8.5}$$

where C_y is the controlled operation and the local unitary operations on polarization and atom reads

$$U_p = \frac{1}{\sqrt{2}}\begin{bmatrix} \cos(\lambda/2) & -\sin(\lambda/2) \\ \sin(\lambda/2) & \cos(\lambda/2) \end{bmatrix}, \; U_a = \begin{pmatrix} e^{-i\lambda/2} & 0 \\ 0 & e^{i\lambda/2} \end{pmatrix}. \tag{8.6}$$

The coherent control channel can be implemented by using the setup in Fig. 8.1 [127]. In Fig. (8.1) we show an implementation scheme for the Eq. (8.5). A three-level (Λ-system) atom is trapped in a cavity and the photon is prepared in the target state $|T\rangle = 1/\sqrt{2}(|L\rangle + |R\rangle)$. The photon p enters the cavity axis with the help of a circulator (C). Since a photon interaction with the atom-cavity results in the C_z operation. The required C_y operation is achieved using STIRAP technique, which involves applying classical pulses (Ω) on the atom, in addition to the C_z operation. Once the C_y operation is completed.

The unitary operations U_p and U_a are applied on the photon and the atom respectively. Electro-optical-modulator (EOM) is used for the unitary operation on the photon and STIRAP protocol is used for the unitary operation on the atom. Since STIRAP lasts for

few micro seconds a quantum memory (QM)can be used to store the photon. After the unitary operation U_a on the atom. The photon is retrieved form the memory to repeat the second C_y operation. Thus two photon reflections from an atom-cavity setup, three unitary rotations on the atom and a unitary operation on the photon are needed to realize the coherent feedback control (8.5).

Experimental realizations for the controlled operations are shown by trapping atoms in Fabry-Perot [127] and photonic crystal cavities [128]. These atom-cavity systems typically interact with a weak coherent pulses ($|\alpha|^2 \sim 0.1$) to realize the C_z operation. The efficiency of a controlled atom-photon gate is obtained to be $\eta_z \sim 0.8$ [127]. Assuming unit efficiency for local unitary operations, the maximum efficiency of the coherent channel can be estimated as η_z^2. The coherent control is strongest when $\lambda = \pi/2$, i.e. the target state is reached in a single iteration. In the weaker limit $\lambda \neq \pi/2$, the channel converges to $\lambda = \pi/2$ by successive iterations with ancilla. Thus for n-iterations the maximum efficiency drops to η_z^{2n}. Also a single iteration requires the STIRAP protocol to be performed thrice, further a single STIRAP involves applying multiple classical pulses. Thus making this protocol, resource intensive and inefficient for the atomic state preparation. To improve the efficiency and reduce the complexities of STIRAP, in the following section we study the swap operation in atom-cavity setups.

8.3 State preparation with off-resonant pulses

Coherent feedback control (Sec. 8.1) results in a target state upon successive controllers interactions. In Sec. 7.3 we showed that a swap operation can be realized between polarization and atomic states. With an ideal swap operation only at exact resonance.

Here we show that swap operation along with the coherent control becomes an effective tool for the atomic state preparation. This protocol works with off-resonant pulses and does not depend on the initial state of the atom. The precision can be improved by increasing the number of controller photons.

Since the atom-cavity system with $\Delta = 0$ results in swap operation followed by $\sigma_z \otimes \sigma_z$ Eq. (7.23), the initial state of the photon and atom is written as

$$|\chi\rangle = \sigma_z |T\rangle_p \otimes |\phi\rangle_a \,, \tag{8.7}$$

where $|T\rangle_p = \alpha_p |R\rangle - \beta_p |L\rangle$ with $|\alpha_p|^2 + |\beta_p|^2 = 1$, is the ideal target state of the photon and $|\phi\rangle_a$ is an unknown state of the atom. On resonance the swap operation Eq. (7.23) gives

$$\mathbb{S}_{\Delta=0} |\chi\rangle = \sigma_z |\phi\rangle_p \otimes |T\rangle_a , \tag{8.8}$$

on using Eq. (8.7) the Kraus operators for the Eq. (7.23) are obtained to be

$$K_1 = \begin{pmatrix} \alpha & 0 \\ b\beta & a\alpha \end{pmatrix}, \qquad K_2 = \begin{pmatrix} a\beta & b\alpha \\ 0 & \beta \end{pmatrix}. \tag{8.9}$$

On using Eq. (7.24) it's easy to verify that the target state $|T\rangle$ satisfies the conditions Eq. (8.1) and Eq. (8.2). Thus irrespective of initial state of the atom, the target state is reached upon sequential interaction with photons.

Since the strength of Kraus operators depends on the initial state of controller photons, to quantify the protocol we initialize the atom in farthest state (zero fidelity) i.e. in the orthogonal state $|T_\perp\rangle$. Then the total initial state reads

$$|\chi\rangle = \sigma_z |T\rangle_p \otimes |T_\perp\rangle_a , \tag{8.10}$$

and the state of atom after n-interactions is obtained by $\rho_n = \$^n(|\chi\rangle\langle\chi|)$. The fidelity is defined with the ideal target state, $\mathcal{F} = \left(\mathrm{tr}\sqrt{\sqrt{\rho_n}\ |T\rangle\langle T|\ \sqrt{\rho_n}}\right)^2$. The average fidelity $\overline{\mathcal{F}}$ is obtained by averaging over large number of random trails.

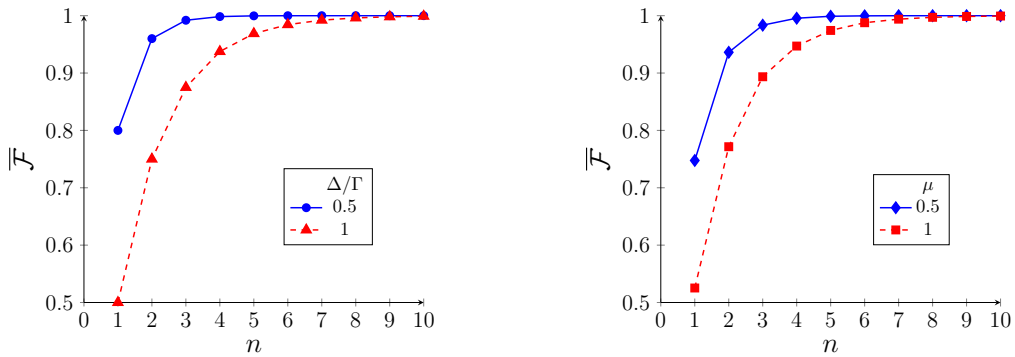

(a) (b)

FIGURE 8.2: Averaged (over 50 trails) fidelity to reach the orthogonal state as a function of controller qubits. a Here the detuning ratio (Δ/Γ) is set to 1. b Average fidelity with Gaussian randomness for the ratio Δ/Γ, where we considered a Gaussian with mean and variance equal to μ.

In Fig. 8.2a we show the average fidelity ($\overline{\mathcal{F}}$) with the target state as a function of number of controllers (n). Here we assume identical detuning for all the controllers. The controller qubits are initialized in a superposition state along with the atom in the corresponding orthogonal state Eq. (8.10). Then the fidelity is averaged over random trials. As expected, the fidelity saturates to one with increase in the number of controllers and for higher detunings we require more photons to reach the unit fidelity.

In Fig. 8.2b we consider the scenario where each sequential photon comes with a random detuning. This can arise due to imperfections in the photon source. The detunings are randomly chosen form a Gaussian noise of the form $\Delta/\Gamma = \mathcal{N}(\mu, \sigma)$, where μ and σ are the mean and standard deviation of the Gaussian distribution. For simplicity we assume $\sigma = \mu$. From Fig. 8.2b we can see that the fidelity converges similar to Fig. 8.2a, where all the photons are assumed to have identical detuning.

Thus the atom-cavity setup effectively swaps the polarization state to the atom, irrespective of the initial state of the atom. Unlike the protocol in Sec. 8.2, here photons interact only once and unitary operations are not required on the atom or the photon. Further with a single-photon source producing 10^9photons/sec [33], ultra high fidelities can be achieved in time scale of $\sim$ 10ns.

Swap operation is theoretically well studied in variety of systems e.g. nitrogen-vacancy centres [129], quantum dots [130], ion-cavity setup [131] and atom-cavity setup [32] but the experimental demonstration has been achieved only in the atom-cavity setup with the protocol known as single-photon Raman interaction (SPRINT) [126, 125]. In SPRINT a Λ-system is trapped in a cavity, with the bad cavity parameters. Since we work in the same regime as SPRINT our protocol is feasible with the existing experimental atom-cavity setups.

8.4 Quantum channel transparency (QCT)

In Chapter. 2 we showed that an interaction with environment will result in the decoherence (decay of off-diagonal terms) of a quantum system and for any practical implementation it is vital to maintain the coherence for longer times. The usual techniques to suppress the noise assume a particular environment and are limited in application.

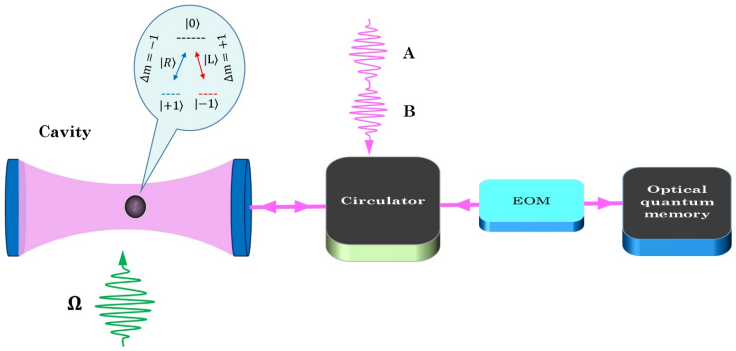

FIGURE 8.3: Experimental setup for realizing the QCT unitary operation. (Figure obtained with permission [30]).

QCT is a protocol where the Linblad evolution of a system is suppressed by interacting the system with ancillary systems. In QCT the environment effects are formulated in the form of Linblad operators without assuming a specific noise model. Hence it works for any general environment. QCT relies on performing an unitary operations of the form [30]

$$\begin{aligned} U_{ABS} =& \ |00\rangle\langle 00|^{AB} \otimes \mathbb{1}^S + |01\rangle\langle 01|^{AB} \otimes \sigma_z^S + |10\rangle\langle 10|^{AB} \otimes \sigma_x^S - i\,|11\rangle\langle 11|^{AB} \otimes \sigma_y^S. \\ V_{ABS} =& (H \otimes H \otimes \mathbb{1})\ U_{ABS}\ (H \otimes H \otimes \mathbb{1}) \qquad \text{with} \quad H = \begin{pmatrix} 1 & 1 \\ 1 & -1 \end{pmatrix} \end{aligned} \tag{8.11}$$

where A, B represent the ancilla's and S the system. H is Hadamard operation on the ancilla's A and B

In the following we implement the U_{ABS} operation using atom-photon gates, with atom and photons as the system and the ancilla's. We first decompose U_{ABS} as a product of two controlled operators

$$U_{ABS} = \left(\mathbb{1}_B \otimes C_x^{AS}\right)\left(\mathbb{1}_A \otimes C_z^{BS}\right), \tag{8.12}$$

where $C_x^{AS} = |0\rangle\langle 0|^A \otimes \mathbb{1}^S + |1\rangle\langle 1|^A \otimes \sigma_x^S$ and $C_z^{BS} = |0\rangle\langle 0|^B \otimes \mathbb{1}^S + |1\rangle\langle 1|^B \otimes \sigma_z^S$ are respectively the control-NOT Eq. (7.9) and control-Phase gates Eq. (7.7) acting on one photon and the atom. Therefore, the unitary U_{ABS} can be implemented by sequentially interacting the two photons with the atom-cavity system similarly the unitary V_{ABS} by performing a Hadamard operation on the ancillas.

In Fig. (8.3) we present an experimental setup to realize the QCT. The photons are initiated in the states $(|R\rangle + |L\rangle)/\sqrt{2}$. In order to implement U_{ABS} operation, we make two photons A and B interact with the atom S inside the cavity. Let the two photons be τ time apart where the photon B comes first. The interaction of the photon B with the atom results in the C_z^{BS} operation. Then applying Hadamard operation on the atom using STIRAP technique with the help of a classical laser pulses (Ω) followed by the interaction of the photon A yields C_x^{AS} operation. Both operations together result in U_{ABS}. Afterward, the two photons can be stored in an optical quantum memory [20, 132, 22] to be used subsequently to implement $U_{ABS}^{\dagger}$ and V_{ABS} operations. Circulators [107] are used to direct the photons towards the cavity and optical quantum memory. The electro-optic-modulator (EOM) [133, 134] is used to perform Hadamard operation on the photons in order to convert U_{ABS} into V_{ABS}.

Chapter 9

Conclusion

Quantum computer is a developing technology that helps us to solve complex problems that are impossible to model on classical super computers. Although quantum supremacy was demonstrated with boson sampling, at present quantum computers are far from performing any practical computations. To perform practical error-free computations it is essential to scale up the quantum systems and with the present day gate-errors a million qubits are required to perform error-free computations. In most quantum computer platforms the three steps, i.e. preparation, operation and measurement are performed using light-matter interactions. Besides advantages in computations light-matter interactions are also necessary to design quantum repeaters. The tools required for quantum repeaters are beam splitters, photonic detectors and photonic quantum memories. This highlights the importance of quantum memory and quantum gates in photonic quantum computers.

In this thesis, we have reviewed various important photonic quantum memories. In particular, we have presented a novel photonic quantum memory called I-AFC. In I-AFC a frequency comb is constructed using different transitions of a single atom. This AFC is important for trapped ions and on-chip quantum computation, single-atom quantum memory, and microwave- to-optical transducers. The spacing between the neighbouring teeth in the comb which characterize the time of the photon echo is controlled by an external magnetic field. Therefore, the time of the photon echo can be controlled by tuning the magnetic field.

I-AFC based quantum memory is robust against non-uniformity in the comb spacing, and non-uniform and fluctuating optical depths. The fluctuations in the comb spacing

can affect the quantum memory efficiency in a strong way. However, this effect can be easily mitigated by increasing the finesse of the I-AFC, which can be done by applying stronger magnetic field. This shows that even the imperfect atomic systems in the extreme environmental conditions can be used for efficient I-AFC based quantum memories. We considered the example of a Cs and Rb atoms and showed that it is robust against fluctuations.

Further, we review the light matter interactions in atom-cavity setups. These setups are used to implement atom-photon and photon-photon quantum gate operations. In such gate operations, the Λ-type atoms are trapped inside an optical cavity. Using the same setup we develop methods to implement QCT protocol and state preparation method using coherent feedback control techniques.

In QCT the effects of bath are removed by interacting the system with ancillas and in the thesis we showed that the required interaction can be implemented using atom-cavity gates and quantum memories. The QCT can be also used to protect quantum information in an atomic system inside a cavity, e.g. an unknown superposition state of the atom can be preserved indefinitely by repeating the QCT protocol.

We also proposed a method for atomic state preparation using coherent feedback control scheme and the weak swap operation in atom-cavity setups. We showed that a weak swap converges to an ideal swap upon the sequential interaction of the controller photons. Using this protocol the fidelity can be increased to any precision by increasing the the number of controller photons. Unlike the existing protocols this method doesn't require information about the initial state of the system and can be implemented with off-resonant pulses. We also discussed the experimental feasibilities of this scheme. Hence, it can be an alternative scheme for atomic state preparation.

In future we plan to design a single atom quantum memory using I-AFC. Such a memory can be easily integrated on a chip and can also be used as single photon source. Following the work in [135] we also plan to improve the storage time of I-AFC by switching on and off the magnetic fields, this will avoid the requirement of spin state transfer for quantum memories. Further, we intend to use our understanding of coherent feedback control and weak swap operation to develop efficient methods to create cat states and GKP type states.

Appendix A

Light-matter interactions

A.1 Adiabatic theorem

In STIRAP we showed that the dark state can be adiabatically followed to realize any superposition state, by avoiding the leakage into the excited state. Here we derive the adiabatic condition required such that a system starting in an eigenstate will remains in the same state upto an overall phase.

The evolution of the system is governed by the Schrödinger equation

$$i\hbar\frac{\partial}{\partial t}\left|\psi\right\rangle = H(t)\left|\psi\right\rangle, \tag{A.1}$$

where the eigenvectors of the Hamiltonian satisfy

$$H(t)\left|m(t)\right\rangle = E_m(t)(t)\left|m(t)\right\rangle \tag{A.2}$$

On writing Eq. (A.1) in the Hamiltonian basis results

$$i\hbar\frac{\partial}{\partial t}\sum_m C_m(t)\left|m(t)\right\rangle = \sum_m C_m(t)E_m(t)\left|m(t)\right\rangle, \tag{A.3}$$

and the inner product with $|n\rangle$ gives

$$i\hbar\left(\dot{C}_n + \sum_m (t)C_m(t)(t)\left\langle n\middle|\dot{m(t)}\right\rangle\right) = C_nE_n, \tag{A.4}$$

$$i\hbar\dot{C}_n - C_nE_n + C_n(t)\left\langle n|\dot{n}\right\rangle = \sum_{m\neq n} C_m(t)\left\langle n(t)\middle|\dot{m(t)}\right\rangle. \tag{A.5}$$

On differentiating Eq. (A.2) and inner-product with $|n\rangle$ yields

$$\begin{aligned} \langle n(t)|\,\dot{H}(t)\,|m(t)\rangle + \langle n(t)|\,H(t)\,|\dot{m}(t)\rangle &= E_m(t)\left\langle n\middle|\dot{m(t)}\right\rangle \quad \forall\ m \neq n, \\ \frac{\langle n(t)|\,\dot{H}(t)\,|m(t)\rangle}{E_m(t) - E_n} &= \left\langle n(t)\middle|\dot{m(t)}\right\rangle \end{aligned} \tag{A.6}$$

Substituting Eq. (A.6) in Eq. (A.5) results

$$i\hbar\dot{C}_n - C_n E_n + C_n\,\langle n(t)|\dot{n}(t)\rangle = \sum_{m\neq n} C_m(t)\frac{\langle n(t)|\,\dot{H}(t)\,|m(t)\rangle}{E_m - E_n}, \tag{A.7}$$

thus when the right side of Eq. (A.7) becomes negligible, i.e. $\dfrac{\langle n(t)|\,\dot{H}(t)\,|m(t)\rangle}{E_m - E_n} \ll 1$ the system starting in n^{th} eigenvector will remain in the same state upto an overall phase. In STIRAP experiments the Λ-system is kept in the dark states and requires shaping the pulses such that Eq. (A.7) remains homogenous at all times.

A.2 Wave equation in Heisenberg picture

In semi-classical theory we only quantized the atom and treated the light as a classical electromagnetic field. In order to describe the system and light using quantum mechanics we quantize the electromagnetic fields also. The fields are represented by the operators $\hat{E}$ and $\hat{B}$. To derive the electric and magnetic field operators we start by writing the Maxwell-equations in vector $\mathbf{A}$ and scalar ϕ potentials. In the Coulomb gauge ($\boldsymbol{\nabla}\cdot\mathbf{A} = 0$) the field equations are written as [136]

$$-\nabla^2\mathbf{A} + \frac{1}{c^2}\frac{\partial}{\partial t}\left(\boldsymbol{\nabla}\phi + \frac{\partial}{\partial t}\mathbf{A}\right) = \mu_0\mathbf{J} \qquad \mathbf{E} = -\boldsymbol{\nabla}\phi - \frac{\partial}{\partial t}\mathbf{A} \tag{A.8}$$

$$-\nabla^2\phi = \sigma/\epsilon_0, \qquad \mathbf{B} = \boldsymbol{\nabla}\times\mathbf{A} \tag{A.9}$$

with $1/c^2 = \epsilon_0\mu_0$. $\mathbf{J}$ and σ are the charge and current densities.

Helmholtz theorem states that a vector field $\mathbf{V}$ can be split into $\mathbf{V} = \mathbf{J}_T + \mathbf{J}_L$ such that $\boldsymbol{\nabla}\cdot\mathbf{V}_T = 0$ and $\boldsymbol{\nabla}\times\mathbf{V}_L = 0$. On using the Helmholtz theorem on $\mathbf{J}$ and $\mathbf{E}$ simplifies the field equations as

$$\nabla^2\mathbf{A} + \frac{1}{c^2}\frac{\partial}{\partial t^2}\mathbf{A} = \mu_0\mathbf{J}_T \qquad \mathbf{E}_T = -\frac{\partial}{\partial t}\mathbf{A} \tag{A.10}$$

$$\frac{1}{c^2}\frac{\partial}{\partial t}\boldsymbol{\nabla}\phi = \mu_0 \mathbf{J}_L \qquad\qquad \mathbf{E}_L = -\boldsymbol{\nabla}\phi \tag{A.11}$$

and in the region with $\mathbf{J}_T = 0$, the field equation is further simplified as

$$\nabla^2 \mathbf{A} + \frac{1}{c^2}\frac{\partial}{\partial t^2}\mathbf{A} = 0 \tag{A.12}$$

For quantization the solutions of vector field are typically solved in a cavity of length L and volume $V = L^3$. Further to incorporate travelling waves periodic boundary conditions are invoked [136]. On solving Eq. (A.12) under periodic boundary conditions yields

$$\mathbf{A} = \sum_{\mathbf{k}} \sum_{\lambda=1,2} \mathbf{e}_{\mathbf{k}\lambda} A_{\mathbf{k}\lambda} e^{-i(\omega_k t - \mathbf{k}\cdot\mathbf{r})} + c.c \tag{A.13}$$

where $\omega_k = ck$. Then electric and magnetic fields are given as

$$\mathbf{E}_T(\mathbf{r},t) \equiv -\frac{\partial}{\partial t}\mathbf{A} = \sum_{\mathbf{k},\lambda} i\omega_k \mathbf{e}_{\mathbf{k},\lambda} A_{\mathbf{k},\lambda} e^{i(\mathbf{k}.\mathbf{r}-\omega t)} + h.c, \tag{A.14}$$

$$\mathbf{B}(\mathbf{r},t) \equiv \boldsymbol{\nabla} \times \mathbf{A} = \sum_{\mathbf{k},\lambda} ik \mathbf{e}_{\mathbf{k},\lambda} \hat{a}_{\mathbf{k},\lambda} e^{i(\mathbf{k}.\mathbf{r}-\omega t)} + h.c, \tag{A.15}$$

where $\mathbf{k}$ and λ are mode and polarization indices, $V = L^3$ is quantization volume and ω is the mode frequency. The total energy of the electromagnetic field is obtained by

$$\mathsf{E} = \frac{1}{2}\int dV [\epsilon_0 \mathbf{E}_T(\mathbf{r},t)\cdot\mathbf{E}_T(\mathbf{r},t) + 1/\mu_0 \mathbf{B}(\mathbf{r},t)\cdot\mathbf{B}(\mathbf{r},t)] \tag{A.16}$$

and in terms of vector potential the energy is obtained as [136]

$$\mathsf{E} = \epsilon_0 V \sum_{\mathbf{k},\lambda} \omega_k^2 (A_{k\lambda} A_{k\lambda}^*) + c.c. \tag{A.17}$$

The operator from of the vector field is obtained by elevating $\mathbf{A}$ to the operator $\hat{A}$ and comparing the energy with the Hamiltonian of a cavity i.e $H = \frac{1}{2}\sum_{v,k} \hbar\omega_k \hat{a}_{k\lambda}\hat{a}_{k\lambda}^\dagger + h.c.$ yields

$$\hat{E}(\mathbf{r},t) = \sum_{\mathbf{k},\lambda} \sqrt{\frac{\hbar\omega_k}{2\epsilon_0 V}} \mathbf{e}_{\mathbf{k},\lambda} \hat{a}_{\mathbf{k},\lambda} e^{i(\mathbf{k}.\mathbf{r}-\omega t)} + h.c, \tag{A.18}$$

where the electric field operators satisfy the bosonic relations

$$\left[\hat{a}_{\mathbf{k},\lambda}, \hat{a}^{\dagger}_{\mathbf{k}',\lambda'}\right] = \delta_{\mathbf{k},\mathbf{k}',\lambda,\lambda'}. \tag{A.19}$$

The equivalence of field operators with simple harmonic oscillator (SHO) gives the intuition to interpret photons as excitations of SHO modes [36, 137, 136]. So far we discussed discrete modes which describe monochromatic pulses in a physical world. To incorporate electromagnetic pulses with narrow spectral widths we use continuous-mode operators [136]. The continuous-mode operators are obtained by changing $\hat{a} \to (\Delta\omega)^{1/2}\,\hat{a}(\omega)$ and $\sum_k \to 1/\Delta\omega \int d\omega$[1]

$$E(z) = \int \sqrt{\frac{\hbar\omega}{4\pi\epsilon_0 cA}} a(\omega) e^{i\omega z/c}\, d\omega + h.c, \tag{A.20}$$

where the continuous operators satisfy $\left[\hat{a}(\omega), \hat{a}^{\dagger}(\omega')\right] = \delta(\omega - \omega')$. Assuming that input pulse has a narrow width around ω_0[2] gives

$$E(z) = \sqrt{\frac{\hbar\omega_0}{4\pi\epsilon_0 cA}} \int a(\omega) e^{i\omega z/c}\, d\omega + h.c. \tag{A.21}$$

The evolution of the operator $\mathcal{E}(z) = (L/2\pi c)^{1/2} \int \hat{a}(\omega) e^{i\omega z/c}\, d\omega$ is obtained by

$$i\hbar \frac{\mathrm{d}}{\mathrm{d}t}\mathcal{E}(z) = [\mathcal{E}(z), H], \tag{A.22}$$

for example the Hamiltonian $H = \int \hbar\omega \hat{a}^{\dagger}(\omega)\hat{a}(\omega)\, d\omega$ gives

$$\begin{aligned} \frac{\mathrm{d}\mathcal{E}}{\mathrm{d}t} &= -i/\hbar[\mathcal{E}, H], \\ &= -i\sqrt{\frac{L}{2\pi c}} \int \omega \hat{a}(\omega) e^{i\omega z/c}\, d\omega \equiv -c\frac{\mathrm{d}\mathcal{E}}{\mathrm{d}z}, \end{aligned} \tag{A.23}$$

and in free space Eq. (A.23) gives

$$\left(\frac{\partial}{\partial t} + c\frac{\partial}{\partial z}\right)\mathcal{E}(z,t) = 0 \quad \Rightarrow \quad \mathcal{E}(z,t) = \sqrt{\frac{L}{2\pi c}} \int \hat{a}(\omega) e^{-i\omega(t - z/c)}\, d\omega, \tag{A.24}$$

which is identical to the forward mode equation obtained in Sec. 2.3[3].

[1] Since propagation is taken to be along $\hat{z}$, $\Delta\omega = 2\pi c/L$, also polarization index is dropped for simplicity.
[2] Narrow band light is the typical source in experiments.
[3] Backward mode equation can be obtained by taking $e^{-i\omega z/c}$ in Eq. (A.21)

A.3 Langevin equations for N three-level atoms

In the following we derive Langevin equations for N atoms with Λ-configuration. The Hamiltonian for the Λ-system interacting with a probe ($\mathcal{E}$) and a control (Ω) pulse is written as

$$H_0 = \int \hbar\omega \hat{a}^\dagger(\omega)\hat{a}(\omega)\, d\omega + \hbar\omega_{eg}\sum_{j=1}^{N}\sigma_{ee}^{j} + \hbar\omega_{sg}\sum_{j=1}^{N}\sigma_{ss}^{j}, \tag{A.25a}$$

$$V = -g\hbar\sum_{j=1}^{N}\sigma_{eg}^{j}\mathcal{E}(z) + \text{H.c.} - \hbar\sum_{j=1}^{N}\Omega(z_j,t)e^{-i\omega_2(t-z_j/c)}\,\sigma_{es}^{j} + h.c, \tag{A.25b}$$

In order to treat the operators like functions we introduce continuous limit approximation [138]

$$\hat{\sigma}_{ab}(z) = \frac{1}{N_z}\sum_{i=1}^{N_z}\hat{\sigma}_{ab}^{i}. \tag{A.26}$$

The summation is over N_z atoms in a thin strip positioned around z that is thick enough to contain $N_z \gg 1$ atoms but thin enough to consider the resulting excitations and de-excitations continuous. Then on using $\delta_{zz'} \to \Delta z\,\delta(z-z')$[4] the commutator relation [138, 48]

$$\left[\hat{\sigma}_{ab}(z), \hat{\sigma}_{cd}(z')\right] = \frac{\delta_{zz'}}{N_z}\left[\delta_{bc}\hat{\sigma}_{ad}(z) - \delta_{da}\hat{\sigma}_{cb}(z)\right], \tag{A.27}$$

in the continuous limit is written as

$$\left[\hat{\sigma}_{ab}(z), \hat{\sigma}_{cd}(z')\right] = \frac{1}{\eta(z)}\delta(z-z')\left[\delta_{bc}\hat{\sigma}_{ad}(z) - \delta_{da}\hat{\sigma}_{cb}(z)\right], \tag{A.28}$$

with $\eta(z)$ being the linear density. Similarly on replacing $\sum_i \hat{\sigma}^i \to \int \eta(z)\hat{\sigma}\, dz$ the Hamiltonian in the continuous limit is given as

$$H = \int \hbar\omega \hat{a}^\dagger(\omega)\hat{a}(\omega)\, d\omega + \hbar\omega_{eg}\int \eta(z)\hat{\sigma}_{ee} + \hbar\omega_{sg}\int \eta(z)\hat{\sigma}_{ss} - \hbar\int dz\ \eta(z)\Big[g\hat{\sigma}_{eg}\mathcal{E}(z) + \Omega(z,t)\hat{\sigma}_{es}e^{-i\omega_2(t-z/c)} + H.c\Big], \tag{A.29}$$

[4] Note that $\hat{\sigma}_{ab}$ at z an z' commute

Then the Heisenberg equations with out noise terms are obtained by using Eq. (A.28)

$$\begin{aligned}
\frac{\partial \mathcal{E}}{\partial t} + c\frac{\partial \mathcal{E}}{\partial z} &= ig^*\eta(z)L\sigma_{ge}, \\
\frac{\partial}{\partial t}\sigma_{ss} &= -i\Omega\sigma_{es}e^{-i\omega_2(t-z/c)} + i\Omega^*\sigma_{se}e^{i\omega_2(t-z/c)}, \\
\frac{\partial}{\partial t}\sigma_{ee} &= ig\mathcal{E}\hat{\sigma}_{eg} - ig^*\mathcal{E}^\dagger\hat{\sigma}_{ge} + i\Omega\sigma_{es}e^{-i\omega_2(t-z/c)} - i\Omega^*\sigma_{se}e^{i\omega_2(t-z/c)}, \\
\frac{\partial}{\partial t}\sigma_{ge} &= -i\omega_{eg}\sigma_{ge} + ig\mathcal{E}(\sigma_{gg} - \sigma_{ee}) + i\Omega\sigma_{gs}e^{-i\omega_2(t-z/c)}, \\
\frac{\partial}{\partial t}\sigma_{gs} &= -i\omega_{sg}\sigma_{gs} - ig\mathcal{E}\sigma_{es} + i\Omega^*\sigma_{ge}e^{i\omega_2(t-z/c)}, \\
\frac{\partial}{\partial t}\sigma_{se} &= -i\omega_{es}\sigma_{se} + ig\mathcal{E}\sigma_{sg} + i\Omega(\sigma_{ss} - \sigma_{ee})e^{-i\omega_2(t-z/c)}.
\end{aligned} \tag{A.30}$$

On applying the following transformations

$$\begin{aligned}
\sigma_{ge} &= \tilde{\sigma}_{ge}e^{-i\omega_1(t-z/c)}, & \sigma_{se} &= \tilde{\sigma}_{se}e^{-i\omega_2(t-z/c)}, \\
\sigma_{gs} &= \tilde{\sigma}_{gs}e^{-i(\omega_1-\omega_2)(t-z/c)}, & \mathcal{E} &= \tilde{\mathcal{E}}e^{-i\omega_1(t-z/c)},
\end{aligned} \tag{A.31}$$

note that these transformations are equivalent to changing to a rotating frame at the Hamiltonian level. On adding the noise gives

$$\begin{aligned}
\frac{\partial \tilde{\mathcal{E}}}{\partial t} + c\frac{\partial \tilde{\mathcal{E}}}{\partial z} &= ig^*\eta(z)L\tilde{\sigma}_{ge}, \\
\frac{\partial}{\partial t}\tilde{\sigma}_{ss} &= -\gamma_2\tilde{\sigma}_{ss} - i\Omega\tilde{\sigma}_{es} + i\Omega^*\tilde{\sigma}_{se} + \hat{F}_{ss}, \\
\frac{\partial}{\partial t}\tilde{\sigma}_{ee} &= -\gamma_1\tilde{\sigma}_{ee} + ig\mathcal{E}\tilde{\sigma}_{eg} - ig^*\mathcal{E}^\dagger\tilde{\sigma}_{ge} + i\Omega\tilde{\sigma}_{es} - i\Omega^*\tilde{\sigma}_{se} + \hat{F}_{ee}, \\
\frac{\partial}{\partial t}\tilde{\sigma}_{ge} &= -(\gamma_{ge} + i\Delta_1)\tilde{\sigma}_{ge} + ig\tilde{\mathcal{E}}(\tilde{\sigma}_{gg} - \tilde{\sigma}_{ee}) + i\Omega\tilde{\sigma}_{gs} + \hat{F}_{ge}, \\
\frac{\partial}{\partial t}\tilde{\sigma}_{gs} &= -\gamma_{gs}\tilde{\sigma}_{gs} - i(\Delta_1 - \Delta_2)\tilde{\sigma}_{gs} - ig\tilde{\mathcal{E}}\tilde{\sigma}_{es} + i\Omega^*\tilde{\sigma}_{ge} + \hat{F}_{gs}, \\
\frac{\partial}{\partial t}\tilde{\sigma}_{se} &= -(\gamma_{se} + i\Delta_2)\tilde{\sigma}_{se} + ig\tilde{\mathcal{E}}\tilde{\sigma}_{sg} + i\Omega(\tilde{\sigma}_{ss} - \tilde{\sigma}_{ee}) + \hat{F}_{se}.
\end{aligned} \tag{A.32}$$

Assuming a weak probe interaction i.e. $\tilde{\sigma}_{gg} \approx 1$ and defining atomic polarization and spin waves as $\sqrt{N}\tilde{\sigma}_{ge} = P$, $\sqrt{N}\tilde{\sigma}_{gs} = S$, $\sqrt{N}\hat{F}_{ge} = \hat{F}_p$, $\sqrt{N}\hat{F}_{gs} = \hat{F}_s$ gives

$$\begin{aligned}
\frac{\partial\tilde{\mathcal{E}}}{\partial t} + c\frac{\partial\tilde{\mathcal{E}}}{\partial z} &= i\frac{g^*\eta(z)L}{\sqrt{N}}P, \\
\frac{\partial}{\partial t}P &= -(\gamma_{ge} + i\Delta_1)P + ig\sqrt{N}\tilde{\mathcal{E}} + i\Omega S + \hat{F}_p, \\
\frac{\partial}{\partial t}S &= -\gamma_{gs}S - i(\Delta_1 - \Delta_2)S - ig\sqrt{N}\tilde{\mathcal{E}}\tilde{\sigma}_{es} + i\Omega^* P + \hat{F}_s, \\
\frac{\partial}{\partial t}\tilde{\sigma}_{se} &= -(\gamma_{se} + i\Delta_2)\tilde{\sigma}_{se} + ig\sqrt{N}\tilde{\mathcal{E}}S^\dagger + \hat{F}_{se},
\end{aligned} \tag{A.33}$$

and on using Eq. (2.64) the expectation values of noise operators are obtained as [138]

$$\left\langle F_p^\dagger(z,t)F_p(z',t')\right\rangle = \left\langle F_s^\dagger(z,t)F_s(z',t')\right\rangle = 0, \tag{A.34a}$$

$$\left\langle F_p(z,t)F_p^\dagger(z',t')\right\rangle = \left\langle F_s(z,t)F_s^\dagger(z',t')\right\rangle = \frac{N}{\eta(z)}\delta(z-z')\delta(t-t'), \tag{A.34b}$$

since normally ordered correlations are zero, vacuum modes will be the only contributing noise and hence the noise terms in Eq. (A.33) are dropped.

The Eqs. (A.33-A.34) are derived under the approximation $\hat{\sigma}_{gg} \approx 1$, which is usually valid as there are no thermal excitations in the system with optical transition $|e\rangle - |g\rangle$ of the order $10^4 K$ and the transition $|g\rangle - |s\rangle$ typically being dipole forbidden.

Assuming the transition $|g\rangle - |s\rangle$ to be dipole forbidden ($\gamma_{sg} = 0$), resonant driving-field ($\Delta_2 = 0$), homogeneous linear density ($\eta = N/L$) and retaining to the first order in $\tilde{\mathcal{E}}$ Eq. (A.33) gives

$$\left(\frac{\partial}{\partial t} + c\frac{\partial}{\partial z}\right)\tilde{\mathcal{E}} = i\tilde{g}^* P, \tag{A.35a}$$

$$\frac{\partial}{\partial t}P = -(\gamma_{ge} + i\Delta_1)P + i\tilde{g}\tilde{\mathcal{E}} + i\Omega S, \tag{A.35b}$$

$$\frac{\partial}{\partial t}S = -i\Delta_1 S + i\Omega^* P, \tag{A.35c}$$

where $\tilde{g} = \sqrt{N}g$. To summarize the steps in deriving Eq. (A.35). We started with a basic Hamiltonian for a N three-level atoms and changed to continuous modes. Then the equations are transformed to a rotating frame. And the noise is added using Langevin equations, further Einstein formulae is used to see vacuum modes as the only noise and finally approximated the equations to the first order in probe-field.

A.4 Adiabatic approximation of Langevin equations

Here we discuss an approximate technique known as adiabatic approximation [5] [139] to solve the Heisenberg-Langevin equations of a three-level atom interacting with light, Eq. (A.35). We start by writing them in a general form

$$\frac{\partial}{\partial t}P = -\Gamma P + \mathcal{R}(\tilde{\mathcal{E}}, S, t) \tag{A.36}$$

$$\frac{\partial}{\partial t}S = \mathcal{G}(S, P, t) \tag{A.37}$$

where $\mathcal{R}$ and $\mathcal{G}$ are any general functions and $\Gamma = \gamma + i\Delta$. Our goal is to obtain the conditions such that $\frac{\partial}{\partial t}P = 0$.

We start by writing $P(t)$ in terms of $S(t)$. On integrating Eq. (A.36) and with $P(-\infty) = 0$ gives

$$P(t) = \int_{-\infty}^{t} e^{-\Gamma(t-t')}\mathcal{R}(\tilde{\mathcal{E}}, S, t')\, dt', \tag{A.38}$$

$$= \frac{\mathcal{R}}{\Gamma} - \frac{1}{\Gamma}\int_{-\infty}^{t} e^{-\Gamma(t-t')}\frac{\partial}{\partial S}\mathcal{R}(\tilde{\mathcal{E}}, S, t')\frac{\partial S}{\partial t'}\, dt', \tag{A.39}$$

where $\frac{\partial}{\partial t'}S = \mathcal{G}$ and to eliminate $P(t)$ in $\mathcal{G}(S, P, t')$ we replace it by the first order approximation i.e. $\mathcal{G}\left(S, \frac{\mathcal{R}}{\Gamma}, t'\right)$. On repeating the integration by parts gives

$$\begin{aligned}
P(t) &= \frac{\mathcal{R}}{\Gamma} - \frac{1}{\Gamma}\int_{-\infty}^{t} e^{-\Gamma(t-t')}\mathcal{G}\frac{\partial \mathcal{R}}{\partial S}\, dt', \\
&= \frac{\mathcal{R}}{\Gamma} - \frac{\mathcal{G}}{\Gamma}\partial_S\left(\frac{\mathcal{R}}{\Gamma}\right) + \int_{-\infty}^{t} e^{-\Gamma(t-t')}\partial_{t'}\left[\frac{\mathcal{G}}{\Gamma}\partial_S\left(\frac{\mathcal{R}}{\Gamma}\right)\right] dt', \\
&= \frac{\mathcal{R}}{\Gamma} - \frac{\mathcal{G}}{\Gamma}\partial_S\left(\frac{\mathcal{R}}{\Gamma}\right) + \frac{\mathcal{G}}{\Gamma}\partial_S\left[\frac{\mathcal{G}}{\Gamma}\partial_S\left(\frac{\mathcal{R}}{\Gamma}\right)\right] - \int_{-\infty}^{t} e^{-\Gamma(t-t')}\partial_{t'}\left[\frac{\mathcal{G}}{\Gamma}\partial_S\left\{\frac{\mathcal{G}}{\Gamma}\partial_S\left(\frac{\mathcal{R}}{\Gamma}\right)\right\}\right] dt', \\
&= \frac{\mathcal{R}}{\Gamma} - \frac{\mathcal{G}}{\Gamma}\partial_S\left(\frac{\mathcal{R}}{\Gamma}\right) + \frac{\mathcal{G}}{\Gamma}\partial_S\left[\frac{\mathcal{G}}{\Gamma}\partial_S\left(\frac{\mathcal{R}}{\Gamma}\right)\right] - \frac{\mathcal{G}}{\Gamma}\partial_S\left[\frac{\mathcal{G}}{\Gamma}\partial_S\left\{\frac{\mathcal{G}}{\Gamma}\partial_S\left(\frac{\mathcal{R}}{\Gamma}\right)\right\}\right] + \dots
\end{aligned} \tag{A.40}$$

and if we wish to approximate the series only by the first term then $P = \mathcal{R}/\Gamma$, note that this could also have been achieved simply by setting $\frac{\partial}{\partial t}P = 0$[6]

[5] Not to be confused with adiabatic elimination and adiabatic theorem.
[6] In the quantum optics literature this is known as adiabatic approximation.

Assuming that the series converges Eq. (A.40) gives

$$\begin{aligned} P(t) &= \left[1 - \frac{\mathcal{G}}{\Gamma}\frac{\partial}{\partial S} + \left(\frac{\mathcal{G}}{\Gamma}\frac{\partial}{\partial S}\right)^2 - \left(\frac{\mathcal{G}}{\Gamma}\frac{\partial}{\partial S}\right)^3 + \dots\right]\frac{\mathcal{R}}{\Gamma}, \\ P(t) &= \left[\frac{1}{1 + \left(\frac{\mathcal{G}}{\Gamma}\frac{\partial}{\partial S}\right)}\right]\frac{\mathcal{R}}{\Gamma}, \end{aligned} \tag{A.41}$$

suppose we approximated the series to m^{th} term and we wish to drop the remaining terms, then to see the conditions required for this approximation, we split the series into two parts

$$P(t) = \sum_{k=0}^{m}\left(-\frac{\mathcal{G}}{\Gamma}\frac{\partial}{\partial S}\right)^k\frac{\mathcal{R}}{\Gamma} + \underbrace{\sum_{l=0}^{\infty}\left(-\frac{\mathcal{G}}{\Gamma}\frac{\partial}{\partial S}\right)^{l+m+1}\frac{\mathcal{R}}{\Gamma}}_{\mathcal{X}} \tag{A.42}$$

and the second term can be simplified as

$$\begin{aligned} \mathcal{X} &= \sum_{l=0}^{\infty}\left(-\frac{\mathcal{G}}{\Gamma}\frac{\partial}{\partial S}\right)^{l+m+1}\frac{\mathcal{R}}{\Gamma} \equiv \left[\frac{1}{1 + \left(\frac{\mathcal{G}}{\Gamma}\frac{\partial}{\partial S}\right)}\right]\left(-\frac{\mathcal{G}}{\Gamma}\frac{\partial}{\partial S}\right)^{m+1}\frac{\mathcal{R}}{\Gamma}, \\ \left[1 + \left(\frac{\mathcal{G}}{\Gamma}\frac{\partial}{\partial S}\right)\right]\mathcal{X} &= \left(-\frac{\mathcal{G}}{\Gamma}\frac{\partial}{\partial S}\right)^{m+1}\frac{\mathcal{R}}{\Gamma}, \end{aligned} \tag{A.43}$$

the above equation gives a measure for the approximated series and when $\mathcal{X}$ is much less compared to remaining m terms we can afford to drop it.

In the typical adiabatic approximation we stop with fist term thus $m = 1$ in the Eq. A.43 gives

$$\mathcal{X}(S) = \mathcal{X}(-\infty)\exp\left(-\frac{\Gamma S}{G}\right) - \int_{-\infty}^{S} e^{-\Gamma/G(S-S')}\frac{\partial}{\partial S'}\frac{\mathcal{R}}{\Gamma}\,dS' \tag{A.44}$$

where $\mathcal{X}(-\infty) = 0$ and $\mathcal{R}$ is typically linear in S which simplifies the above to

$$\mathcal{X}(S) = \left(\frac{\partial}{\partial S}\frac{\mathcal{R}}{\Gamma}\right)\frac{\mathcal{G}}{\Gamma} \equiv \left(\frac{i\Omega}{\Gamma}\right)\frac{\mathcal{G}}{\Gamma}, \tag{A.45}$$

now one can adiabatically approximate $P(t)$ by setting $\frac{\partial}{\partial t}P = 0$ if

$$\left|\frac{\mathcal{R}}{\Gamma}\right| \gg |\mathcal{X}(S)| \gg \left|\frac{\Omega}{\Gamma}\right|\left|-\frac{\Delta S}{\Gamma} + \frac{\Omega^*}{\Gamma}\frac{\mathcal{R}}{\Gamma}\right| \gg \left|\frac{\Omega}{\Gamma}\right|\left[\left|\frac{\Delta S}{\Gamma}\right| + \left|\frac{\Omega^*}{\Gamma}\frac{\mathcal{R}}{\Gamma}\right|\right], \tag{A.46}$$

since $S_{\max} = 1$ and if $|\Gamma| > \Delta$ and $|\Gamma| \gg |\Omega|$ are satisfied we can safely proceed with adiabatic approximation in fact the only required condition is $|\Gamma| \gg |\Omega|$ as $|\Gamma| > |\Delta|$ is trivial. Thus an adiabatic solution for three-level system can be obtained by setting $\partial P/\partial t = 0$.

Appendix B

Calculations for CRIB

Here we give calculations for the absorption, forward mode and backward mode in CRIB memories. The equations are same for AFC memory also, with the inhomogeneous broadening replaced by AFC-comb, i.e. $G(\Delta) \rightarrow n(\delta)$. We split the time scale from $-\infty \rightarrow 0$ for absorption and $0 \rightarrow \infty$ for emission. We further split the emission into backward mode and forward mode. Then dynamical equations equations for the forward mode are given by Eq. (3.28a)-(3.28d)

$$\frac{\partial}{\partial t}\sigma_f(z,t) = -i(\Delta_0 + \Delta')\sigma_f + id_{eg}E_f(z,t), \tag{B.1a}$$

$$\left(\frac{\partial}{\partial t} + c\frac{\partial}{\partial z}\right)E_f(z,t) = i\beta\int_{-\infty}^{\infty} G(\Delta_0)G'(\Delta')\sigma_f(z,t)\,d\Delta_0 d\Delta', \tag{B.1b}$$

where $\beta = g^2N/d_{eg}$ and $G(\Delta)$ is normalized spectral distribution for the inhomogeneous broadening. The backward mode equations are similarly given as:

$$\frac{\partial}{\partial t}\sigma_b(z,t) = -i(\Delta_0 + \Delta')\sigma_b + id_{eg}E_b(z,t), \tag{B.1c}$$

$$\left(\frac{\partial}{\partial t} - c\frac{\partial}{\partial z}\right)E_b(z,t) = i\beta\int_{-\infty}^{\infty} G(\Delta_0)G'(\Delta')\sigma_b(z,t)\,d\Delta_0 d\Delta'. \tag{B.1d}$$

where $G(\Delta_0)$ and $G'(\Delta')$ are the initial and broadened distributions.

Absorption

We assume that absorption happens in forward mode and in the time $-\infty \rightarrow 0$. Here we will use the approach of Fourier transform to solve the differential equations. Since the absorption happens in negative times, Fourier transform (FT) for the absorption can be

defined as

$$\mathrm{A}(z,\omega) = \int_{-\infty}^{0} e^{i\omega t}\mathcal{A}(z,t)\,dt, \tag{B.2}$$

On solving Eq. (B.1a) with initial condition $\sigma_f(z,-\infty,\Delta_0,\Delta') = 0$ gives

$$\sigma_f(z,t) = id_{eg}\int_{-\infty}^{t} e^{-i(\Delta'+\Delta_0)(t-s)}E_f(z,s)\,ds, \tag{B.3}$$

On applying Fourier transform Eq. (B.3) gives,

$$\begin{aligned}\sigma_f(z,\omega) =& id\int_{-\infty}^{0} e^{i\omega t}\,dt\int_{0}^{\infty} e^{-i(\Delta'+\Delta_0)x}\mathcal{E}_f(z,t-x)\,dx\\ =& id\int_{0}^{\infty} e^{-i(\Delta'+\Delta_0)x}e^{i\omega x}E_f(z,\omega)\,dx,\end{aligned} \tag{B.4}$$

where $x = t - s$ is used. Similarly applying FT on the Eq. (B.1b) yields

$$\left(-i\omega + c\frac{\partial}{\partial z}\right)E_f(z,\omega) = i\tilde{p}\int_{-\infty}^{\infty} G(\Delta)G'(\Delta')\sigma_f(z,\omega,\Delta_0,\Delta')\,d\Delta_0 d\Delta'. \tag{B.5}$$

On substituting Eq. (B.4) in Eq. (B.5) gives

$$\left[\frac{\partial}{\partial z} - \frac{i\omega}{c} + \kappa H(\omega)\right]E_f(z,\omega) = 0, \tag{B.6}$$

with

$$H(\omega) \equiv \int_{0}^{\infty} dx\, e^{i\omega x}\int_{-\infty}^{\infty} G(\Delta_0)G'(\Delta')e^{-i(\Delta'+\Delta_0)x}\,d\Delta_0 d\Delta', \qquad \kappa \equiv \frac{|g|^2 N}{c}. \tag{B.7}$$

Then the solution of absorption is written as

$$E_f(z,\omega) = E_f(0,\omega)\,e^{i\omega z/c}\,e^{-\kappa H(\omega)z}. \tag{B.8}$$

Backward

We assume that absorption is finished by $t = 0$. The detunings are reversed, i.e. $\Delta_0+\Delta' \to \Delta_0-\Delta'$ and the phase shift $\exp(-2i\omega_0 z/c)$ is applied to couple to the backward

mode. Since the backward mode evolves in the time 0 to ∞, the FT can be defined as

$$\mathrm{A}(z,\omega) \equiv \int_0^\infty e^{i\omega t}\mathrm{A}(z,t)\,dt. \tag{B.9}$$

The backward mode dynamics are given by

$$\frac{\partial}{\partial t}\sigma_b(z,t) = -i(\Delta_0-\Delta')\sigma_b + id_{eg}E_b(z,t), \tag{B.10a}$$

$$\left(\frac{\partial}{\partial t} - c\frac{\partial}{\partial z}\right)E_b(z,t) = i\beta\int_{-\infty}^{\infty} G(\Delta_0)G'(\Delta')\sigma_b(z,t)\,d\Delta_0 d\Delta'. \tag{B.10b}$$

The initial value for the backward mode will be final value of the forward mode hence we write the initial condition for the backward mode as

$$\sigma_b(z,0) = \sigma_f(z,0) = id_{eg}\int_{-\infty}^{0} e^{i(\Delta'+\Delta_0)s}\mathcal{E}_f(z,s)\,ds = idE_f(z,\Delta'+\Delta_0). \tag{B.11}$$

On solving Eq. (B.10a) with the above initial condition gives

$$\sigma_b(z,t) = \sigma(z,0,\Delta_0,\Delta')e^{i(\Delta_0-\Delta')t} + id\int_0^t e^{-i(\Delta'-\Delta_0)(t-s)}E_b(z,s)\,ds \tag{B.12}$$

Note that lower limit can be extended to $-\infty$ since $E_b(z,t)=0$ for $-\infty$ to 0. On taking FT of wave equation Eq. (B.10b) and substituing Eq. (B.11), Eq. (B.12) and Eq. (B.8) yields

$$\begin{aligned}
E_b(z,\omega) =& 2\pi\kappa e^{-(i\omega z/c-\kappa F(\omega)z)}\int_{-\infty}^{\infty} G(\Delta_0)G'(-\omega+\Delta_0)E_f(0,-\omega+2\Delta_0)\\
&\int_L^z e^{i2\Delta_0 z'/c}e^{-\kappa F(\omega)z'}e^{-\kappa H(-\omega+2\Delta_0)z'}\,dz',\\
E_b(0,\omega) =& 2\pi\kappa\int_{-\infty}^{\infty} E_f(0,-\omega+2\Delta_0)\frac{G(\Delta_0)G'(-\omega+\Delta_0)}{2i\Delta_0/c-\kappa[(H(-\omega+2\Delta_0)+F(\omega)]}e^{i\omega z/c}\\
&\left[e^{i2\Delta_0 z/c}e^{-\kappa H(-\omega+2\Delta_0)z} - e^{i2\Delta_0 L/c}e^{\kappa F(\omega)(z-L)}e^{-\kappa H(-\omega+2\Delta_0)L}\right]d\Delta_0.
\end{aligned} \tag{B.13}$$

Assuming that initial distribution to be $G(\Delta_0)=\delta(\Delta_0)$ Eq. (B.13) is simplified as

$$E_b(0,\omega) = E_f(0,-\omega)\frac{-2\pi G'(-\omega)}{H(-\omega)+F(\omega)}\left[1-e^{-\kappa[(H(-\omega)+F(\omega)]L}\right]. \tag{B.14}$$

Assuming that $G'(\Delta')$ is constant $(1/\gamma)$ on the interval $[-\gamma/2, \gamma/2]$ and zero elsewhere gives

$$\begin{aligned} F(\omega) &= \int_0^\infty dx\, e^{i\omega x} \int_{-\infty}^{\infty} G(\Delta_0)G'(\Delta')e^{i(\Delta'-\Delta_0)x}\, d\Delta_0 d\Delta', \\ &= \pi \int_{-\infty}^{\infty} \delta(\Delta'+\omega)G'(\Delta')\, d\Delta', \\ &= \pi/\gamma, \end{aligned} \tag{B.15}$$

and the same simplification gives $H(\omega) = \pi/\gamma$. Then the final output in the time domain is obtained to be

$$\begin{aligned} E_b(0,t) &= -\frac{\gamma}{2\pi}\left(1-e^{-\alpha L}\right) \int_{-\infty}^{\infty} E_f(0,-\omega)G'(-\omega)e^{i\omega t}\, d\omega, \\ &= -\frac{\gamma}{2\pi}\left(1-e^{-\alpha L}\right) \int_{-\gamma/2}^{\gamma/2} E_f(0,-\omega)(1/\gamma)e^{i\omega t}\, d\omega, \end{aligned} \tag{B.16}$$

where $\alpha = \kappa 2\pi/\gamma$.

Forward

At $t = 0$ the absorption is completed and the detuning is reversed, i.e. $\Delta_0 + \Delta' \to \Delta_0 - \Delta'$ but the phase shift $\exp(-2i\omega_0 z/c)$ is not applied and the light will continue to propagate in the forward direction. The wave equation Eq. (B.5) remains same as in absorption

$$\left(-i\omega + c\frac{\partial}{\partial z}\right) E_f(z,\omega) = i\tilde{p} \int_{-\infty}^{\infty} G(\Delta)G'(\Delta')\sigma_f(z,\omega,\Delta_0,\Delta')\, d\Delta_0 d\Delta'. \tag{B.17}$$

Since the forward propagation happens in the time $-\infty$ to ∞ and the detunings are reversed, the σ evolution is same as Eq. (B.12) but with E_b replaced by E_F

$$\sigma_f(z,t) = \sigma_f(z,0,\Delta_0,\Delta')e^{i(\Delta_0-\Delta')t} + id \int_{-\infty}^{t} e^{-i(\Delta'-\Delta_0)(t-s)} E_f(z,s)\, ds. \tag{B.18}$$

On taking FT of Eq. (B.18) and substituting in Eq. (B.17) gives

$$\left[\frac{\partial}{\partial z} - \frac{i\omega}{c} + \kappa F(\omega)\right] \mathcal{E}_f(z,\omega) = -\kappa \int_{-\infty}^{\infty} G(\Delta_0)G'(-\omega+\Delta_0)\mathcal{E}_f(z,-\omega+2\Delta_0)\, d\Delta_0, \tag{B.19}$$

then the solution is obtained as

$$\begin{aligned} E_f(z,\omega) &= -\kappa e^{[i\omega z/c-\kappa F(\omega)z]} \int_{-\infty}^{\infty} G(\Delta_0)G'(-\omega+\Delta_0)\mathcal{E}_f(0,-\omega+2\Delta_0) \\ &\qquad \times \int_0^z e^{-2i\omega z'/c} e^{i2\Delta_0 z'/c} e^{\kappa F(\omega)z'} e^{-\kappa H(-\omega+2\Delta_0)z'}\, dz', \\ &= -\kappa z \int_{-\infty}^{\infty} \mathcal{E}_f(0,-\omega+2\Delta_0)G(\Delta_0)G'(-\omega+\Delta_0) \\ &\qquad \times \operatorname{sinhc}\left[\frac{\kappa z}{2}\{F(\omega)-H(-\omega+2\Delta_0)\}-\frac{iz}{c}(\omega-\Delta_0)\right] \\ &\qquad \times \exp\left[\frac{iz}{c}\Delta_0-\frac{\kappa z}{2}\{F(\omega)+H(-\omega+2\Delta_0)\}\right] d\Delta_0, \end{aligned} \tag{B.20}$$

as in backward-scattering we assume $G(\Delta_0)=\delta(\Delta_0)$ to obtain

$$\begin{aligned} E_f(L,\omega) = -\kappa L E_f(0,-\omega)G'(-\omega), \times \operatorname{sinhc}&\left[\frac{\kappa L}{2}\{F(\omega)-H(-\omega)\}-\frac{iL}{c}\omega\right], \\ &\times \exp\left[-\frac{\kappa L}{2}\{F(\omega)+H(-\omega)\}\right], \end{aligned} \tag{B.21}$$

using the same arguments ($F(\omega)=H(\omega)=\pi/\gamma$) as in back scattering gives

$$E_f(L,\omega) = -\kappa L E_f(0,-\omega)G'(-\omega) \times \frac{\sin(\omega L/c)}{\omega L/c} \times \exp\left(-\frac{\alpha L}{2}\right). \tag{B.22}$$

Appendix C

Calculations for I-AFC in Cs atom

Here we show the calculations for the eigenstates and energies for Cesium atom. We choose the basis $|F, M_F, I, J\rangle$ to write the matrix i.e.

$$\sum_{F,F',M_F,M_{F'}} \left|F', M_{F'}\right\rangle\!\left\langle F', M_{F'}\right| H' \left|F, M_F\right\rangle\!\left\langle F, M_F\right| \tag{C.1}$$

where summation is over all values of F and M_F. Then the hyperfine terms can be obtained as [40]

$$\langle H_{\rm hfs}\rangle = \frac{A}{2}[F(F+1) - I(I+1) - J(J+1)]. \tag{C.2}$$

To evaluate the terms like $\langle F', M_{F'}|H_B|F, M_F\rangle$ we use the Clebsch–Gordan(CG) coefficients as

$$|F, M_F, I, J\rangle = \sum_{M_J,M_I} \mathcal{C}^{J,I,F}_{M_J,M_I,M_F} \left|J, M_J\right\rangle \left|I, M_I\right\rangle \tag{C.3}$$

once the matrix for H' is formed its eigenvalues and vectors will give the transition energies and states.

The transition dipole moments ($|\mathbf{d}|$) between the eigen vectors is written as

$$\begin{aligned}\sum_{m,n} c_m^* c_n \langle F_m, M_F^m, I, J_m|d_q|F_n, M_F^n, I, J_n\rangle = &\sum_{m,n} c_m^* c_n \langle F_m|\mathbf{d}|F_n\rangle \mathcal{C}^{F_n,1,F_m}_{M_F^n,q,M_F^m}.\\ \langle F_m|\mathbf{d}|F_n\rangle = &\langle J_m|\mathbf{d}|J_n\rangle (-1)^{F_n+J_m+1+I}\\ &\sqrt{(2F_n+1)(2J_m+1)(2J_n+1)}\begin{Bmatrix} J_m & J_n & 1\\ F_n & F_m & I\end{Bmatrix}\end{aligned} \tag{C.4}$$

where c_m and c_n are elements of the eigen vector, $\mathbf{d} = e\mathbf{r}$ is the dipole operator and the last

term in curly braces is the Wigner 6-j symbol. The matrix element $\langle J_m|\mathbf{d}|J_n\rangle$ between the excited and ground state, for example for Cs atom it is given to be $0.23ea_o$ [140, 141] and q can take values ±1. Also the selection rules can be obtained by writing CG coefficient ($\mathcal{C}$) in 3-j symbol

$$\mathcal{C}^{F_n,1,F_m}_{M_F^n,q,M_F^m} = (-1)^{F_n-1+M_F^m}\sqrt{2F_m+1}\begin{pmatrix} F_n & 1 & F_m \\ M_F^n & q & -M_F^m \end{pmatrix} \tag{C.5}$$

Eq. (C.5) exists only when the following conditions are satisfied

$$\begin{aligned} M_F^n + q - M_F^m = 0 &\Longrightarrow \Delta M_F = 0, \pm 1 \\ |F_n - 1| \leq F_m \leq F_n + 1 &\Longrightarrow \Delta F = 0, \pm 1 \end{aligned} \tag{C.6}$$

To calculate the comb structure of I-AFC. We start with a ground $|g\rangle$ and excited state $|e\rangle$. Then perturbation matrix for excited and ground levels are obtained.

C.1 Excited state

Energy level	J	I	F	Hyperfine constant (A) in MHz
$5p^6 8p$	3/2	7/2	5, 4, 3, 2	7.626

TABLE C.1: Details for the excited state

Perturbation matrix (H'_e) for the excited level is obtained by solving Eq. (C.1)–(C.3).

$$H'_e = \begin{bmatrix} D_1 & F_1 & 0 & 0 \\ (F_1)^{\mathsf{T}} & D_2 & F_2 & 0 \\ 0 & (F_2)^{\mathsf{T}} & D_3 & F_3 \\ 0 & 0 & (F_3)^{\mathsf{T}} & D_4 \end{bmatrix} \tag{C.7}$$

where i and j, are defined as

$$\begin{aligned} i &= \frac{1}{2} g_J \mu_B B = \frac{1}{2} \times 2 \times 1.4\, 10^{10}\, B, \\ j &= \frac{1}{2} g_I \mu_N B = \frac{1}{2} \times 0.7369 \times \frac{1.4\, 10^{10}}{1836.15}\, B, \end{aligned} \tag{C.8}$$

and

$$D_1 = diag\Big(A\frac{21}{4},\cdots,A\frac{21}{4}\Big)+ diag\Big((3i-7j),\ \frac{4}{5}(3i-7j),\ \frac{3}{5}(3i-7j),\frac{2}{5}(3i-7j),\ \frac{1}{5}(3i-7j),\ 0,\ -\frac{1}{5}(3i-7j),\ -\frac{2}{5}(3i-7j),\ -\frac{3}{5}(3i-7j),\ -\frac{4}{5}(3i-7j),\ -(3i-7j)\Big)$$

$$D_2 = diag\Big(\frac{A}{4},.,.,.,\ \frac{A}{4},.,.,.,\ \frac{A}{4}\Big)+ diag\Big(\frac{8}{5}(i-4j),\ \frac{6}{5}(i-4j),\ \frac{4}{5}(i-4j),\ \frac{2}{5}(i-4j),\ -\frac{2}{5}(i-4j),\ -\frac{4}{5}(i-4j),\ -\frac{6}{5}(i-4j),\ -\frac{8}{5}(i-4j)\Big)$$

$$D_3 = diag\Big(-A\frac{15}{4},.,.,.,.,\ -A\frac{15}{4},.,.,.,.,\ -A\frac{15}{4}\Big)+ diag\Big(-6j,\ -4j,\ -2j,\ 0,\ 6j,\ 4j,\ 2j\Big)$$

$$D_4 = diag\Big(-A\frac{27}{4},.,\ -A\frac{27}{4},.,\ -A\frac{27}{4}\Big)+ diag\Big(-2(i+3j),\ -2(i+j),\ 0,\ 2(i+3j),\ 2(i+j)\Big)$$

$$F_1 = (i+j)\begin{bmatrix} 0 & 0 & 0 & 0 & 0 & 0 & 0 & 0 & 0 \\ \frac{\sqrt{21}}{5} & 0 & 0 & 0 & 0 & 0 & 0 & 0 & 0 \\ 0 & \frac{4}{5}\sqrt{\frac{7}{3}} & 0 & 0 & 0 & 0 & 0 & 0 & 0 \\ 0 & 0 & \frac{7}{5} & 0 & 0 & 0 & 0 & 0 & 0 \\ 0 & 0 & 0 & \frac{2}{5}\sqrt{14} & 0 & 0 & 0 & 0 & 0 \\ 0 & 0 & 0 & 0 & \sqrt{\frac{7}{3}} & 0 & 0 & 0 & 0 \\ 0 & 0 & 0 & 0 & 0 & \frac{2}{5}\sqrt{14} & 0 & 0 & 0 \\ 0 & 0 & 0 & 0 & 0 & 0 & \frac{7}{5} & 0 & 0 \\ 0 & 0 & 0 & 0 & 0 & 0 & 0 & \frac{4}{5}\sqrt{\frac{7}{3}} & 0 \\ 0 & 0 & 0 & 0 & 0 & 0 & 0 & 0 & \frac{\sqrt{21}}{5} \\ 0 & 0 & 0 & 0 & 0 & 0 & 0 & 0 & 0 \end{bmatrix}$$

$$F_2 = (i+j)\begin{bmatrix} 0 & 0 & 0 & 0 & 0 & 0 & 0 \\ \sqrt{\frac{5}{3}} & 0 & 0 & 0 & 0 & 0 & 0 \\ 0 & 2\sqrt{\frac{5}{7}} & 0 & 0 & 0 & 0 & 0 \\ 0 & 0 & \frac{5}{\sqrt{7}} & 0 & 0 & 0 & 0 \\ 0 & 0 & 0 & 4\sqrt{\frac{5}{21}} & 0 & 0 & 0 \\ 0 & 0 & 0 & 0 & \frac{5}{\sqrt{7}} & 0 & 0 \\ 0 & 0 & 0 & 0 & 0 & 2\sqrt{\frac{5}{7}} & 0 \\ 0 & 0 & 0 & 0 & 0 & 0 & \sqrt{\frac{5}{3}} \\ 0 & 0 & 0 & 0 & 0 & 0 & 0 \end{bmatrix} \qquad F_3 = (i+j)\begin{bmatrix} 0 & 0 & 0 & 0 & 0 \\ \sqrt{\frac{15}{7}} & 0 & 0 & 0 & 0 \\ 0 & 2\sqrt{\frac{6}{7}} & 0 & 0 & 0 \\ 0 & 0 & 3\sqrt{\frac{3}{7}} & 0 & 0 \\ 0 & 0 & 0 & 2\sqrt{\frac{6}{7}} & 0 \\ 0 & 0 & 0 & 0 & \sqrt{\frac{15}{7}} \\ 0 & 0 & 0 & 0 & 0 \end{bmatrix}$$

The eigenvalues of M_e give the energy splitting of the excited state and the eigenvectors give the corresponding states.

C.2 Ground state

Energy level	J	I	F	Hyperfine constant (A) in MHz
$5p^6$6s	1/2	7/2	4, 3	2298.157943

TABLE C.2: Details for the ground state

$$H'_g = \begin{bmatrix} D_0 & F \\ (F)^{\mathsf{T}} & D \end{bmatrix} \tag{C.9}$$

where

$$D_0 = diag\Big(A\frac{7}{4}, ., ., ., ., A\frac{7}{4}, ., ., ., ., A\frac{7}{4}\Big) + diag\Big((i-7j),\ \frac{3}{4}(i-7j),\ \frac{1}{2}(i-7j),\ \frac{1}{4}(i-7j),\ 0,\ -\frac{1}{4}(i-7j),\ -\frac{1}{2}(i-7j),\ -\frac{3}{4}(i-7j),\ (-i+7j)\Big)$$

$$D = diag\Big(-A\frac{9}{4}, ., ., -A\frac{9}{4}, ., ., -A\frac{9}{4}\Big) + diag\Big(-\frac{3}{4}(i+9j),\ -\frac{1}{2}(i+9j),\ -\frac{1}{4}(i+9j),\ 0,\ \frac{1}{4}(i+9j),\ \frac{1}{2}(i+9j),\ \frac{3}{4}(i+9j)\Big)$$

$$F=(i+j)\begin{bmatrix} 0 & 0 & 0 & 0 & 0 & 0 & 0 \\ \frac{\sqrt{7}}{4} & 0 & 0 & 0 & 0 & 0 & 0 \\ 0 & \frac{\sqrt{3}}{2} & 0 & 0 & 0 & 0 & 0 \\ 0 & 0 & \frac{\sqrt{15}}{4} & 0 & 0 & 0 & 0 \\ 0 & 0 & 0 & 1 & 0 & 0 & 0 \\ 0 & 0 & 0 & 0 & \frac{\sqrt{15}}{4} & 0 & 0 \\ 0 & 0 & 0 & 0 & 0 & \frac{\sqrt{3}}{2} & 0 \\ 0 & 0 & 0 & 0 & 0 & 0 & \frac{\sqrt{7}}{4} \\ 0 & 0 & 0 & 0 & 0 & 0 & 0 \end{bmatrix}$$

Eigenvalues and eigenvectors hold same interpretation as in the excited state. Now we have 32 excited, 16 ground states and hence (32×16) transitions and the transition amplitudes are numerically calculated using Eq. (C.4).

The atomic transitions are divided into selection rules $\Delta m = +1\,(-1)$ which interact with the polarization $|L\rangle$ ($|R\rangle$). The transitions of I-AFC for the Cesium atom numerically are written as

Transition frequency in MHz	Energy difference (Δ_n) in MHz	Transition amplitude ($\lvert d_n\rvert^2$) in $(ea_o)^2$
7242.76	-931.6	0.0164
7427.04	-747.317	0.0319
7815.46	-358.897	0.0245
8174.36	0	0.0183
8509.73	335.368	0.0129
8825.77	651.409	0.0081
9125.56	951.205	0.0039

TABLE C.3: Transition frequencies and amplitudes for the selection rule $\Delta M_F = -1$ (i.e.. q=1 in Eq. (C.5))

We also calculate the transitions and energies for Rubidium using similar techniques.

Transition frequency in MHz	Energy difference (Δ_n) in MHz	Transition amplitude ($\|d_n\|^2$) in $(ea_o)^2$
1467.76	-1105.29	0.0119
1871.67	-701.379	0.021
2237.08	-335.975	0.0283
2573.05	0	0.0346
2885.59	312.539	0.04
3178.89	605.845	0.0447
3320.06	747.013	0.0135

TABLE C.4: Transition frequencies and amplitudes for the selection rule $\Delta M_F = 1$ (i.e.. q=-1 in Eq. (C.5))

Appendix D

Calculations for swap operation

The swap operation in atom-cavity system was first proposed in [32]. Instead of the following [32] we derive the equations using the approach developed in [101, 100].

To derive the Eq. (7.22) we first set the initial conditions. The initial state is given by Eq. (7.20) and the input pulse is assumed to have a Gaussian profile with mean frequency ω_L and width $\bar{w}$

$$f_{\text{inp}}(\omega', -\infty) = \mathbf{N} \int \exp\left\{-\frac{(\omega' - \omega_L)^2}{\bar{\omega}}\right\} d\omega' \tag{D.1}$$

here $|f_{\text{inp}}(\omega', -\infty)|^2 = 1$ and $\mathbf{N}$ is the normalization constant. Since the frequencies are defined relative to cavity frequency $\omega = \omega' - \omega_c$, we write

$$f_{\text{inp}}(\omega, -\infty) = \mathbf{N} \int \exp\left\{-\frac{(\omega - \Delta)^2}{\bar{\omega}}\right\} d\omega \tag{D.2}$$

where $\Delta = \omega_L - \omega_c = \omega_L - \omega_a$ is atom-light detuning. Thus the initial condition Eq. (7.20) changes to

$$|\Psi\rangle(-\infty) = \int f_{\text{inp}}(\omega - \Delta, -\infty)\hat{a}_R^\dagger \, d\omega \, |0\rangle \, |1\rangle \, . \tag{D.3}$$

The pulse profile in the time domain is obtained by taking Fourier transforms, which we define as:

$$f(t) = \int f(\omega) e^{-i\omega t} \, d\omega, \qquad f(\omega) = \frac{1}{2\pi} \int f(t) e^{i\omega t} \, dt. \tag{D.4}$$

The equations of motions on using Eq. (7.18) and Eq. (7.19) reads

$$\begin{aligned} \frac{\partial}{\partial t} f_R(\omega, t) &= -\sqrt{\Gamma} e^{i\omega t} f_0(t), \\ \frac{\partial}{\partial t} f_L(\omega, t) &= -\sqrt{\Gamma} e^{i\omega t} f_0(t), \\ \frac{\partial}{\partial t} f_0(t) &= \sqrt{\Gamma} \int e^{-i\omega t} (f_R + f_L)\, d\omega, \end{aligned} \tag{D.5}$$

and with $F(\omega, t) \equiv f_R + f_L$, Eq. (D.5) gives

$$\frac{\partial}{\partial t} F(\omega, t) = -2\sqrt{\Gamma} e^{i\omega t} f_0(t), \tag{D.6a}$$

$$\frac{\partial}{\partial t} f_0(t) = \sqrt{\Gamma} \int e^{-i\omega t} F(\omega, t)\, d\omega. \tag{D.6b}$$

On solving Eq. (D.6a) gives

$$F = f_{\text{inp}}(\omega - \Delta, -\infty) - 2\sqrt{\Gamma} \int_{-\infty}^{t} e^{i\omega t'} f_0(t')\, dt', \tag{D.7}$$

and substituting it in the Eq. (D.6b) gives

$$\begin{aligned} \frac{\partial}{\partial t} f_0(t) &= \sqrt{\Gamma} \int e^{-i\omega t} f_{\text{inp}}(\omega - \Delta, -\infty)\, d\omega - 2\Gamma \int \int_{-\infty}^{t} e^{-i\omega(t-t')} f_0(t')\, dt'\, d\omega, \\ &= \sqrt{\Gamma} e^{-i\Delta t} f_{\text{inp}}(t, -\infty) - 2\pi\Gamma f_0(t), \end{aligned} \tag{D.8}$$

where the relations $\int e^{-i\omega(t-t')} d\omega = 2\pi\delta(t - t')$ and $2\int_{-\infty}^{t} \delta(t - t') f_0(t')\, dt' = f_0(t)$ are used. Then the transformation $f_0(t) = e^{-i\Delta t} \tilde{f}_0(t)$ gives

$$\frac{\partial}{\partial t} \tilde{f}_0(t) + (-i\Delta + 2\pi\Gamma) \tilde{f}_0(t) = \sqrt{\Gamma} f_{\text{inp}}(t, -\infty). \tag{D.9}$$

In the adiabatic limit where the width of input pulse ($\mathcal{T}^{-1}$) is assumed to be shorter than the decay rate ($\Gamma \gg \mathcal{T}^{-1}$), we set $\frac{\partial}{\partial t} \tilde{f}_0(t) = 0$. Then the Eq. (D.9) gives

$$f_0(t) = \frac{\sqrt{\Gamma}}{-i\Delta + 2\pi\Gamma} e^{-i\Delta t} f_{\text{inp}}(t, -\infty). \tag{D.10}$$

On assuming the input photon to be right circularly polarized and substituting the above in the Eq. (D.5) gives

$$\begin{aligned} f_R(\omega,t) &= f_{\text{inp}}(\omega-\Delta,\infty) - \frac{2\pi\Gamma}{-i\Delta+2\pi\Gamma}\frac{1}{2\pi}\int_{-\infty}^{t} f_{\text{inp}}(t',-\infty)e^{i(\omega-\Delta)t'}\,dt', \\ f_R(\omega,\infty) &= \frac{-i\Delta}{\Gamma'-i\Delta} f_{\text{inp}}(\omega-\Delta,-\infty), \end{aligned} \tag{D.11}$$

where the angular frequency is defined as $2\pi\Gamma = \Gamma'$ and similarly we obtain

$$f_L(\omega,\infty) = \frac{-\Gamma'}{\Gamma'-i\Delta} f_{\text{inp}}(\omega-\Delta,-\infty). \tag{D.12}$$

Bibliography

[1] Morten Kjaergaard, Mollie E. Schwartz, Jochen Braumüller, Philip Krantz, Joel I.-J. Wang, Simon Gustavsson, and William D. Oliver. Superconducting qubits: Current state of play. *Annual Review of Condensed Matter Physics*, 11(1):369–395, 2020.

[2] Alexandre Blais, Arne L. Grimsmo, S. M. Girvin, and Andreas Wallraff. Circuit quantum electrodynamics. *Rev. Mod. Phys.*, 93:025005, May 2021.

[3] Colin D. Bruzewicz, John Chiaverini, Robert McConnell, and Jeremy M. Sage. Trapped-ion quantum computing: Progress and challenges. *Applied Physics Reviews*, 6(2):021314, Jun 2019.

[4] Xiaoling Wu, Xinhui Liang, Yaoqi Tian, Fan Yang, Cheng Chen, Yong-Chun Liu, Meng Khoon Tey, and Li You. A concise review of rydberg atom based quantum computation and quantum simulation*. *Chinese Physics B*, 30(2):020305, Feb 2021.

[5] Erika Janitz, Mihir K. Bhaskar, and Lilian Childress. Cavity quantum electrodynamics with color centers in diamond. *Optica*, 7(10):1232–1252, Oct 2020.

[6] Anasua Chatterjee, Paul Stevenson, Silvano De Franceschi, Andrea Morello, Nathalie P. de Leon, and Ferdinand Kuemmeth. Semiconductor qubits in practice. *Nature Reviews Physics*, 3(3):157–177, Feb 2021.

[7] J. Eli Bourassa, Rafael N. Alexander, Michael Vasmer, Ashlesha Patil, Ilan Tzitrin, Takaya Matsuura, Daiqin Su, Ben Q. Baragiola, Saikat Guha, Guillaume Dauphinais, Krishna K. Sabapathy, Nicolas C. Menicucci, and Ish Dhand. Blueprint for a scalable photonic fault-tolerant quantum computer. *Quantum*, 5:392, Feb 2021.

[8] Sara Bartolucci, Patrick Birchall, Hector Bombin, Hugo Cable, Chris Dawson, Mercedes Gimeno-Segovia, Eric Johnston, Konrad Kieling, Naomi Nickerson, Mihir

Pant, Fernando Pastawski, Terry Rudolph, and Chris Sparrow. Fusion-based quantum computation, 2021.

[9] Daniel Gottesman, Alexei Kitaev, and John Preskill. Encoding a qubit in an oscillator. *Physical Review A*, 64(1):012310, 2001.

[10] Xing Rong, Jianpei Geng, Fazhan Shi, Ying Liu, Kebiao Xu, Wenchao Ma, Fei Kong, Zhen Jiang, Yang Wu, and Jiangfeng Du. Experimental fault-tolerant universal quantum gates with solid-state spins under ambient conditions. *Nature communications*, 6(1):1–7, 2015.

[11] Mark Saffman. Quantum computing with neutral atoms. *National Science Review*, 6(1):24–25, 2019.

[12] Christian Weedbrook, Stefano Pirandola, Raúl García-Patrón, Nicolas J Cerf, Timothy C Ralph, Jeffrey H Shapiro, and Seth Lloyd. Gaussian quantum information. *Reviews of Modern Physics*, 84(2):621, 2012.

[13] Swapnil Nitin Shah. Realizations of measurement based quantum computing, 2021.

[14] Robert Raussendorf and Hans J Briegel. A one-way quantum computer. *Physical Review Letters*, 86(22):5188, 2001.

[15] Nicolas Sangouard, Christoph Simon, Hugues De Riedmatten, and Nicolas Gisin. Quantum repeaters based on atomic ensembles and linear optics. *Reviews of Modern Physics*, 83(1):33, 2011.

[16] Charles H Bennett, Gilles Brassard, Sandu Popescu, Benjamin Schumacher, John A Smolin, and William K Wootters. Purification of noisy entanglement and faithful teleportation via noisy channels. *Physical review letters*, 76(5):722, 1996.

[17] L-M Duan, Mikhail D Lukin, J Ignacio Cirac, and Peter Zoller. Long-distance quantum communication with atomic ensembles and linear optics. *Nature*, 414(6862):413–418, 2001.

[18] Gavin Brennen, Elisabeth Giacobino, and Christoph Simon. Focus on quantum memory. *New Journal of Physics*, 17(5):050201, 2015.

[19] Khabat Heshami, Duncan G. England, Peter C. Humphreys, Philip J. Bustard, Victor M. Acosta, Joshua Nunn, and Benjamin J. Sussman. Quantum memories: emerging applications and recent advances. *Journal of Modern Optics*, 63(20):2005–2028, Mar 2016.

[20] Yunfei Wang, Jianfeng Li, Shanchao Zhang, Keyu Su, Yiru Zhou, Kaiyu Liao, Shengwang Du, Hui Yan, and Shi-Liang Zhu. Efficient quantum memory for single-photon polarization qubits. *Nature Photonics*, 13(5):346, 2019.

[21] Gabriel Hetet, JJ Longdell, AL Alexander, Ping Koy Lam, and MJ Sellars. Electro-optic quantum memory for light using two-level atoms. *Physical review letters*, 100(2):023601, 2008.

[22] Mahdi Hosseini, Ben M Sparkes, Geoff Campbell, Ping K Lam, and Ben C Buchler. High efficiency coherent optical memory with warm rubidium vapour. *Nature communications*, 2:174, 2011.

[23] T Chaneliere, J Ruggiero, M Bonarota, M Afzelius, and JL Le Gouët. Efficient light storage in a crystal using an atomic frequency comb. *New Journal of Physics*, 12(2):023025, 2010.

[24] Andreas Reiserer and Gerhard Rempe. Cavity-based quantum networks with single atoms and optical photons. *Rev. Mod. Phys.*, 87:1379–1418, Dec 2015.

[25] Mark Saffman. Quantum computing with neutral atoms. *National Science Review*, 6(1):24–25, 09 2018.

[26] Bastian Hacker, Stephan Welte, Severin Daiss, Armin Shaukat, Stephan Ritter, Lin Li, and Gerhard Rempe. Deterministic creation of entangled atom–light schrödinger-cat states. *Nature Photonics*, 13(2):110–115, 2019.

[27] Andrew D Ludlow, Martin M Boyd, Jun Ye, Ekkehard Peik, and Piet O Schmidt. Optical atomic clocks. *Reviews of Modern Physics*, 87(2):637, 2015.

[28] Mikael Afzelius, Imam Usmani, Atia Amari, Björn Lauritzen, Andreas Walther, Christoph Simon, Nicolas Sangouard, Jiří Minář, Hugues De Riedmatten, Nicolas Gisin, et al. Demonstration of atomic frequency comb memory for light with spin-wave storage. *Physical review letters*, 104(4):040503, 2010.

[29] Chanchal, G. P. Teja, Christoph Simon, and Sandeep K. Goyal. Storing vector-vortex states of light in an intra-atomic frequency-comb quantum memory. *Phys. Rev. A*, 104:043713, Oct 2021.

[30] Rajeev Gangwar, Mohit Lal Bera, GP Teja, Sandeep K Goyal, and Manabendra Nath Bera. Making noisy quantum channels transparent. *arXiv preprint arXiv:2106.04425*, 2021.

[31] Thomas Konrad, Amy Rouillard, Michael Kastner, and Hermann Uys. Robust control of quantum systems by quantum systems. *Phys. Rev. A*, 104:052614, Nov 2021.

[32] Kazuki Koshino, Satoshi Ishizaka, and Yasunobu Nakamura. Deterministic photon-photon $\sqrt{\text{swap}}$ gate using a Λ system. *Phys. Rev. A*, 82:010301, Jul 2010.

[33] Natasha Tomm, Alisa Javadi, Nadia Olympia Antoniadis, Daniel Najer, Matthias Christian Löbl, Alexander Rolf Korsch, Rüdiger Schott, Sascha René Valentin, Andreas Dirk Wieck, Arne Ludwig, and et al. A bright and fast source of coherent single photons. *Nature Nanotechnology*, 16(4):399–403, Jan 2021.

[34] Leslie Allen and Joseph H Eberly. *Optical resonance and two-level atoms*, volume 28. Courier Corporation, 1987.

[35] Leonard Mandel and Emil Wolf. *Optical coherence and quantum optics*. Cambridge university press, 1995.

[36] Marlan O Scully and M Suhail Zubairy. Quantum optics, 1999.

[37] Howard Carmichael. *An open systems approach to quantum optics: lectures presented at the Université Libre de Bruxelles, October 28 to November 4, 1991*, volume 18. Springer Science & Business Media, 2009.

[38] Heinz-Peter Breuer, Francesco Petruccione, et al. *The theory of open quantum systems*. Oxford University Press on Demand, 2002.

[39] Pierre Meystre and Murray Sargent. *Elements of quantum optics*. Springer Science & Business Media, 2013.

[40] Brian Harold Bransden and Charles Jean Joachain. *Physics of atoms and molecules*. Pearson Education India, 2003.

[41] K. Bergmann, H. Theuer, and B. W. Shore. Coherent population transfer among quantum states of atoms and molecules. *Rev. Mod. Phys.*, 70:1003–1025, Jul 1998.

[42] Mustafa Demirplak and Stuart A. Rice. Adiabatic population transfer with control fields. *The Journal of Physical Chemistry A*, 107(46):9937–9945, 2003.

[43] Mustafa Demirplak and Stuart A. Rice. Assisted adiabatic passage revisited. *The Journal of Physical Chemistry B*, 109(14):6838–6844, 2005. PMID: 16851769.

[44] Michael Fleischhauer, Atac Imamoglu, and Jonathan P. Marangos. Electromagnetically induced transparency: Optics in coherent media. *Reviews of Modern Physics*, 77(2):633–673, 2005.

[45] R. M. Whitley and C. R. Stroud. Double optical resonance. *Phys. Rev. A*, 14:1498–1513, Oct 1976.

[46] EetGORRIOLS Arimondo and G Orriols. Nonabsorbing atomic coherences by coherent two-photon transitions in a three-level optical pumping. *Nuovo Cimento Lettere*, 17:333–338, 1976.

[47] CW Gardiner and MJ Collett. Input and output in damped quantum systems: Quantum stochastic differential equations and the master equation. *Physical Review A*, 31(6):3761, 1985.

[48] Alexey V Gorshkov, Axel André, Mikhail D Lukin, and Anders S Sørensen. Photon storage in λ-type optically dense atomic media. i. cavity model. *Physical Review A*, 76(3):033804, 2007.

[49] Claude Cohen-Tannoudji, Jacques Dupont-Roc, and Gilbert Grynberg. *Atom-photon interactions: basic processes and applications*. 1998.

[50] Michael Fleischhauer and Mikhail D Lukin. Quantum memory for photons: Dark-state polaritons. *Physical Review A*, 65(2):022314, 2002.

[51] Lene Vestergaard Hau, Stephen E Harris, Zachary Dutton, and Cyrus H Behroozi. Light speed reduction to 17 metres per second in an ultracold atomic gas. *Nature*, 397(6720):594, 1999.

[52] Michael M Kash, Vladimir A Sautenkov, Alexander S Zibrov, Leo Hollberg, George R Welch, Mikhail D Lukin, Yuri Rostovtsev, Edward S Fry, and Marlan O Scully. Ultraslow group velocity and enhanced nonlinear optical effects in a coherently driven hot atomic gas. *Physical Review Letters*, 82(26):5229, 1999.

[53] SE Harris and Lene Vestergaard Hau. Nonlinear optics at low light levels. *Physical Review Letters*, 82(23):4611, 1999.

[54] Michael Fleischhauer and Aaron S Manka. Propagation of laser pulses and coherent population transfer in dissipative three-level systems: An adiabatic dressed-state picture. *Physical Review A*, 54(1):794, 1996.

[55] D. Budker, D. F. Kimball, S. M. Rochester, and V. V. Yashchuk. Nonlinear magneto-optics and reduced group velocity of light in atomic vapor with slow ground state relaxation. *Phys. Rev. Lett.*, 83:1767–1770, Aug 1999.

[56] David Höckel and Oliver Benson. Electromagnetically induced transparency in cesium vapor with probe pulses on the single-photon level. *Physical review letters*, 105(15):153605, 2010.

[57] Young-Wook Cho and Yoon-Ho Kim. Storage and retrieval of thermal light in warm atomic vapor. *Physical Review A*, 82(3):033830, 2010.

[58] Jürgen Appel, Eden Figueroa, Dmitry Korystov, M Lobino, and AI Lvovsky. Quantum memory for squeezed light. *Physical review letters*, 100(9):093602, 2008.

[59] DF Phillips, A Fleischhauer, A Mair, RL Walsworth, and Mikhail D Lukin. Storage of light in atomic vapor. *Physical Review Letters*, 86(5):783, 2001.

[60] Stefan Riedl, Matthias Lettner, Christoph Vo, Simon Baur, Gerhard Rempe, and Stephan Dürr. Bose-einstein condensate as a quantum memory for a photonic polarization qubit. *Physical Review A*, 85(2):022318, 2012.

[61] Matthias Lettner, Martin Mücke, Stefan Riedl, Christoph Vo, Carolin Hahn, Simon Baur, Jörg Bochmann, Stephan Ritter, Stephan Dürr, and Gerhard Rempe. Remote entanglement between a single atom and a bose-einstein condensate. *Physical Review Letters*, 106(21):210503, 2011.

[62] Rui Zhang, Sean R Garner, and Lene Vestergaard Hau. Creation of long-term coherent optical memory via controlled nonlinear interactions in bose-einstein condensates. *Physical review letters*, 103(23):233602, 2009.

[63] T Chaneliere, DN Matsukevich, SD Jenkins, S-Y Lan, TAB Kennedy, and Alex Kuzmich. Storage and retrieval of single photons transmitted between remote quantum memories. *Nature*, 438(7069):833, 2005.

[64] Han Zhang, Xian-Min Jin, Jian Yang, Han-Ning Dai, Sheng-Jun Yang, Tian-Ming Zhao, Jun Rui, Yu He, Xiao Jiang, Fan Yang, et al. Preparation and storage of frequency-uncorrelated entangled photons from cavity-enhanced spontaneous parametric downconversion. *Nature Photonics*, 5(10):628, 2011.

[65] Xiao-Hui Bao, Andreas Reingruber, Peter Dietrich, Jun Rui, Alexander Dück, Thorsten Strassel, Li Li, Nai-Le Liu, Bo Zhao, and Jian-Wei Pan. Efficient and long-lived quantum memory with cold atoms inside a ring cavity. *Nature Physics*, 8(7):517, 2012.

[66] Yu-Ao Chen, Shuai Chen, Zhen-Sheng Yuan, Bo Zhao, Chih-Sung Chuu, Jörg Schmiedmayer, and Jian-Wei Pan. Memory-built-in quantum teleportation with photonic and atomic qubits. *Nature Physics*, 4(2):103, 2008.

[67] K Akiba, K Kashiwagi, T Yonehara, and M Kozuma. Frequency-filtered storage of parametric fluorescence with electromagnetically induced transparency. *Physical Review A*, 76(2):023812, 2007.

[68] Georg Heinze, Christian Hubrich, and Thomas Halfmann. Stopped light and image storage by electromagnetically induced transparency up to the regime of one minute. *Physical review letters*, 111(3):033601, 2013.

[69] Mattias Nilsson and Stefan Kröll. Solid state quantum memory using complete absorption and re-emission of photons by tailored and externally controlled inhomogeneous absorption profiles. *Optics communications*, 247(4-6):393–403, 2005.

[70] Mattias Nilsson and Stefan Kröll. Solid state quantum memory using complete absorption and re-emission of photons by tailored and externally controlled inhomogeneous absorption profiles. *Optics communications*, 247(4-6):393–403, 2005.

[71] SA Moiseev and Stefan Kröll. Complete reconstruction of the quantum state of a single-photon wave packet absorbed by a doppler-broadened transition. *Physical review letters*, 87(17):173601, 2001.

[72] Annabel L Alexander, Jevon J Longdell, Matthew J Sellars, and Neil B Manson. Photon echoes produced by switching electric fields. *Physical review letters*, 96(4):043602, 2006.

[73] Annabel L Alexander, Jevon J Longdell, Matthew J Sellars, and Neil B Manson. Photon echoes produced by switching electric fields. *Physical review letters*, 96(4):043602, 2006.

[74] Nicolas Sangouard, Christoph Simon, Mikael Afzelius, and Nicolas Gisin. Analysis of a quantum memory for photons based on controlled reversible inhomogeneous broadening. *Physical Review A*, 75(3):032327, 2007.

[75] Björn Lauritzen, Jiří Minář, Hugues De Riedmatten, Mikael Afzelius, Nicolas Sangouard, Christoph Simon, and Nicolas Gisin. Telecommunication-wavelength solid-state memory at the single photon level. *Physical review letters*, 104(8):080502, 2010.

[76] Mikael Afzelius, Christoph Simon, Hugues de Riedmatten, and Nicolas Gisin. Multimode quantum memory based on atomic frequency combs. *Phys. Rev. A*, 79(5):052329, may 2009.

[77] Hugues De Riedmatten, Mikael Afzelius, Matthias U Staudt, Christoph Simon, and Nicolas Gisin. A solid-state light–matter interface at the single-photon level. *Nature*, 456(7223):773, 2008.

[78] Juan Luis Rubio, Daniel Viscor, Jordi Mompart, and Verònica Ahufinger. Atomic-frequency-comb quantum memory via piecewise adiabatic passage. *Physical Review A*, 98(4):043834, 2018.

[79] G P Teja, Christoph Simon, and Sandeep K Goyal. Photonic quantum memory using an intra-atomic frequency comb. *Physical Review A*, 99(5):052314, 2019.

[80] Pierre Meystre and Murray Sargent. *Elements of quantum optics*. Springer Science & Business Media, 2007.

[81] Y-W Liu and PEG Baird. Measurement of the caesium 6s1/2? 8p1/2 transition frequency. *Applied Physics B: Lasers and Optics*, 71(4):567–572, 2000.

[82] Daniel F Walls and Gerard J Milburn. *Quantum optics*. Springer Science & Business Media, 2007.

[83] Andreas Reiserer and Gerhard Rempe. Cavity-based quantum networks with single atoms and optical photons. *Reviews of Modern Physics*, 87(4):1379, 2015.

[84] D. E. Chang, J. S. Douglas, A. González-Tudela, C.-L. Hung, and H. J. Kimble. Colloquium: Quantum matter built from nanoscopic lattices of atoms and photons. *Rev. Mod. Phys.*, 90:031002, Aug 2018.

[85] Qiong Chen, Wanli Yang, Mang Feng, and Jiangfeng Du. Entangling separate nitrogen-vacancy centers in a scalable fashion via coupling to microtoroidal resonators. *Physical Review A*, 83(5):054305, may 2011.

[86] Chris O'Brien, Tian Zhong, Andrei Faraon, and Christoph Simon. Nondestructive photon detection using a single rare-earth ion coupled to a photonic cavity. *Physical Review A*, 94(4):043807, 2016.

[87] CY Hu and JG Rarity. Extended linear regime of cavity-qed enhanced optical circular birefringence induced by a charged quantum dot. *Physical Review B*, 91(7):075304, 2015.

[88] Kevin M Birnbaum, Andreea Boca, Russell Miller, Allen D Boozer, Tracy E Northup, and H Jeff Kimble. Photon blockade in an optical cavity with one trapped atom. *Nature*, 436(7047):87–90, 2005.

[89] Christoph Hamsen, Karl Nicolas Tolazzi, Tatjana Wilk, and Gerhard Rempe. Two-photon blockade in an atom-driven cavity qed system. *Phys. Rev. Lett.*, 118:133604, Mar 2017.

[90] Axel Kuhn, Markus Hennrich, T Bondo, and Gerhard Rempe. Controlled generation of single photons from a strongly coupled atom-cavity system. *Applied Physics B*, 69(5-6):373–377, 1999.

[91] Martin Mücke, Joerg Bochmann, Carolin Hahn, Andreas Neuzner, Christian Nölleke, Andreas Reiserer, Gerhard Rempe, and Stephan Ritter. Generation of single photons from an atom-cavity system. *Physical Review A*, 87(6):063805, 2013.

[92] Nikolay V. Vitanov, Andon A. Rangelov, Bruce W. Shore, and Klaas Bergmann. Stimulated raman adiabatic passage in physics, chemistry, and beyond. *Rev. Mod. Phys.*, 89:015006, Mar 2017.

[93] Girish S Agarwal. *Quantum optics*. Cambridge University Press, 2012.

[94] Jean-Michel Raimond and Serge Haroche. Exploring the quantum. *Oxford University Press*, 82:86, 2006.

[95] M Brune, F Schmidt-Kaler, Abdelhamid Maali, J Dreyer, E Hagley, JM Raimond, and S Haroche. Quantum rabi oscillation: A direct test of field quantization in a cavity. *Physical review letters*, 76(11):1800, 1996.

[96] Guan Yu Wang, Qian Liu, Hai Rui Wei, Tao Li, Qing Ai, and Fu Guo Deng. Universal quantum gates for photon-atom hybrid systems assisted by bad cavities. *Scientific Reports*, 6:1–9, 2016.

[97] Alexandre Baksic, Hugo Ribeiro, and Aashish A Clerk. Speeding up adiabatic quantum state transfer by using dressed states. *Physical review letters*, 116(23):230503, 2016.

[98] Xi Chen, I Lizuain, A Ruschhaupt, D Guéry-Odelin, and JG Muga. Shortcut to adiabatic passage in two-and three-level atoms. *Physical review letters*, 105(12):123003, 2010.

[99] Yan-Xiong Du, Zhen-Tao Liang, Yi-Chao Li, Xian-Xian Yue, Qing-Xian Lv, Wei Huang, Xi Chen, Hui Yan, and Shi-Liang Zhu. Experimental realization of stimulated raman shortcut-to-adiabatic passage with cold atoms. *Nature Communications*, 7(1), Aug 2016.

[100] Julio Gea-Banacloche and William Wilson. Photon subtraction and addition by a three-level atom in an optical cavity. *Phys. Rev. A*, 88:033832, Sep 2013.

[101] Julio Gea-Banacloche. Space-time descriptions of quantum fields interacting with optical cavities. *Phys. Rev. A*, 87:023832, Feb 2013.

[102] Q. A. Turchette, C. J. Hood, W. Lange, H. Mabuchi, and H. J. Kimble. Measurement of conditional phase shifts for quantum logic. *Phys. Rev. Lett.*, 75:4710–4713, Dec 1995.

[103] L-M Duan and HJ Kimble. Scalable photonic quantum computation through cavity-assisted interactions. *Physical review letters*, 92(12):127902, 2004.

[104] Xin-Wen Wang, Deng-Yu Zhang, Shi-Qing Tang, and Li-Jun Xie. Nondestructive greenberger-horne-zeilinger-state analyzer. *Quantum information processing*, 12(2):1065–1075, 2013.

[105] Joerg Bochmann, Martin Mücke, Christoph Guhl, Stephan Ritter, Gerhard Rempe, and David L Moehring. Lossless state detection of single neutral atoms. *Physical review letters*, 104(20):203601, 2010.

[106] Roger Gehr, Jürgen Volz, Guilhem Dubois, Tilo Steinmetz, Yves Colombe, Benjamin L Lev, Romain Long, Jérôme Esteve, and Jakob Reichel. Cavity-based single atom preparation and high-fidelity hyperfine state readout. *Physical review letters*, 104(20):203602, 2010.

[107] Bastian Hacker, Stephan Welte, Gerhard Rempe, and Stephan Ritter. A photon–photon quantum gate based on a single atom in an optical resonator. *Nature*, 536(7615):193–196, 2016.

[108] Edo Waks, Eleni Diamanti, and Yoshihisa Yamamoto. Generation of photon number states. *New Journal of Physics*, 8(1):4, 2006.

[109] Chunle Xiong, X Zhang, Z Liu, Matthew J Collins, A Mahendra, LG Helt, Michael J Steel, D-Y Choi, CJ Chae, PHW Leong, et al. Active temporal multiplexing of indistinguishable heralded single photons. *Nature communications*, 7(1):1–6, 2016.

[110] David P. DiVincenzo. The physical implementation of quantum computation. *Fortschritte der Physik*, 48(9-11):771–783, Sep 2000.

[111] Emanuel Knill. Quantum computing with realistically noisy devices. *Nature*, 434(7029):39–44, 2005.

[112] Jani Tuorila, Matti Partanen, Tapio Ala-Nissila, and Mikko Möttönen. Efficient protocol for qubit initialization with a tunable environment. *npj Quantum Information*, 3(1):1–12, 2017.

[113] T. P. Harty, D. T. C. Allcock, C. J. Ballance, L. Guidoni, H. A. Janacek, N. M. Linke, D. N. Stacey, and D. M. Lucas. High-fidelity preparation, gates, memory, and readout of a trapped-ion quantum bit. *Phys. Rev. Lett.*, 113:220501, Nov 2014.

[114] A. H. Myerson, D. J. Szwer, S. C. Webster, D. T. C. Allcock, M. J. Curtis, G. Imreh, J. A. Sherman, D. N. Stacey, A. M. Steane, and D. M. Lucas. High-fidelity readout of trapped-ion qubits. *Phys. Rev. Lett.*, 100:200502, May 2008.

[115] Roger Gehr, Jürgen Volz, Guilhem Dubois, Tilo Steinmetz, Yves Colombe, Benjamin L. Lev, Romain Long, Jérôme Estève, and Jakob Reichel. Cavity-based single atom preparation and high-fidelity hyperfine state readout. *Phys. Rev. Lett.*, 104:203602, May 2010.

[116] A. Reiserer, S. Ritter, and G. Rempe. Nondestructive detection of an optical photon. *Science*, 342(6164):1349–1351, November 2013.

[117] J. Bochmann, M. Mücke, C. Guhl, S. Ritter, G. Rempe, and D. L. Moehring. Lossless state detection of single neutral atoms. *Phys. Rev. Lett.*, 104:203601, May 2010.

[118] Morten Kjaergaard, Mollie E. Schwartz, Jochen Braumüller, Philip Krantz, Joel I.-J. Wang, Simon Gustavsson, and William D. Oliver. Superconducting qubits: Current state of play. *Annual Review of Condensed Matter Physics*, 11(1):369–395, 2020.

[119] Antti Vepsäläinen, Sergey Danilin, and Gheorghe Sorin Paraoanu. Superadiabatic population transfer in a three-level superconducting circuit. *Science Advances*, 5(2):eaau5999, Feb 2019.

[120] Tenghui Wang, Zhenxing Zhang, Liang Xiang, Zhilong Jia, Peng Duan, Weizhou Cai, Zhihao Gong, Zhiwen Zong, Mengmeng Wu, Jianlan Wu, and et al. The experimental realization of high-fidelity "shortcut-to-adiabaticity" quantum gates in a superconducting xmon qubit. *New Journal of Physics*, 20(6):065003, Jun 2018.

[121] Yan-Xiong Du, Zhen-Tao Liang, Yi-Chao Li, Xian-Xian Yue, Qing-Xian Lv, Wei Huang, Xi Chen, Hui Yan, and Shi-Liang Zhu. Experimental realization

of stimulated raman shortcut-to-adiabatic passage with cold atoms. *Nature Communications*, 7(1), Aug 2016.

[122] Jingfu Zhang, Jeong Hyun Shim, Ingo Niemeyer, T. Taniguchi, T. Teraji, H. Abe, S. Onoda, T. Yamamoto, T. Ohshima, J. Isoya, and et al. Experimental implementation of assisted quantum adiabatic passage in a single spin. *Physical Review Letters*, 110(24), Jun 2013.

[123] Brian B. Zhou, Alexandre Baksic, Hugo Ribeiro, Christopher G. Yale, F. Joseph Heremans, Paul C. Jerger, Adrian Auer, Guido Burkard, Aashish A. Clerk, and David D. Awschalom. Accelerated quantum control using superadiabatic dynamics in a solid-state lambda system. *Nature Physics*, 13(4):330–334, Nov 2016.

[124] Shuoming An, Dingshun Lv, Adolfo del Campo, and Kihwan Kim. Shortcuts to adiabaticity by counterdiabatic driving for trapped-ion displacement in phase space. *Nature Communications*, 7(1), Sep 2016.

[125] Orel Bechler, Adrien Borne, Serge Rosenblum, Gabriel Guendelman, Ori Ezrah Mor, Moran Netser, Tal Ohana, Ziv Aqua, Niv Drucker, Ran Finkelstein, et al. A passive photon–atom qubit swap operation. *Nature Physics*, 14(10):996–1000, 2018.

[126] Serge Rosenblum, Orel Bechler, Itay Shomroni, Yulia Lovsky, Gabriel Guendelman, and Barak Dayan. Extraction of a single photon from an optical pulse. *Nature Photonics*, 10(1):19–22, 2016.

[127] Andreas Reiserer, Norbert Kalb, Gerhard Rempe, and Stephan Ritter. A quantum gate between a flying optical photon and a single trapped atom. *Nature*, 508(7495):237–240, 2014.

[128] TG Tiecke, Jeffrey Douglas Thompson, Nathalie Pulmones de Leon, LR Liu, Vladan Vuletić, and Mikhail D Lukin. Nanophotonic quantum phase switch with a single atom. *Nature*, 508(7495):241–244, 2014.

[129] Hai-Rui Wei and Fu-Guo Deng. Compact implementation of the

$(\mathrm{SWAP})^a$

(swap) a gate on diamond nitrogen-vacancy centers coupled to resonators. *Quantum Information Processing*, 14(2):465–477, 2015.

[130] Wen-Qiang Liu and Hai-Rui Wei. Implementations of more general solid-state $(\text{swap})^{1/m}$ and controlled-$(\text{swap})^{1/m}$ gates. *New Journal of Physics*, 21(10):103018, Oct 2019.

[131] Adrien Borne, Tracy E. Northup, Rainer Blatt, and Barak Dayan. Efficient ion-photon qubit swap gate in realistic ion cavity-qed systems without strong coupling. *Optics Express*, 28(8):11822, Apr 2020.

[132] Jinxian Guo, Xiaotian Feng, Peiyu Yang, Zhifei Yu, LQ Chen, Chun-Hua Yuan, and Weiping Zhang. High-performance raman quantum memory with optimal control in room temperature atoms. *Nat. Commun.*, 10(1):148, 2019.

[133] Siyuan Luo, Yanan Wang, Xin Tong, and Zhiming Wang. Graphene-based optical modulators. *Nanoscale Research Letters*, 10(1):1–11, 2015.

[134] Rubab Amin, Jacob B Khurgin, and Volker J Sorger. Waveguide-based electro-absorption modulator performance: comparative analysis. *Opt. Express*, 26(12):15445–15470, 2018.

[135] Zenghui Bao, Zhiling Wang, Yukai Wu, Yan Li, Cheng Ma, Yipu Song, Hongyi Zhang, and Luming Duan. On-demand storage and retrieval of microwave photons using a superconducting multiresonator quantum memory. *Physical Review Letters*, 127(1):010503, 2021.

[136] Rodney Loudon. *The quantum theory of light*. OUP Oxford, 2000.

[137] Christopher Gerry, Peter Knight, and Peter L Knight. *Introductory quantum optics*. Cambridge university press, 2005.

[138] Alexey V. Gorshkov, Axel André, Mikhail D. Lukin, and Anders S. Sørensen. Photon storage in λ-type optically dense atomic media. ii. free-space model. *Phys. Rev. A*, 76:033805, Sep 2007.

[139] Hermann Haken. *Advanced synergetics: Instability hierarchies of self-organizing systems and devices*, volume 20. Springer Science & Business Media, 2012.

[140] MS Safronova, WR Johnson, and A Derevianko. Relativistic many-body calculations of energy levels, hyperfine constants, electric-dipole matrix elements, and static polarizabilities for alkali-metal atoms. *Physical Review A*, 60(6):4476, 1999.

[141] SA Blundell, WR Johnson, and J Sapirstein. Relativistic all-order calculations of energies and matrix elements in cesium. *Physical Review A*, 43(7):3407, 1991.